THE UNIVERSITY OF ASTON IN BIRMINGHAM

"INVESTIGATION OF NEUTRON DIFFUSION PARAMETERS IN LIQUID MODERATORS AND LIQUID MODERATED MULTIPLYING ASSEMBLIES"

Thesis submitted for the Degree of
Doctor of Philosophy

by

L.Twum-Danso, M.Sc.

Department of Physics,

September, 1969

ABSTRACT.

The effect of voids on neutron multiplication in a natural uranium/water moderated subcritical assembly has been investigated. Voids were introduced by bubbling compressed air through the core and covered the range 0% to about 10% void fraction. A 150 Kev S.A.M.E.S. accelerator provided D-D source neutrons to the subcritical assembly and neutron flux measurement was by Indium foil activation with subsequent β-counting on a plastic scintillation counter. The results of the measurement have shown that the system has a positive void coefficient of reactivity, at least, for the size of void fractions used. Good agreement was found with theory and there was also good agreement with the results of other workers, notably Kouts et.al[18].

Fluctuations were also induced in the assembly with the view of predicting the onset of local fluctuations of neutron population in reactors. For this aspect of the work a 3 Curie-Am-Be neutron source was used instead of the S.A.M.E.S accelerator and neutron counting was by means of a Li^6 loaded glass scintillation counter. Results have shown that the onset of fluctuations in a reactor is easily predictable and it is suggested that an on-line computer could be used to monitor this.

ACKNOWLEDGEMENTS.

I would like to thank Dr.P.N.Cooper for suggesting the project and to acknowledge the continued help and guidance offered by him.

I would also like to thank Professor S.E.Hunt for his help and encouragement.

My thanks are due to the Ghana Atomic Energy Commission for financial assistance and also to the University of Aston for the offer of a year's research assistantship.

Thanks are also due to other members of staff and colleagues of the Physics Department for their help and cooperation.

Finally, I would like to thank my wife for much patience and understanding.

L.Twum-Danso.

TABLE OF CONTENTS.

CHAPTER 5 (contd)

LIST OF FIGURES.

LIST OF TABLES.

CHAPTER 1.

THE SUBCRITICAL ASSEMBLY

1.1 Introduction.

The behaviour and properties of nuclear chain reactors can be understood by studying the neutron population which supports the chain. This involves making neutron flux measurements in either subcritical assemblies or proper critical reactors and supporting these experimental results with theoretical calculations. Usually experiment offers a much simpler way of obtaining results than theory - Uncertainties in neutron cross-section data and incomplete understanding of neutron behaviour in reactor systems means that reactor calculations can only depend on approximations and assumptions which are not always rigorous. Calculations therefore tend to be long, tedious and a somewhat uncertain procedure. Nevertheless, for any experimental results to be acceptable they must have the support of theory. Also a combination of theory and experiment enables semi-empirical recipes to be derived for use in predicting the behaviour of generally similar systems.

It was the aim of this work to make measurements of the static neutron diffusion parameters in a light water moderated natural uranium multiplying assembly and compare the results obtained with those obtained from a suitable theoretical model.

1.2 Role of Subcritical Assemblies in Thermal Reactor Physics Research.

Subcritical assemblies or exponential assemblies provide a very important and useful tool for the experimental study of thermal reactor systems. A subcritical assembly is smaller than a critical assembly having a similar lattice and fuel. A self sustaining chain reaction is not possible in such a system though a steady state is possible if an extraneous source is present. The extraneous source makes up the deficit between neutron leakage and absorption on one hand and the production by fission on the other.(1)

Frequently exponential assemblies are used for obtaining the first experimental data concerning the neutron physics properties of a particular reactor. They have been used to determine the optimum proportions of the fuel moderator and other parts of a proposed full-sized operating reactor. Reactor optimization with subcritical assembles can be carried through relatively quickly, safely and cheaply. This is because very little shielding is necessary since the neutron density is generally low. Furthermore, the complicated and often expensive control mechanisms and instrumentation systems of a full critical reactor are unnecessary. Exponential assemblies are easily accessible and in general, moderator to fuel ratios can be varied conveniently. The activation

1.2 (contd)

level of the fuel elements is such that fuel manipulation presents no special problems. The speed with which data can be collected makes them well suited for extensive series of measurements. These merits lead to easy operation and low operating costs which explains why sub-critical assemblies find such wide application in thermal reactor physics research.

It has to be pointed out, however, that exponential experiments are not without their inherent disadvantages -

(i) Higher leakage rates in comparison with critical assemblies - This may necessitate corrections in some of the measurements.

(ii) Source effects which are totally absent in critical experiments may create problems in an exponential experiment.

(iii) The absence of poisonous fission products coupled with the fact that subcritical fuel composition differs from the true composition during an actual core lifetime gives rise to a neutron flux distribution in each lattice cell which is different from that in an actual reactor.

(iv) Exponential experiments are carried out under external circumstances which are different from those in an

1.2 (contd)

(iv) contd.

actual reactor. For example experiments are usually performed at room temperature. However, in some experiments like those described in Chapter 2 it is possible to simulate certain high temperature effects such as boiling.

(v) Furthermore, some measurements such as control rod worth are difficult and not very meaningful to do in exponential assemblies.

Despite these inherent disadvantages subcritical assemblies have had, and will continue to have wide application in reactor physics research.

1.3 Flux Distribution in Subcritical Assembly.

For a relatively large system such as a natural uranium assembly the thermal flux distribution at a distance from the extraneous source can be represented fairly closely by the wave equation:

$$\nabla^2\phi + B_m^2\phi = 0 \qquad 1.1$$

where ϕ represents the thermal neutron flux and B_m^2 the material buckling of the medium of which the assembly is composed.

For equation 1.1 to hold the region in which

1.3 contd.

measurements are made must be at least one slowing down length from the boundaries of the system. For a light water moderated system this is of the order of 5 - 6 cm. Strictly speaking the wave equation (Eqn.1.1) only refers to a homogeneous system. In a heterogeneous system there will be local irregularities due to the lattice structure but the wave equation will give the overall flux distribution.

1.4 Construction of the Subcritical Assembly.

The subcritical assembly was the first major constructional work undertaken on the commencement of this project. A S.A.M.E.S. J type accelerator (Fig.1.1) was also available to provide a source of neutrons for the assembly.

1.4.1 Description of the Subcritical Assembly.

The assembly consists of a stainless steel tank 44 in. × 34.5 in. × 36 in.high. In this tank are arranged vertically 196 fuel elements in an array determined by guide holes drilled in two removable $\frac{1}{2}$ in. aluminium lattice plates. Each fuel element is a rod of natural uranium 1.15 in. diameter and 32 in. long clad in 0.036 in. aluminium. There is an air space of 0.005 in. between the uranium and the

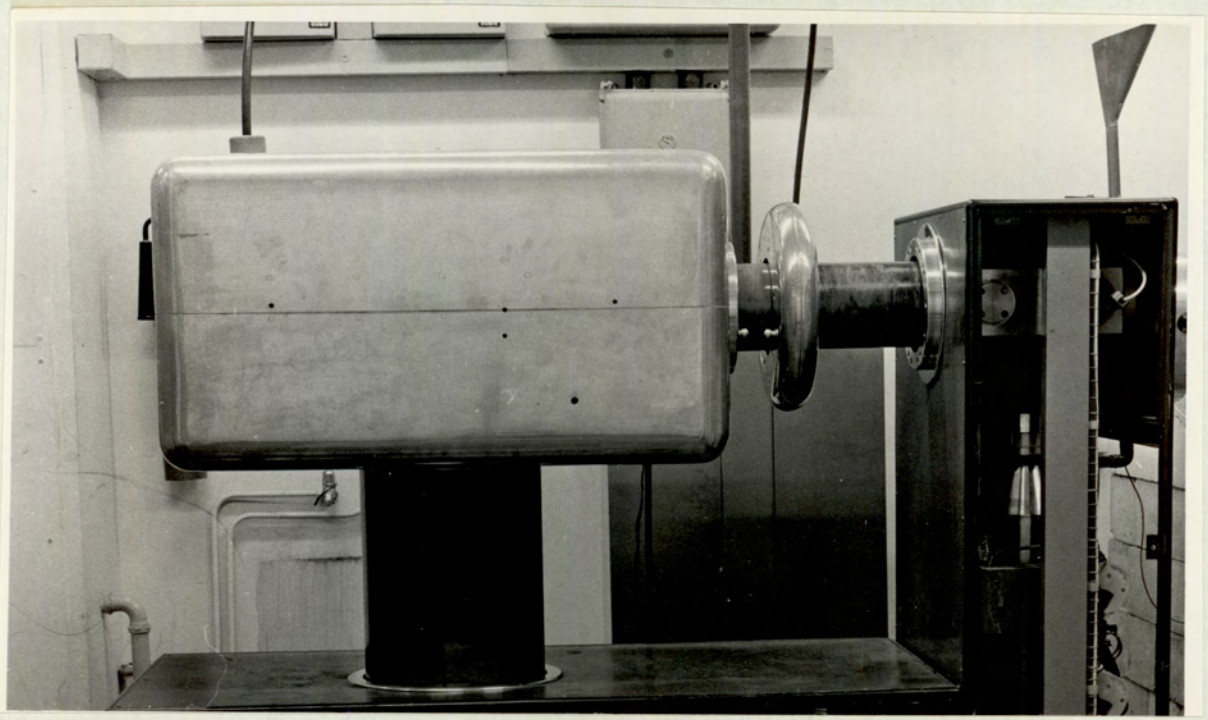

FIG. 1.1

1.4 (contd)

1.4.1 contd.

aluminium can. Each rod weighs 10 kg. giving a total mass of 1.96 tonnes in the core. One of the lattice plates rests on the bottom of the tank while the second is fixed so that its top face is 32 in. from the bottom of the tank. This construction ensures a more stable positioning of the fuel elements in the core of the assembly. The lattice plates contain additional guide holes to take $\frac{1}{2}$ in. diameter solid perspex foil holders.

The lattice plates (like the stainless steel tank) were originally manufactured for a subcritical facility at the Royal Naval College, Greenwich which had an 18 x 18 fuel assembly. (Our facility uses 196 fuel rods in a 14 x 14 lattice assembly).

Polythene spacers were used to reduce the holes in the lattice plates so that they fitted the fuel elements. These spacers also prevented the fuel elements from making direct contact with the lattice plates, thus reducing the risk of electrolytic corrosion of the fuel cans. Figs.1.2 and 1.3 show the top view of the lattice arrangement of the subcritical assembly with and without uranium respectively.

The assembly uses light water moderator and

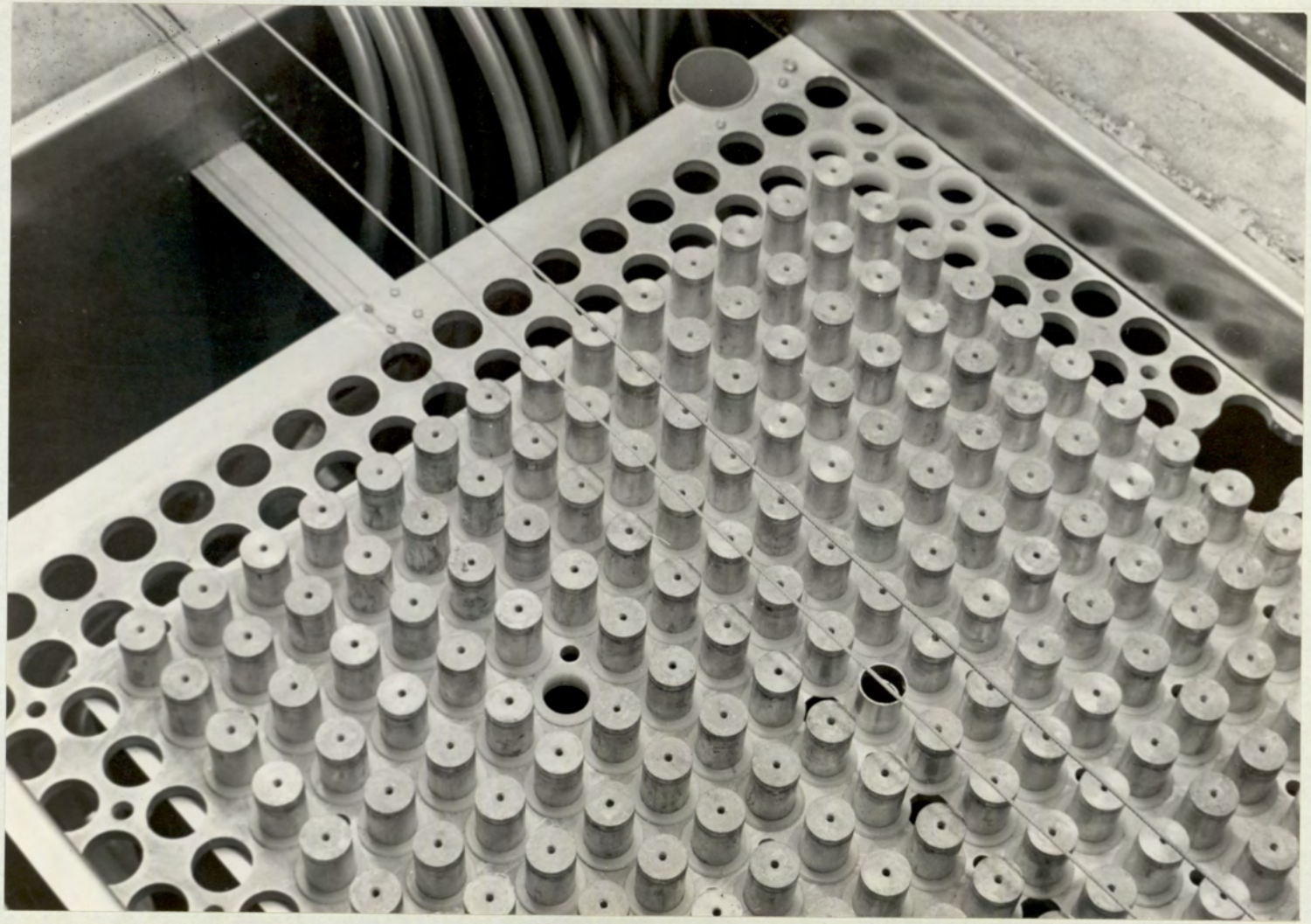

FIG. 1.2

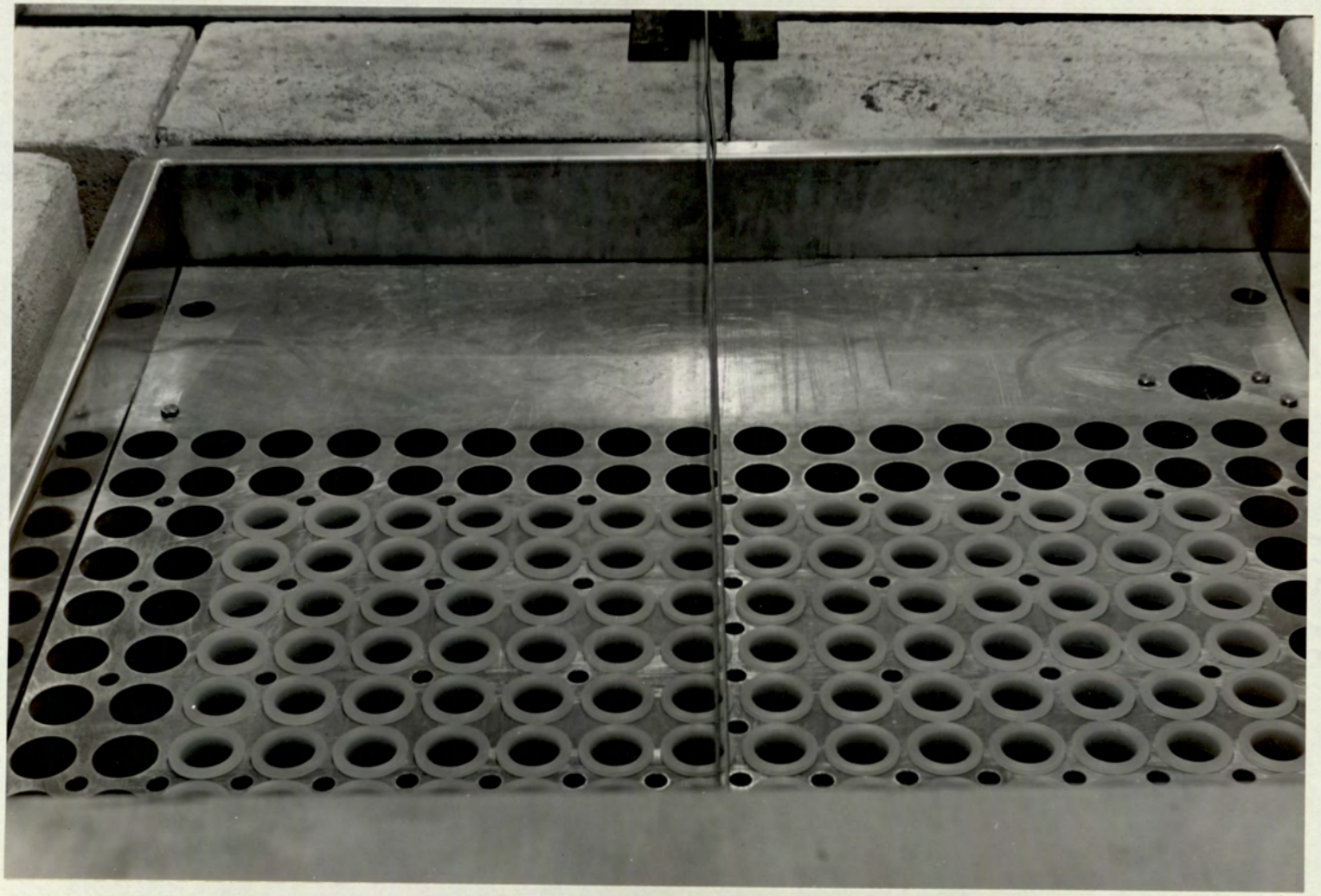

FIG. 1.3

1.4 (contd)

1.4.1 contd.

the arrangement of the core is such that there is about 4 inches of water surrounding three of the vertical faces. The water height is the same as the fuel so that the core is unreflected in the vertical direction. About 15 inches of water adjoins the fourth vertical face and a drift tube from the Sames J type accelerator projects into the water such that the target is close to the edge of the core.

Fig.1.4 shows the plan view of the core of the subcritical assembly.

The bottom lattice plate has thirteen $\frac{1}{2}$ in. aluminium tubes fixed firmly on it. Through these tubes air is blown from the compressors for the purpose of simulating boiling in the subcritical assembly.

Fig.1.5 shows the bottom lattice plate with the $\frac{1}{2}$ in. aluminium tubes in position. There is also a more detailed description of this in Chapter 2 which deals with boiling simulation in the subcritical assembly.

1.4.2 Fuel Canning.

Each uranium fuel rod is protected by an aluminium can 1.16 in. (internal diameter), 0.036 in.

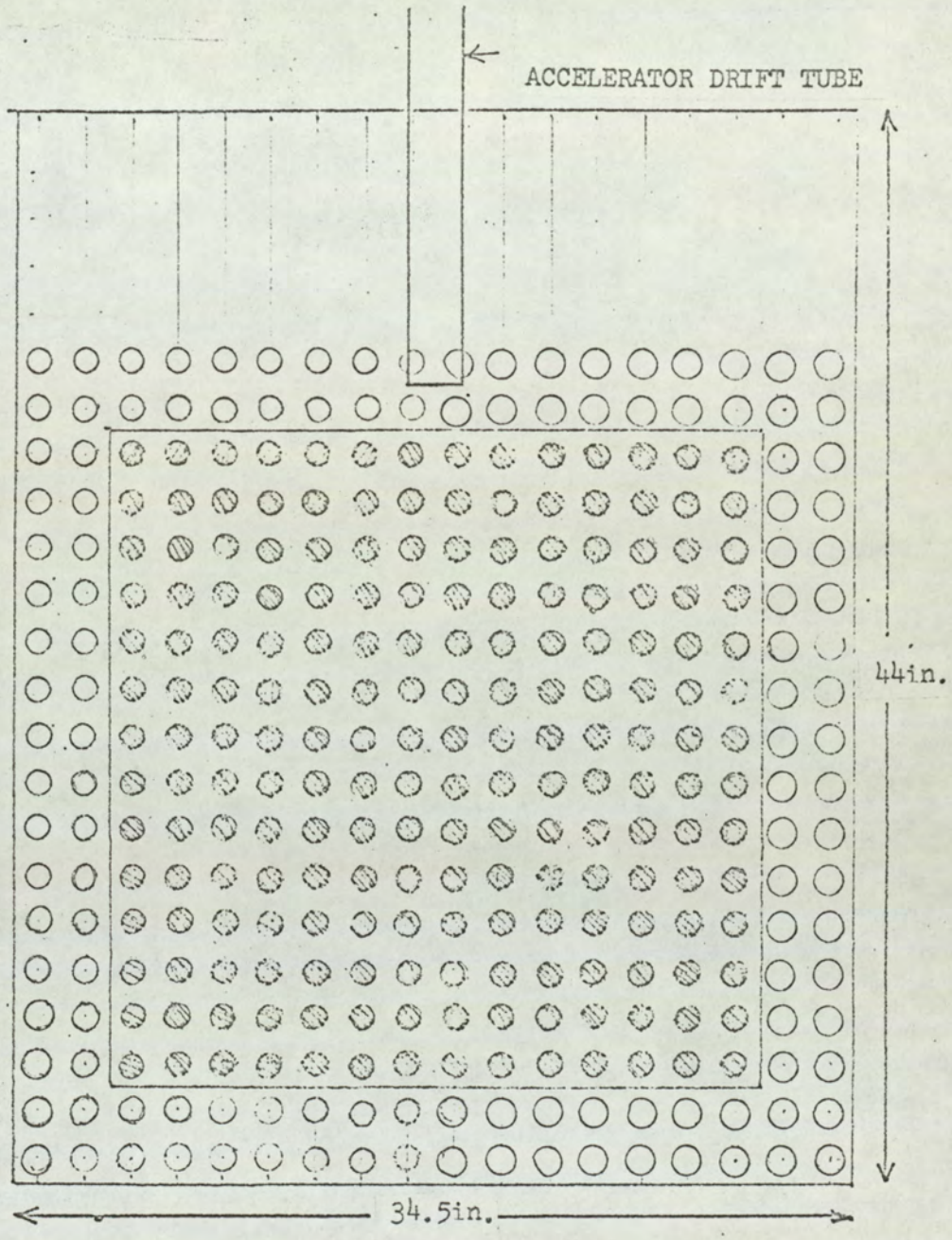

FIG.1.4 PLAN VIEW OF SUBCRITICAL ASSEMBLY CORE

14x14 ASSEMBLY ON 1.90in.SQUARCE PITCH

KEY ⊘ URANIUM BARS

○ VACANT LATTICE POSITIONS

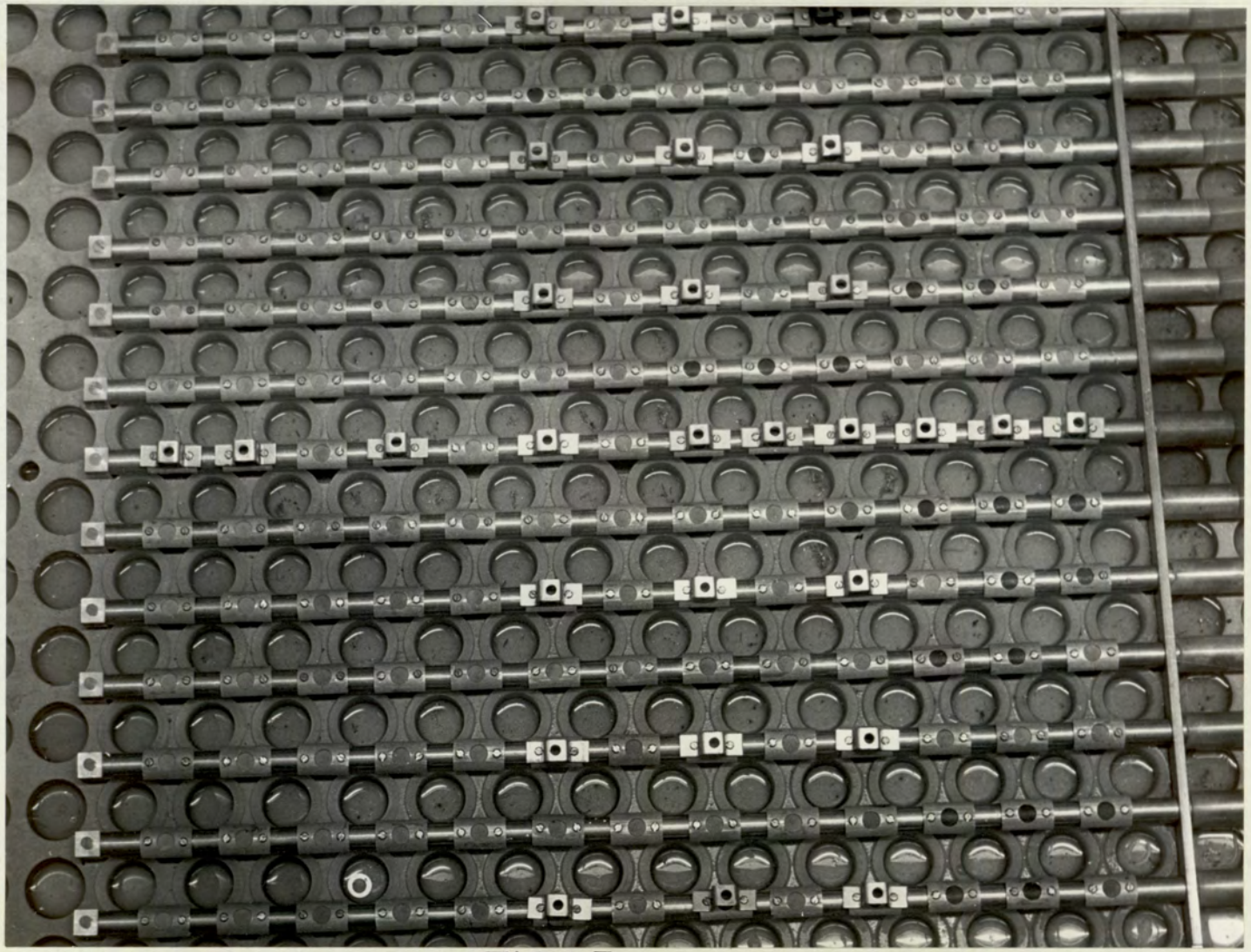

FIG.1.5

1.4 (contd)

1.4.2 contd.

wall thickness fabricated from B.A 99.5% aluminium (U.K.A.E.A. Standard). The cans were manufactured with an internal welded cap at the lower end. Before assembling the uranium in the cans, each can was thoroughly cleaned and degreased to avoid contamination of the uranium. The top end of each can was sealed with an aluminium plug araldited in position to make it water-tight. Epoxy resin was placed in the bottom of each can to form a firm base for the uranium, and also to ensure a leak tight can. A diagram of the fuel element is shown in Fig.1.6.

1.4.3 Water Circulation System.

Water is pumped from a storage tank up into the core tank by means of a stainless steel centrifugal pump and allowed to run out through an overflow pipe. The water in the subcritical assembly is in continuous circulation. It is purified by an ion-exchange column and can be drained from the core when necessary. When drained from the core the water is stored in the storage tank.

Fig.1.7 shows the water flow system in the assembly.

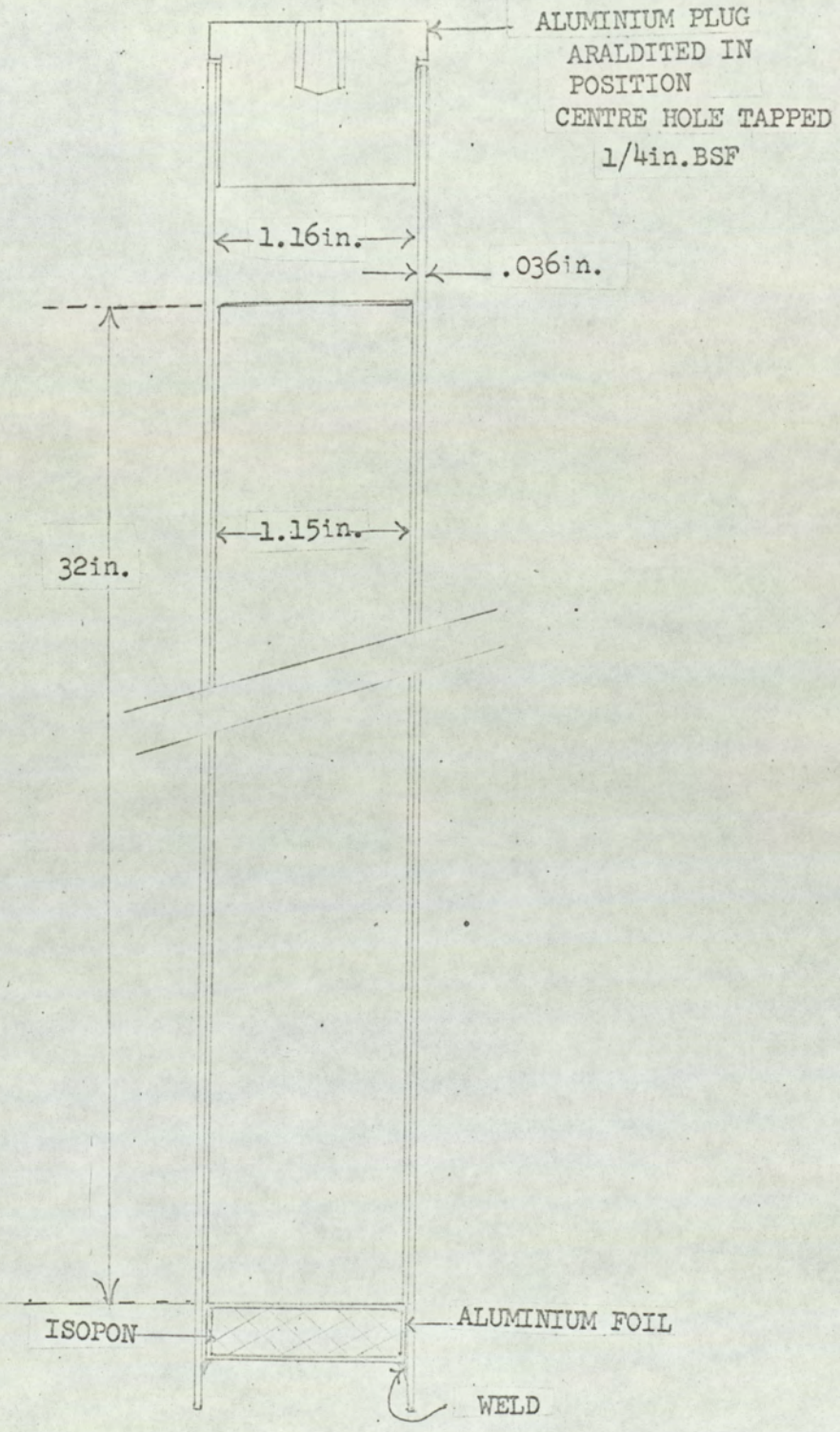

FIG. 1.6 FUEL ELEMENT

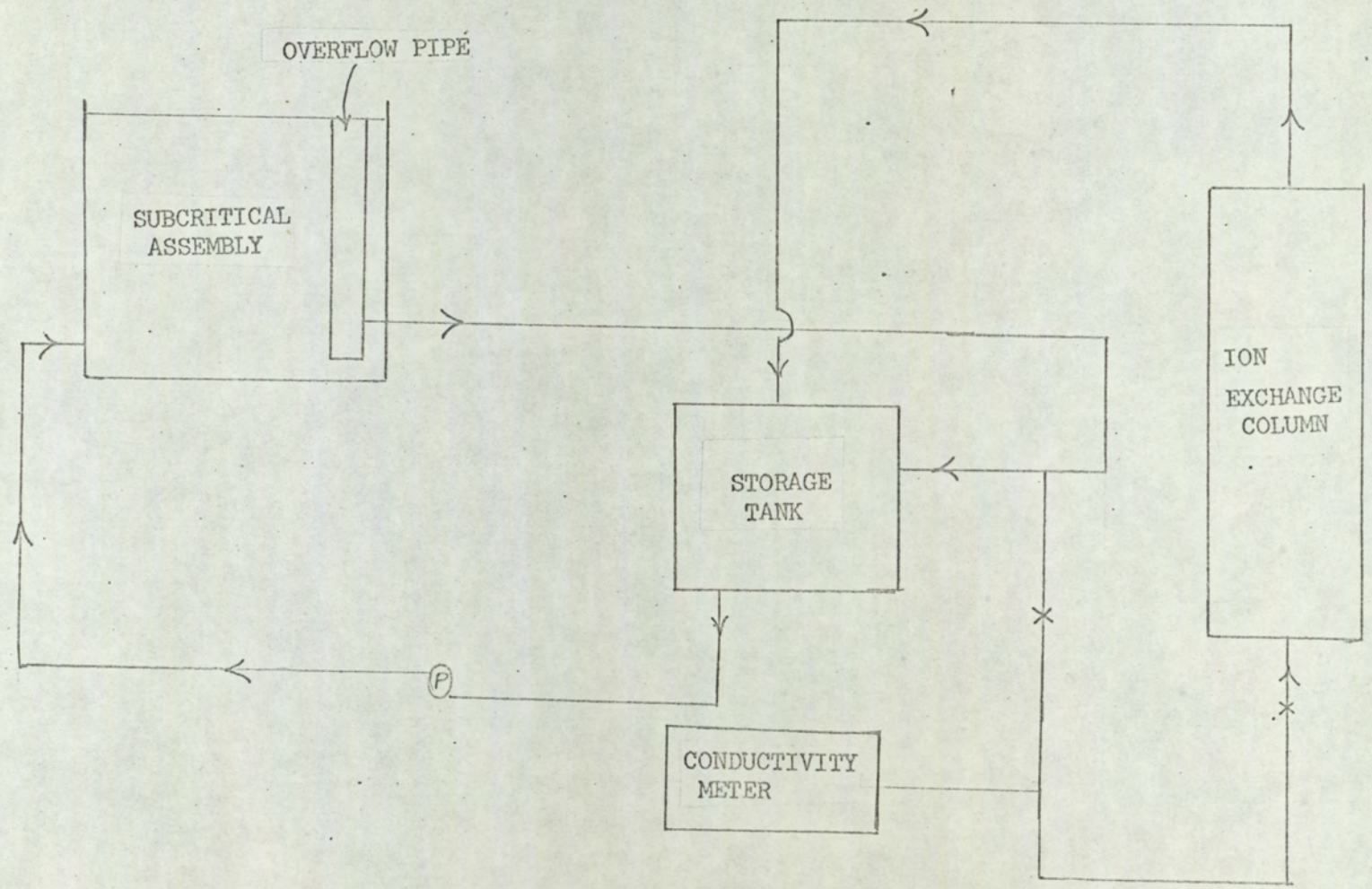

FIG.1.7 WATER CIRCULATION SYSTEM OF SUBCRITICAL ASSEMBLY

1.4 contd.

1.4.4 Target Assembly.

As pointed out in Section 1.4 the S.A.M.E.S. accelerator provided the subcritical assembly with a source of neutrons by the D-D reaction.

Fig.1.8 shows the target assembly to hold the deuterium target. This is at the end of a drift tube (Fig.1.9) which is coupled to the S.A.M.E.S. accelerator.

The deuterium target was obtained from the Radiochemical Centre, Amersham and consists of titanium evaporated on to a copper disc 2.85 cm. diameter, 0.025 cm. thickness, the titanium layer being about 2.5 cm. diameter and about 1 milligram per square centimetre in thickness. Deuterium is absorbed into the titanium to an atomic ratio (D/Ti) of about one.[2]

1.4.5 Neutron Shielding.

The main radiation hazards are neutrons from the core and from the accelerator target. An estimate of the total neutron leakage from the system was obtained from the following considerations (using simple diffusion theory).

Let S neutrons/sec represent the total

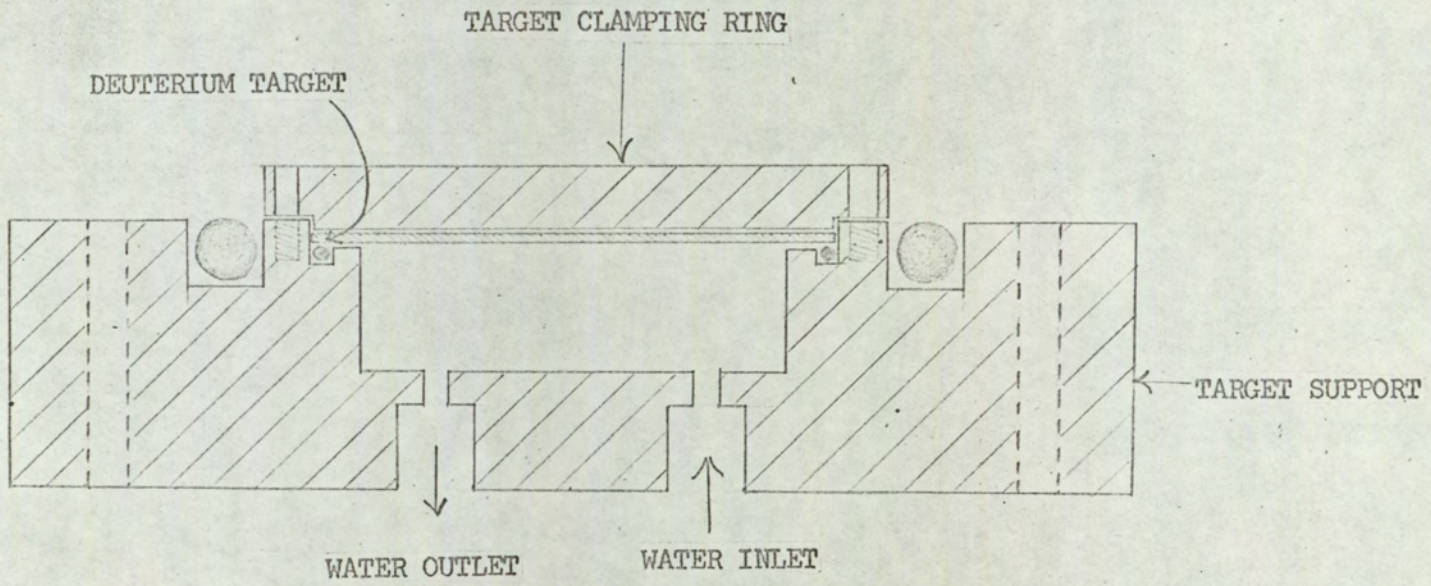

FIG 1.8 TARGET ASSEMBLY

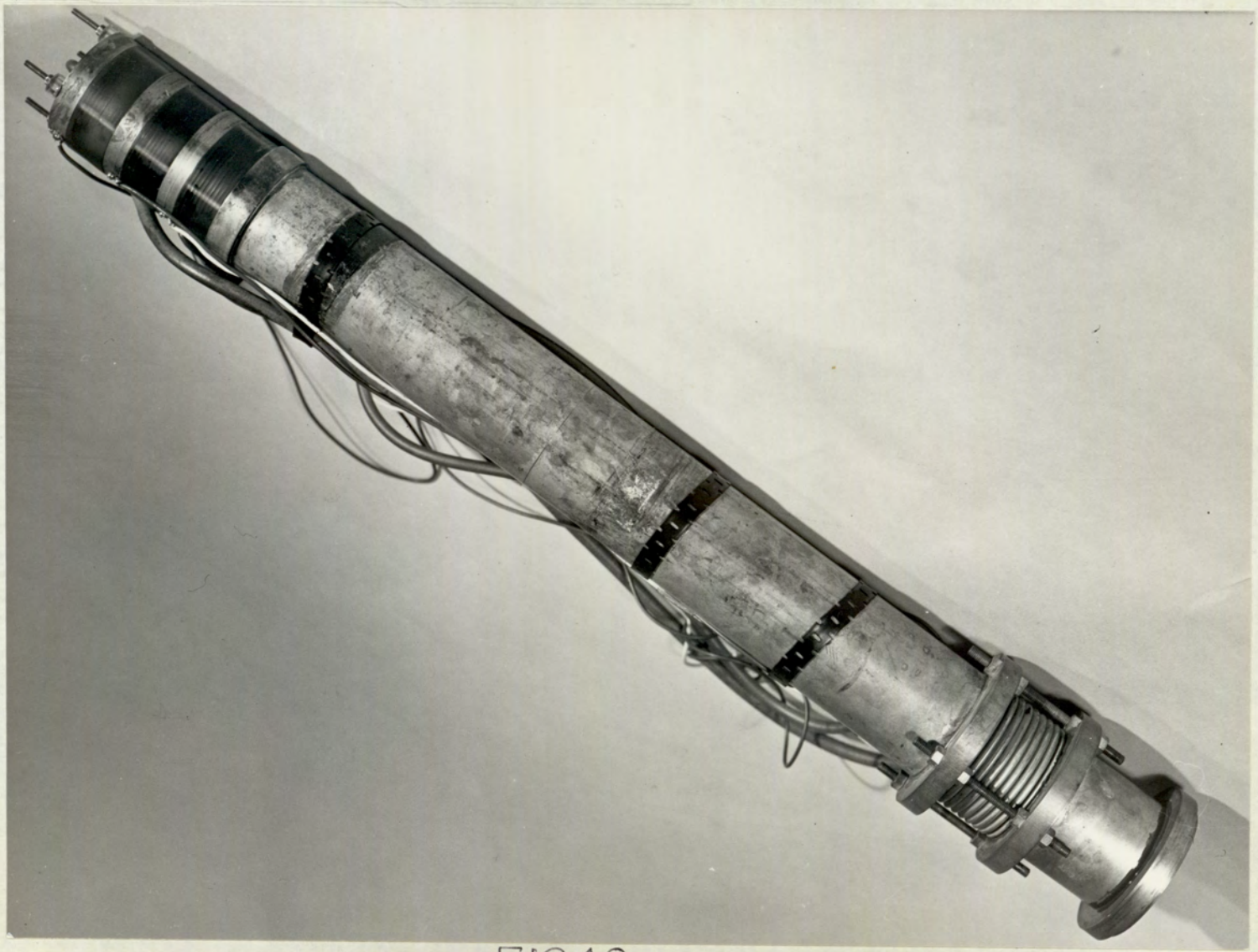

FIG. 1.9

1.4 (contd)

1.4.5 contd.

neutron input rate and M the neutron multiplication rate.

Then the product M × S will give the total number of neutrons present in the core.

$$\text{Now} \quad M = \frac{1}{1 - K_{eff}} \qquad 1.2$$

where K_{eff} = effective multiplication factor.

The fraction ℓ_f of fast neutrons leaking out of the system will be given by

$$\ell_f = \frac{L_f^2 B_g^2}{1 + L_f^2 B_g^2} \qquad 1.3$$

where L_f = Slowing down length of fast neutrons in water, B_g^2 = Geometric buckling of the core.

The total number N_f of fast neutrons leaking out will be given by

$$N_f = \frac{L_f^2 B_g^2}{1 + L_f^2 B_g^2} M \times S \qquad 1.4$$

The number N_{th} of thermal neutrons leaking out of the system will be given by:

1.4 (contd)

1.4.5 contd.

$$N_{th} = \frac{MS}{L_f^2 B_g^2 + 1} \times \frac{L_{th}^2 B_g^2}{L_{th}^2 B_g^2 + 1} \times p \qquad 1.5$$

where L_{th} = thermal diffusion length in water;

p = resonance escape probability.

It now remains to put in values into equations 1.2 - 1.5 so that the total number of both fast and thermal neutrons leaking out of the core can be calculated. The values used in a recent recalculation are given in Table 1.1. These are similar to initial design values and lead to similar conclusions.

TABLE 1.1

Values of Parameters used in Shielding Calculation.

Parameter	Value
K_{eff}	0.76
$B_g^2 (cm^{-2})$	44.31×10^{-4}
$L_f^2 (cm^2)$	27
$L_{th}^2 (cm^2)$	8.1
P	0.79
S (neutrons/sec)	10^8

1.4 contd.

1.4.5 contd.

The results of the computations using the values given in Table 1.1 yield a total leakage of about 10^7 fast neutrons per second and 3×10^6 thermal neutrons from a source of the order of 10^8 fast neutrons per second at the target.

In working out the amount of shielding material required it is assumed, for simplicity, that the leakage neutrons are all coming from the centre of a core 26.6 in. × 26.6 in. × 32 in. high. So that for the purpose of shielding the top of the core the neutrons could be taken as coming from a point in the core 16 inches (about 40 cm.) from the top. Granted this assumption the flux at the top of the core would be given by $\frac{10^7}{4\pi \times 40^2}$ i.e. 10^3 fast neutrons per second. Now as 10 fast neutrons per second are equivalent to 1 m.p.ℓ. i.e. a dose rate of 2.5 m.rem. per hour, the fast flux would have to be reduced by a factor of 100 to bring the dose rate down to 2.5 m.rem per hour. Reference to the literature[3-6] shows that 15 cm. of water will reduce fission neutron dose by a factor of 10. In view of this the top shielding consisted of 12 inches of ordinary water contained in a tank which is movable on rails. Using the same argument as before the flux at the four vertical faces of the

1.4 (contd)

1.4.5 contd.

core was estimated to be of the order of 10^3 fast neutrons per second. For this again 12 inches of water would be adequate to bring about the required reduction in dose rate to give 2.5 m.rem/hour at the surface. Regarding this it is to be remembered that there will be 4 inches of water on three vertical faces and 15 inches on the fourth vertical face when the core is filled with water (Fig.1.4). If the fast neutron shielding effectiveness of concrete is taken as roughly equivalent to that of ordinary water then 9 inches of ordinary concrete all round the tank in addition to the 4 in. of water should be adequate to bring about the required reduction in the fast neutron dose rate i.e. 2.5 m.rem/hr. at the three faces.

The shielding of the fourth vertical face of the core is complicated by the fact that the target is against this face and fast neutrons from a source of the order of 10^8 fast neutrons will be streaming backwards down the drift tube in the direction of the main laboratory working space. Fig.1.10 shows the plan view of the laboratory.

An 18 in. concrete wall was, therefore,

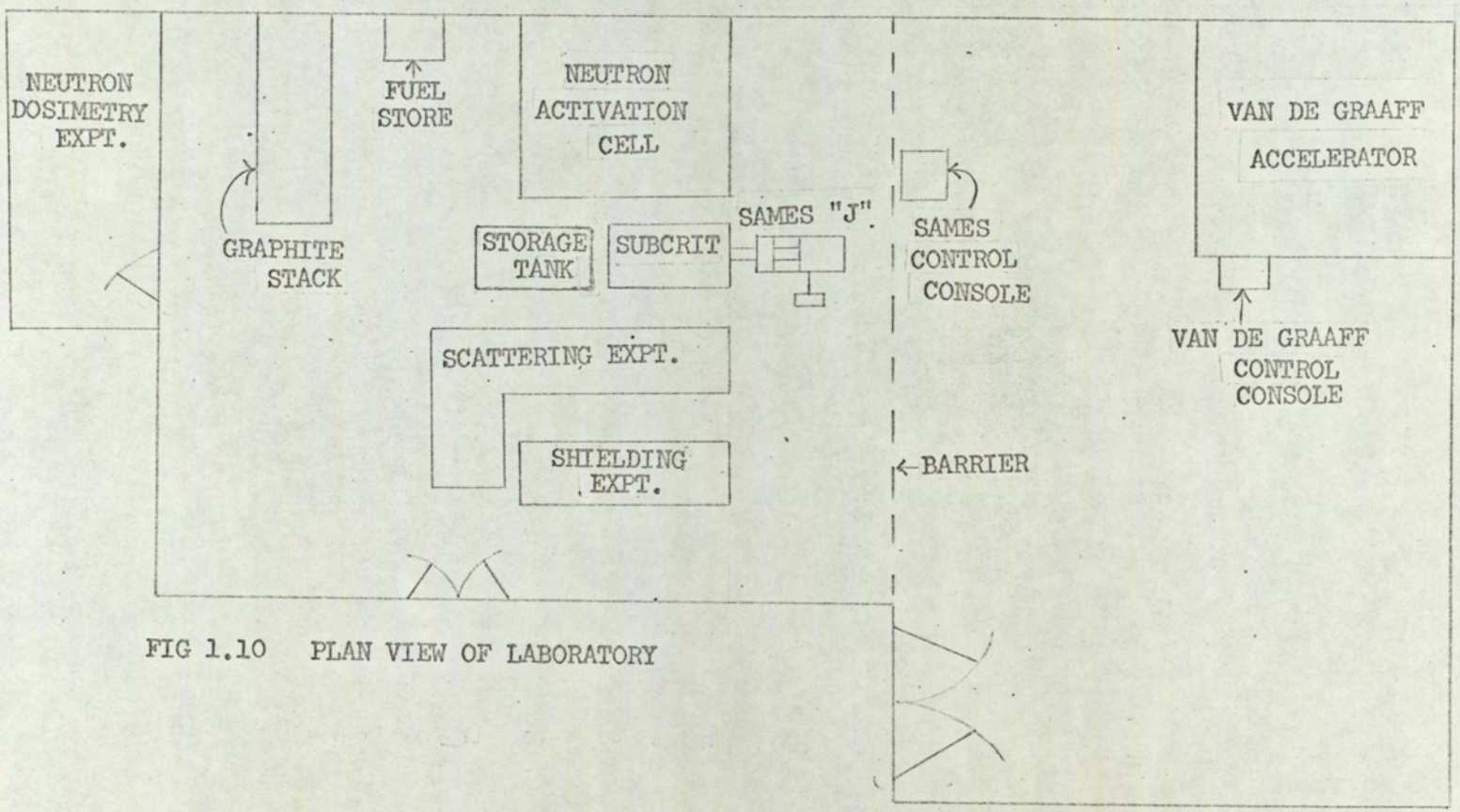

FIG 1.10 PLAN VIEW OF LABORATORY

1.4 (contd)

1.4.5 contd.

erected to separate the accelerator and experimental facilities from the main laboratory. This wall is 9 ft. from the core of the subcritical assembly so that for a fast neutron production rate of 10^8 neutrons per second at the target the flux at the inner surface of this wall will be about 10^2 neutrons per second. The wall thickness is sufficient to bring about a negligible fast neutron dose rate at its outer surface. In deciding upon what thickness of concrete to use for the "catcher wall", account had to be taken of the other experimental facilities using 14 MeV D-T neutrons.

The shielding needed against thermal neutrons was found to be more than adequate for thermal neutrons. In addition there is some gamma radiation from the decay of the natural uranium, which has an activity of about 0.7 Curies. In a dry unshielded core the gamma ray dose rate at the surface of the uranium is only 2.5 m.rem per hour due to self-shielding. Therefore, the shielding will be more than adequate for the natural radioactivity of the fuel.

The tank of the subcritical assembly stands on a plinth of concrete to provide shielding underneath.

1.4 contd.

1.4.5 contd.

This also helps to match the height of the accelerator beam to the centre line of the assembly.

A radiation survey conducted with the S.A.M.E.S. accelerator providing the subcritical assembly with D-D source neutrons showed that the dose at the surface of the top shield was about 0.8 m.p.ℓ. Elsewhere the fast neutron dose was much less than 1 m.p.ℓ, and especially in the main laboratory it was negligible showing that adequate shielding had been provided. Fig.1.11 shows the top shielding and part of the concrete side shielding for the assembly. The storage tank and the Ion Exchange Column can also be seen in Fig.1.11.

1.4.6 Safety Considerations.

Apart from providing adequate shielding to protect personnel from receiving too much radiation dose, special safety precuations had to be taken - These included the provision of fixed neutron and gamma radiation monitors with high level warnings to serve the subcritical assembly and all other facilities operated from the S.A.M.E.S. accelerator. These monitors, tanklid position, and water flow level were all inter-

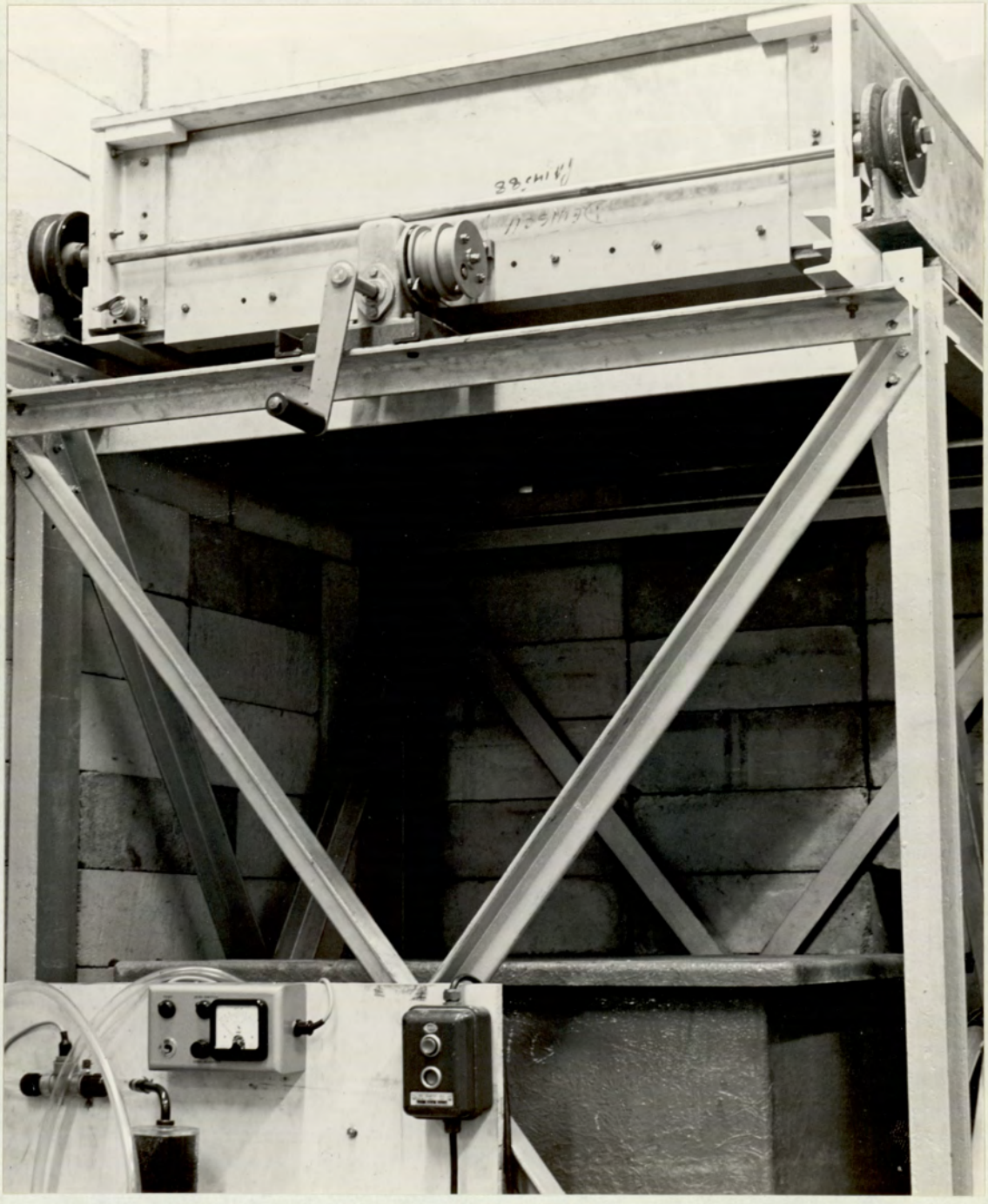

FIG. 1.11

1.4 (contd)

1.4.6 contd.

locked with the accelerator high tension.

CHAPTER 2.

THE SIMULATION OF BOILING.

2.1 Introduction.

The production of voids by actual boiling of the water in the subcritical assembly was impracticable. It was therefore decided to resort to the alternative method of producing voids by simulated boiling. It is to be appreciated that such boiling simulation can only be carried out at room temperatures which limits any study of the effects of boiling on the thermal nuclear reactor parameters to an investigation of voids. In a way this has an advantage over real boiling experiments as the other temperature effects are eliminated. For example, the effect of doppler broadening of Uranium-238 resonances on the neutron multiplication is eliminated as there is no heating of the fuel elements. Another point about simulated boiling is that the method only simulates bulk boiling such as is expected under runaway conditions in a pressurised water reactor or such as takes place near the surface in the boiling water reactor.

2.2 Methods of Simulating Boiling.

The main requirement in any method for simulating voids is a reduction in the hydrogen content of the moderator. This may be brought about in different ways:

(i) Diluting the water with a substance of lower scattering and absorption cross sections - Techniques in the past have used mixtures of light and heavy water - Such

2.2 contd.

(i) contd.

mixtures have lower absorption and scattering cross sections than the corresponding values for light water alone. This means less effective moderating properties which is tantamount to introducing voids in the medium.

(ii) The insertion of small sheets of Aluminium or Magnesium in the water - The trouble with this method is that the thermal neutron spectrum is affected too locally.

(iii) Replacement of the hydrogen of the water by organic material of lower hydrogen content - The organic material may be in the form of small plastic spheres which fill the measurement region, the empty space in the spheres representing the voids.

Small beads of highly expanded polystyrene may be packed into the fuel clusters and the interstices flooded with water as was done by Down et al.[7]

The use of expanded plastic materials like styrofoam does not give a true picture of what takes place in an actual boiling water reactor because of the very high void fraction associated with these substances (98%-99.5%). The other thing about these substances is that they lead to a difficult determination of the void fraction and moderating properties. Furthermore, some

2.2 contd.

discrepancy has been reported between styrofoam and magnesium[8]. The lack of space in the subcritical assembly was another point to consider as this ruled out the use of expanded substances like styrofoam for simulating voids.

In view of these difficulties it was considered preferable to simulate boiling by bubbling air through the assembly as this seemed to present fewer problems. This method has been quite successfully used by Shapiro[9] and Kleijn[10] among others. Air introduces very little foreign material into the assembly which is an advantage as this gives a mixture not too different from the steam-water mixture that obtains in an actual boiling water reactor. On the other hand the determination of the void fraction related to the motion of air bubbles in the liquid presents a problem which is probably not very serious when a static pressure method is adopted for the determination of the average void fraction.

2.3 Description of the Bubbling Equipment.

Two rotary oil free compressors each producing 20 cubic feet per min. free air displacement at a pressure of 3 psi were used. A picture of the compressors is given

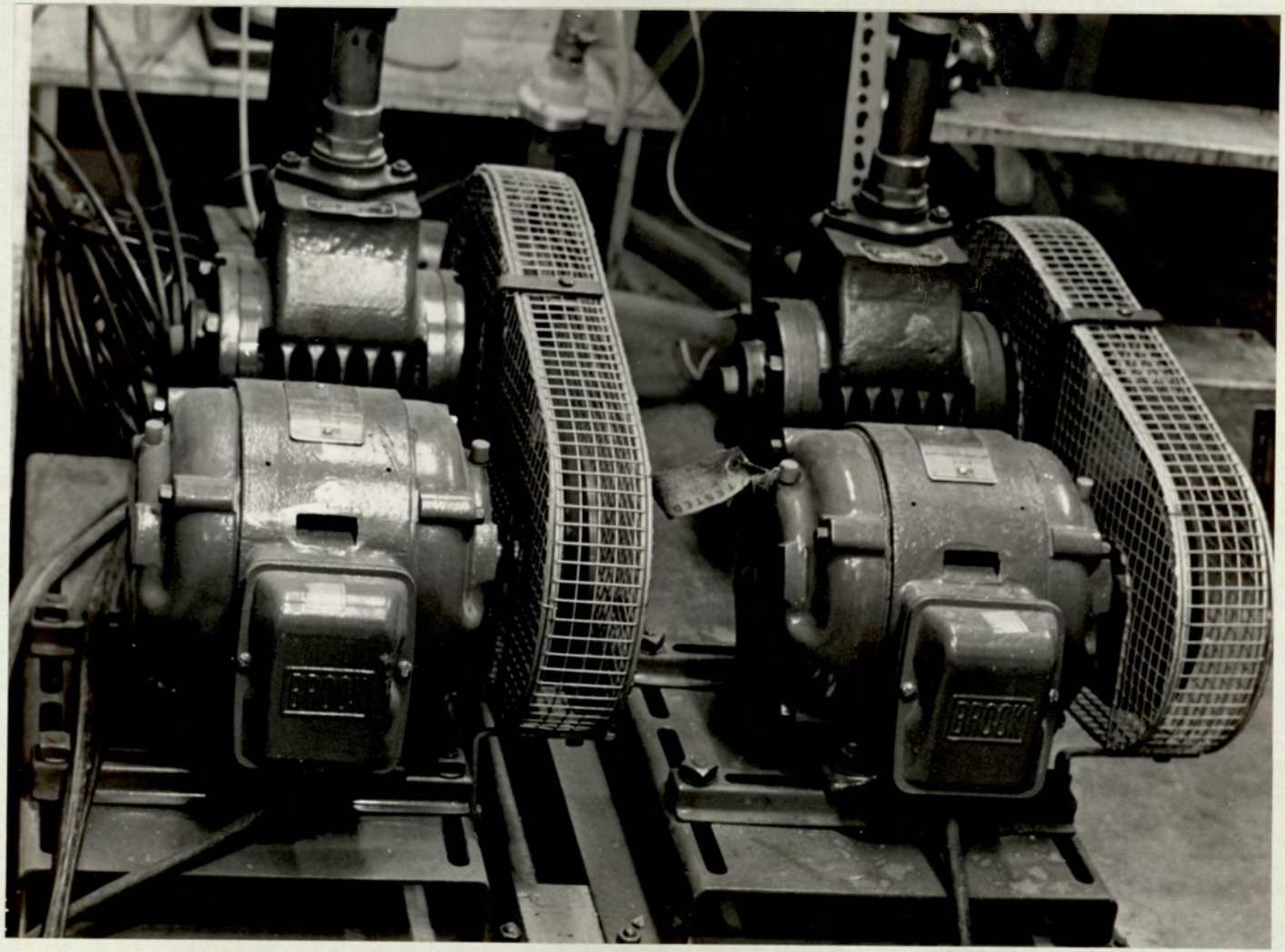

FIG. 2.1

2.3 contd.

in Fig.2.1.

The air from the compressors is blown through a copper tube into the core of the subcritical assembly. There are thirteen $\frac{1}{2}$ in. Aluminium tubes each of length 26 in. fixed in position at the bottom of the core of the subcritical assembly. Each tube is closed at one end while the open end is connected by a plastic tube to the air supply from the compressors. Thirteen equi-spaced $\frac{1}{2}$ in. holes lie along the length of each tube. A piece of porous polythene covers each hole and is held in position by an Aluninium clamp. Air from the compressors is blown through the tubes and then escapes through the polythene, rising upward through the whole body of the water moderator. A valve fitted to one of the compressors helps to regulate the amount of air through the system. This arrangement gives a more or less uniform distribution of bubbles in the body of the core - This can be seen from the uniformity of bubbling at the surface.

2.4 Measurement of the Void Fraction.

2.4.1 Static Measurement.

This method was used to measure the average void fraction caused by the introduction of air bubbles in the assembly. The apparatus consisted

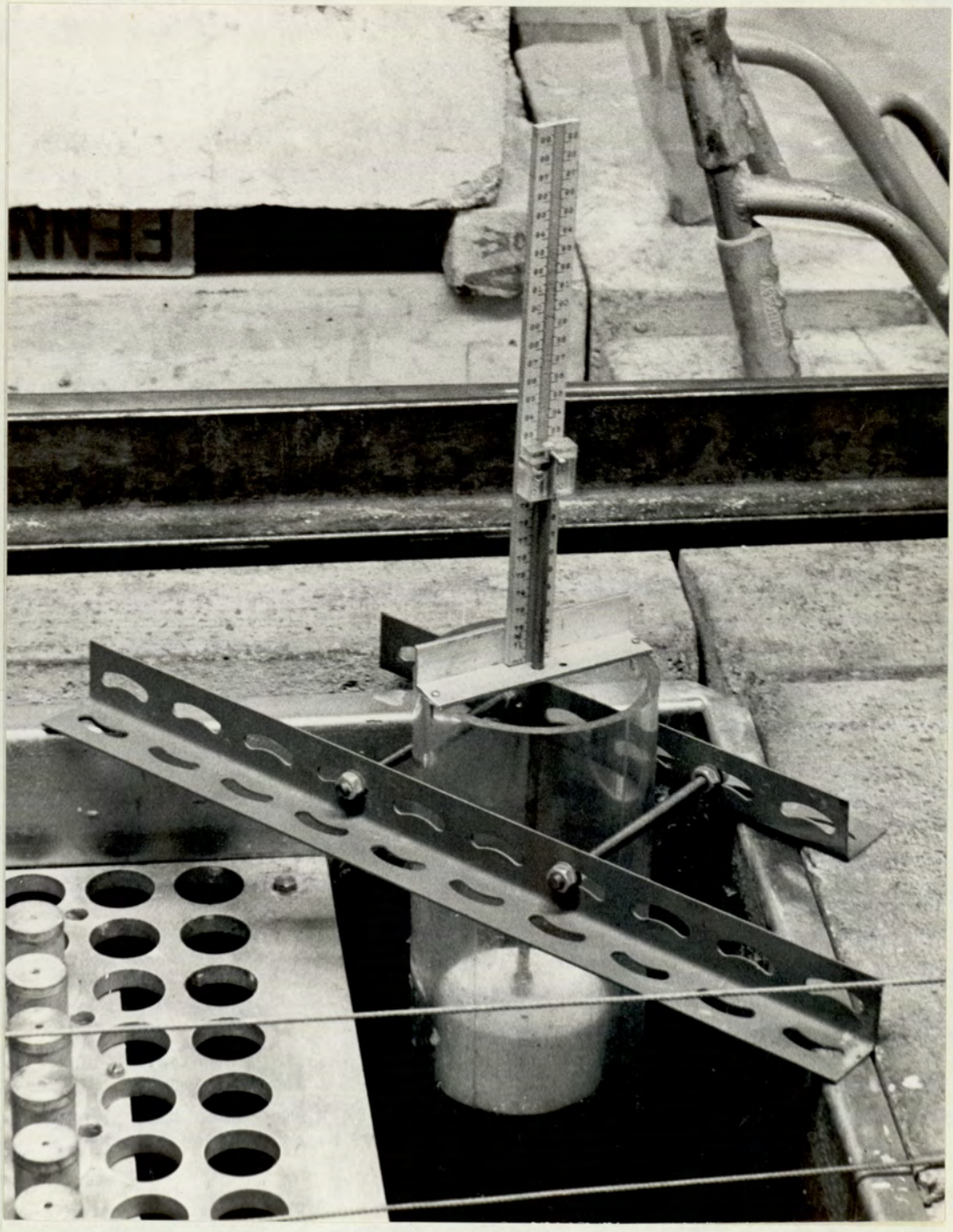

FIG. 2.2

2.4 contd.

2.4.1 contd.

of a plastic tube with a float system and a means of reading the water level inside the tube. A picture of this and its position in relation to the subcritical assembly is given in Fig.2.2. The measurement consisted in reading the level of water in the plastic tube when there was no bubbling and again when bubbling was proceeding. From the difference between the two readings the increase in the volume of water in the tank caused by the bubbling can be determined.

2.4.2 Calculation of Void Fraction.

The void fraction follows simply from this increase in the volume of the water on the basis of the following considerations:

Let the cross sectional area of the uranium be A_u, that of the tank A_t and that of the core A_c. If h represents the height of the core then the volume V_u of the uranium in the core is given by

$$V_u = A_u \times h \qquad 2.1$$

If V_{tw} is the volume of water in the tank and V_{cw} is the volume of water in the core then:

$$V_{tw} = h(A_t - A_u) \qquad 2.2$$

$$V_{cw} = h(A_c - A_u) \qquad 2.3$$

2.4 contd.

2.4.2 contd.

Now it has to be borne in mind that the voids are actually produced in the core and then distributed throughout the whole tank. Also the changes in the water level produced by the bubbles are measured for the entire tank as space limitation did not permit the installation of the measuring tube in the actual core. This means that changes in the water level caused by the bubbling which were directly measurable by this method were changes which applied to the entire tank. Therefore, to get the change in the water level which would have been produced were it possible to confine the bubbles to the core alone it is necessary to apply a correction. This was done by multiplying the changes in the water level measured in the plastic cylindrical tube by a factor S defined by equation 2.4

$$S = \frac{h(A_t - A_u)}{h(A_c - A_u)} = \frac{A_t - A_u}{A_c - A_u} \qquad 2.4$$

Putting in values of A_t and A_u and A_c this correction factor was found to be 2.71. Another correction has to be applied to account for the water which fills the plastic tubes connecting the Aluminium tubes at the

2.4 contd.

2.4.2 contd.

bottom of the core (Fig.1.5) to the copper tube directly connected to the compressors - When the compressors are switched on the air drives out the water from these tubes so that the rise in the water level indicated by the float system is an overestimate of what actually takes place as a result of bubbling. A simple calculation using the dimensions of the tubes, tank and core gives this correction as being of the order of 0.03 cm. This is a very small correction but it could be important in the smaller void fraction measurements.

With the correction factors determined the actual void fraction from any particular measurement is easily determined from the following equation:

$$\alpha = \frac{(x_2 - x_1) \times 2.71}{h} \times 100\% \qquad 2.5$$

where α = the void fraction

x_1 = the initial level of water in the tube

x_2 = level of water in tube while bubbling is proceeding

h = height of the core.

2.5 Results of Void Fraction Measurements.

Void fraction measurements were carried out for different amounts of air blown through the assembly. For each case several readings of the rise in the water level in the plastic tube were taken. The mean of these readings was used for the computation of the void fraction. With the two compressors switched on simultaneously the mean rise in the water level was found to be 2.72 cm. (from six separate measurements). This led to a void fraction of 9.1% with an estimated error of 4%. The corresponding value obtained for one compressor operating at full capacity was 1.85 cm. (from six measurements) leading to a void fraction of 6.1% with error estimated to be 6%. For the third case of one compressor operating at about half its maximum capacity the mean rise in the water level was 0.77 cm. (from six measurements) leading to a void fraction of 2.5% with 13% error.

The observational error was the same no matter the size of the rise of the water in the measuring tube so that it is not unreasonable to expect higher errors associated with smaller void fractions.

2.6 Other Possible Methods of Measuring Void Fraction.

2.6.1 Cadmium Ratio Method.

The theory of the method is given by Thie et al.[11]

2.6 contd.

2.6.1 contd.

and Kleijn[10] among others. The relation between the Cadmium ratio and the void fraction is given by:

$$\alpha = 1 - \left[\frac{Rcd(\alpha) - 1}{Rcd(o) - 1}\right] \times 100\% \qquad 2.6$$

where α = void fraction

$Rcd(\alpha)$ = Cadmium ratio at void fraction α

$Rcd(o)$ = Cadmium ratio at zero void fraction

The method was tried but as it gives the void fraction locally too many measurements would be needed for the average value.

2.6.2 Gamma-Ray Attenuation Technique.

This method which is well reported by many authors[12],[13],[14] was also tried but it did not prove successful because:

(i) The void fraction was too small - The static measurement gave a maximum average void fraction of about 9% but according to Perkins et al.[13] the gamma-ray method is unreliable when the void fraction is less than 25%.

(ii) There was a very high γ-background from the uranium. The counter was shielded but the background could not be reduced sufficiently.

CHAPTER 3.

THERMAL NEUTRON FLUX MEASUREMENT.

3.1 Review of Neutron Flux Measuring Techniques.

Several methods exist in the literature for neutron detection. All these methods emply one or other of the different mechanisms by which neutron interaction with matter takes place. The most useful of these mechanisms are as follows:[15]

(i) Neutron induced transmutations in which the product particles make the detection of neutrons possible. The (n,γ), (n,p), (n,α) and (n,fission) reactions provide examples of these mechanisms with the alpha particle, the proton, gamma ray or the fission products giving instantaneous information concerning the neutron.

(ii) Neutron induced transmutations which result in radioactive product nuclei. The subsequent decay of the radioactive nuclei gives information on the neutron flux which induced the radioactivity. A detector employing this principle is referred to as a neutron activation detector.

(iii) Elastic scattering by neutrons in which the recoil particle is charged and is capable of being detected - Elastic scattering of a neutron by a proton is the most important example of this process. This only applies to high energy neutrons though, as recoil protons from thermal neutron interaction would be too

3.1 contd.

weak to detect.

Because of limited space in the lattice and the availability of a high energy neutron output from an accelerator the foil activation technique was considered the most suitable method to use in the main series of experiments which involved measurement of flux as a function of position.

3.2 The Foil Activation Technique.

By this method the most stable isotope of a suitable detecting foil is first exposed to the neutron flux for a given period. This is called the activation or irradiation process. After this the foil is removed from the neutron field and the activity induced in it determined. The method has a number of advantages which include the following:

(i) Controlled sensitivity over a wide range. - By making suitable choice of materials with different cross sections it is possible to make measurements down to low fluxes (less than 1 neutron/cm^2 sec) and up to the largest values obtainable with a controlled reactor.

(ii) The detectors may be thin foils or small pellets. Consequently it is possible to introduce them in

3.2 contd.

(ii) contd.

the medium in which measurements are made without the introduction of significant voids - This is a particularly important point to consider in measurements concerned with the effect of voids on the static neutron diffusion parameters. For such measurements it is essential that voids not directly introduced by the main void production mechanism of the experimental set up are kept to a minimum. This requirement, therefore, makes the foil activation technique quite ideal for our measurements.

(iii) The effect of neutron absorption can be made negligible either by the selection of the foil or by the application of a small correction.

The main disadvantage of this technique, however, is that it is unsuitable for the measurement of the time dependence of a flux which is continually changing. This is because the measurement of the induced activity has two steps, viz:- the irradiation process and the activity measurement.

This advantage was no drawback in the main flux measurements to determine buckling changes but incore counter techniques had to be used when looking at fluctuations in the neutron population.

3.3 Type of foil Material.

3.3.1 Indium Foil Activation.

Having selected the foil activation technique as the method to use in the main neutron flux measurements the next step was to decide on the type of foil material to use. Following general practice it was decided to use Indium. Indium-115 which is about 96% abundant in natural uranium has a reasonably large capture cross section for thermal neutrons. In particular it has a very large resonance, over 30,000 barns at 1.46 ev.

The capture of a neutron by Indium-115 produces the radioactive isotope Indium-116 by the (n,γ) reaction:

$$_{49}In^{115} + {}_{0}n^{1} \rightarrow {}_{49}In^{116} + {}_{0}\gamma^{0}$$

$_{49}In^{116}$ emits β particles with maximum energy 1.01 Mev to become $_{50}Sn^{116}$ which is stable: $_{49}In^{116} \rightarrow {}_{50}Sn^{116} + \beta^{-} + \nu$. The radioisotope Indium-116 has a metastable and ground state with half lives of 54 min. and 14 sec. respectively.[16] The 14 sec. half life can be eliminated by waiting a short time between the end of the activation and the beginning of the counting so that the 54 min.

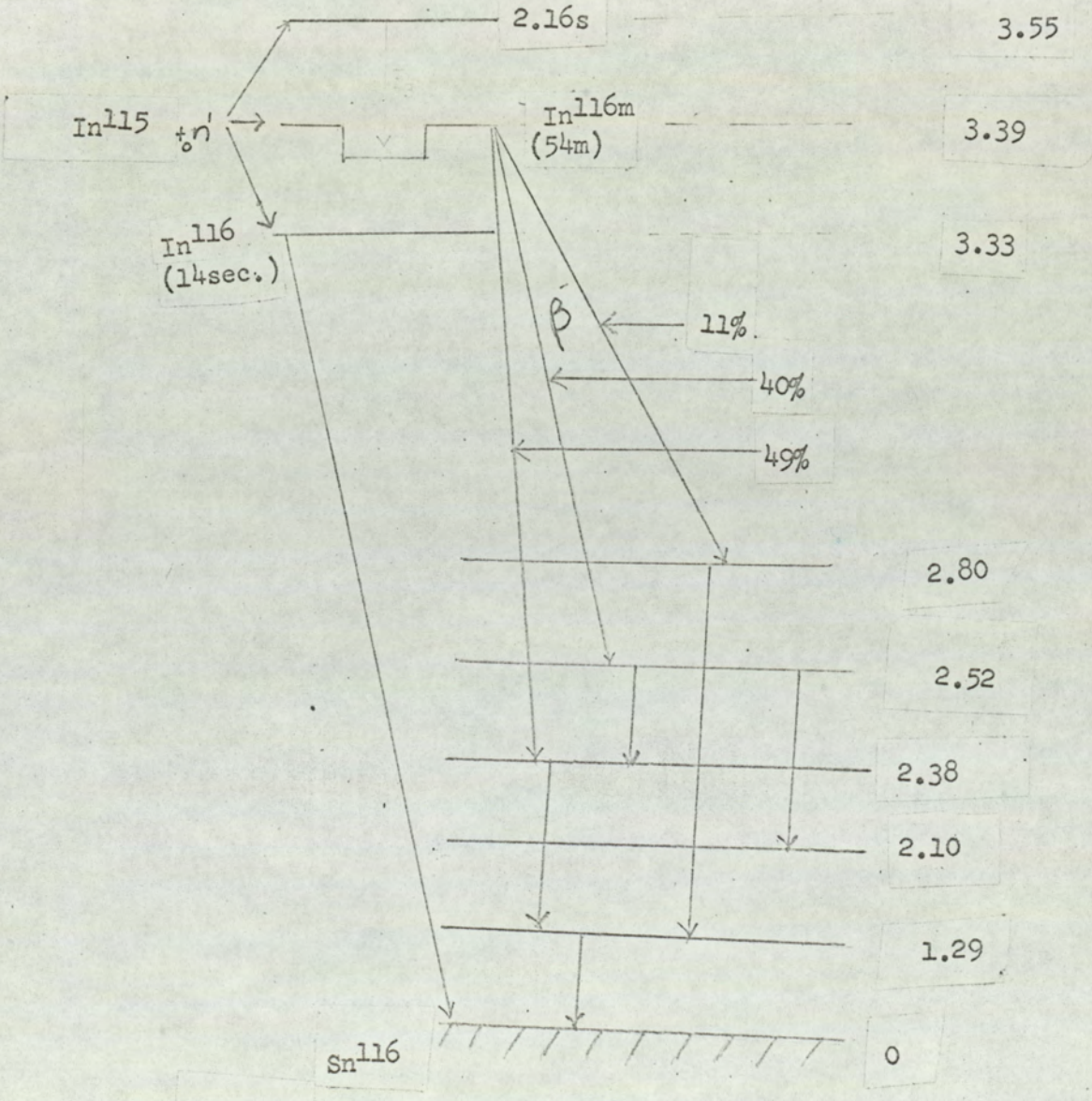

FIG.3.1 DECAY SCHEME OF INDIUM-116

3.3 contd.

3.3.1 contd.

half life can be counted almost exclusively. The half life of 54 min. is long enough for good counting and yet short enough for rapid irradiation. The predominant features of the decay scheme of Indium-116 are shown in Fig.3.1.

3.3.2 Foil Preparation.

A number of Indium foils each of approximately 1 cm. diameter was punched. These were then weighed on a balance accurate to 10^{-4} gram. Indium is very fragile and so to provide durability each foil was araldited on to a thin disc of perspex backing of about the same diameter as the foils. Perspex was used as the backing material for the foils because its low atomic number would decrease the effect of backscattering of β particles. Also the composition of perspex is not too different from that of water. This meant the perspex was not likely to add to the problem of flux perturbation in the vicinity of the foils. The foils were numbered on the perspex backing and grouped according to weight. The diameter of each foil was taken, and this meant making three measurements with the travelling microscope

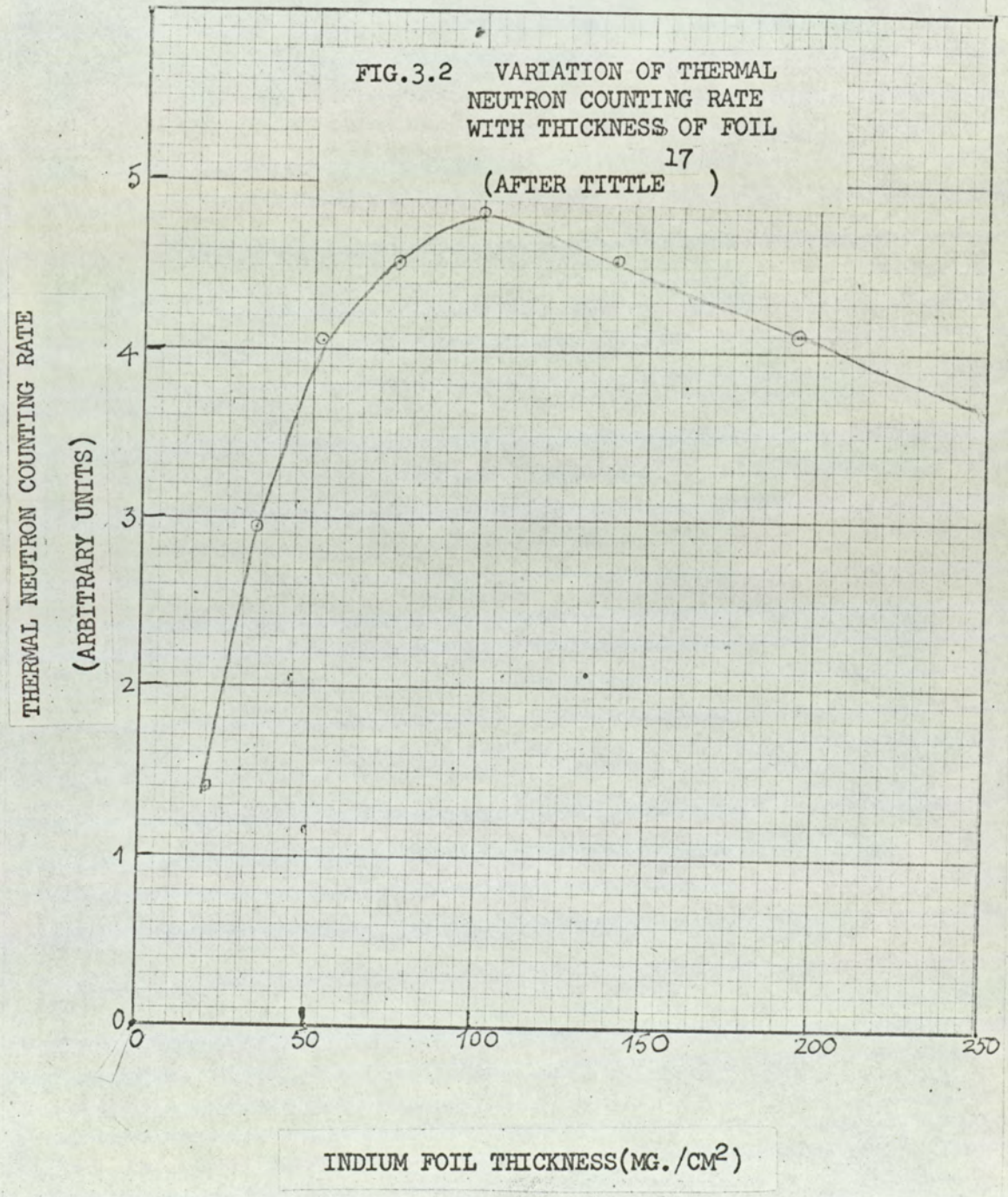
FIG.3.2 VARIATION OF THERMAL NEUTRON COUNTING RATE WITH THICKNESS OF FOIL
(AFTER TITTLE 17)
THERMAL NEUTRON COUNTING RATE
(ARBITRARY UNITS)
0
1
2
3
4
5
0
50
100
150
200
250
INDIUM FOIL THICKNESS(MG./CM2)

3.3 contd.

3.3.2 contd.

and taking the mean of the three readings.

3.3.3 Foil Thickness.

It has been shown that Indium foils give a maximum counting rate at about 100 mg/cm^2. thickness.[17] Fig.3.2 shows the general shape of the variation of thermal neutron counting rate with thickness of foil for 2.5 cm. diameter Indium foils as given in Tittle.[16]

The Indium foils used in this work ranged in thickness from 88 - 100 mg/cm^2 which is close to the optimum thickness. The advantage in using foils whose thickness is near the optimum value is that slight variations in a group of foils will have a minimum effect on their relative sensitivities.

3.3.4 Foil Holders.

Fig.3.3 is a diagram of the type of foil holder used. The material of the foil holder is solid plastic (methyl methacrylate) with the following formula: $C_5H_8O_2$. The foil holders had in them machined depressions for holding the Indium foils.

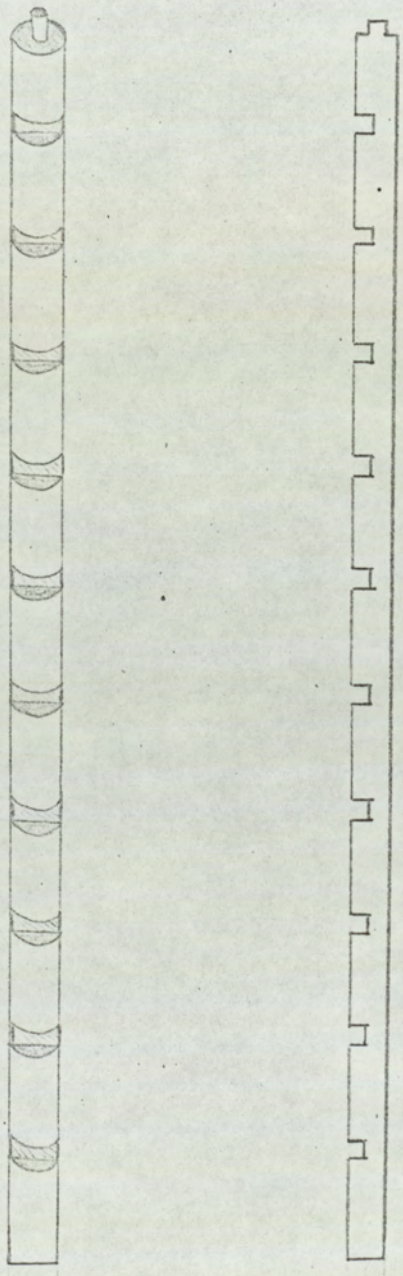

FIG. 3.3 FOIL HOLDER

3.3 contd.

3.3.4 contd.

This material was used because of its composition which may be taken as being close to that of water, and as pointed out in Section 3.3.2, this meant its presence in the subcritical assembly was not likely to add to the problem of flux perturbation in the vicinity of the detecting foils.

There was, however, the problem of bowing which tended to distort the shape of the foil holders with the consequent introduction of errors in the determination of the foil position in the subcritical assembly. This caused some random fluctuations in the foil activity but as flux distributions were the average of several readings the effect of the bowing was minimized.

Aluminium which is quite often used as a foil holder was not considered a satisfactory material because the mismatch of scattering cross sections between Aluminium and water leads to the introduction of flux perturbations into the system. This has been pointed out by Kouts et al.[18] among others.

3.3.5 Foil Positioning.

The foils were fastened on to the foil

3.3 contd.

3.3.5 contd.

holders with Lassothene tape. This is a polythene adhesive tape which is not affected by water.

In deciding upon how much space to leave between the foils for irradiation purposes it has to be borne in mind that if foils are too close flux perturbations are produced which may be large enough to influence the neighbouring foil readings and to affect the final result. Wade[19] in his work on neutron age in mixtures of heavy water and light water found that if foils were spaced about 8 cm. no such interference was observed. In the literature, however, 2-3 mean free paths is considered the minimum separation to use. In our case this is of the order of 2 cm. N.A.Khan et.al.[20] have also reported that interaction between 1 cm. diameter and 0.0127 cm. thick Indium foils became small for interfoil separations greater than 1.8 cm. The minimum spacing between the foils for the measurements reported in this work was one lattice pitch i.e. 1.9 in. (4.8 cm.) Axial flux measurements taken using the minimum spacing of one lattice pitch (4.8 cm.) and again using a minimum separation of two lattice pitches i.e. 9.6 cm. showed no noticeable change in the

3.3 contd.

3.3.5 contd.

flux distribution. This seemed to confirm that the separation of one lattice patch which was the very minimum used in our measurements was satisfactory.

3.4 Determination of the Relative Flux.

As pointed out in Section 3.2 the neutron flux measurement by the foil activation technique is in two parts, viz:- The activation process followed by the measurement of the induced activity. One of the Indium foils for irradiation was made to act as a monitor foil relative to which the activities of all the other foils were measured. The activity measurements were made on twin β sensitive scintillation counters, one for the monitor and the other to be used in turn with for the remaining foils. The foils were placed directly over the scintillator so that the solid angle of collection approached 2π. The monitor counter controls the installation in a preset count mode - Preset time controls both counters. The advantage in using a monitor foil of the same composition as the whole series of activation detectors is that the measurements and counting statistics become independent of the decay time (apart from a relatively small background correction). Each counting channel used a plastic scintillator to record the β activity

3.4 contd.

and covered with .002 cm. Aluminium foil to exclude light.

3.4.1 Irradiation of Foils.

The S.A.M.E.S. accelerator provided the sub-critical assembly with a neutron source:

$$D + D \rightarrow {}_2He^3 + {}_0n^1 + 3.266 \text{ Mev.}$$

The neutrons going off in the forward direction have an energy of about 2.45 Mev. which is not too different from the average energy of fission neutrons (range 0 - 10 Mev, mean 2 Mev). This relatively low energy neutron source is quite an advantage over a D-T source since the thickness of shielding required is about halved for similar yields of neutrons. In addition to this the exponential fall off of flux would be strongly influenced by the long slowing down length for 14 Mev, primary neutrons.

3.4.2 The Plastic Scintillator.

The plastic scintillator employed was a Nuclear Enterprises type NE 102A which is described as consisting of the "scintillation chemicals in polyvinyl toluene"(21). The scintillator is non-hygroscopic and needs no protective coating or entry window. It is less susceptible to thermal

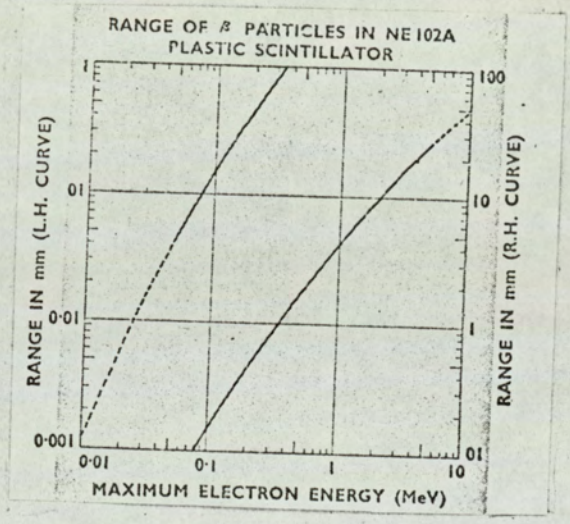

FIG.3.4 RANGE OF β PARTICLES IN NE 102A (21)

3.4 contd.

3.4.2 contd.

or mechanical shock and is easily machined.

The size of scintillator used was 1.5 in. diameter to match the photomultiplier tubes both of which were EMI type 6097B. Nuclear Enterprises[21] give a graph of the range of β particles in NE 102A. Fig.3.4 is a copy of this graph. From considerations of the maximum energy of β particles emitted during the decay of Indium-116 (and this is 1.01 Mev) the thickness of scintillator required for activity measurements was found from the graph (Fig.3.4) to be 5 mm.

3.4.3 The Scintillation Process.

The plastic scintillator NE 102A is an organic material. For the most part organic scintillators are aromatic hydrocarbons. Luminescence in organic materials is a fundamental property of the molecule and is shown not only in the solid state but in the liquid and vapour phases. The chief factor in determining the energy levels of the molecule is the distance between the atoms, and the energy system of the molecule can be represented in principle by a potential energy diagram in which the abscissa is the interatomic

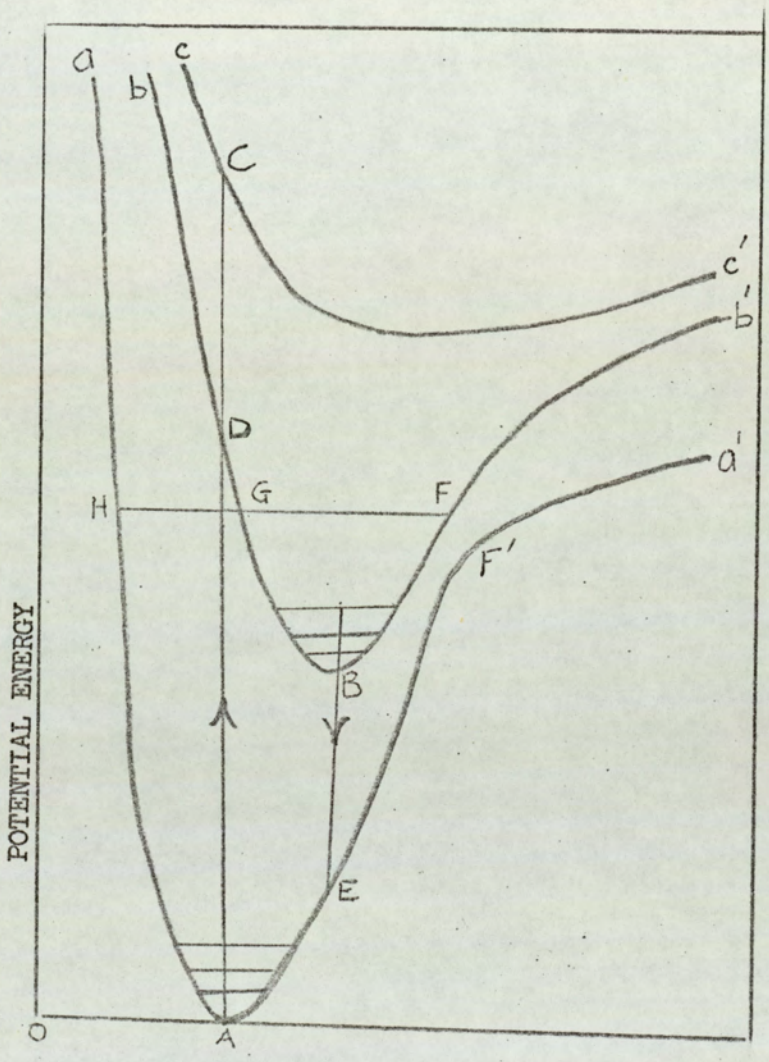

FIG.3.5 MOLECULAR POTENTIAL ENERGY DIAGRAM OF ORGANIC MOLECULE

3.4 contd.

3.4.3 contd.

distance (Fig.3.5). Normally the system is in ground state at A with low energy vibrational states shown by the short horizontal lines. Absorption of energy, for example by radiation raises the system to a higher excited state. This process is represented by a vertical line through A. If the absorbed energy is high the system reaches the point C, the atoms will move apart along cCc' and the molecule will dissociate. On the other hand if the energy of the radiation is less the system reaches the state D, and the molecules will be in the excited state represented by bBb'. Immediately after this transition the system is not in a state of minimum potential energy and so it moves from D to B, the excess vibrational energy being dissipated thermally to its neighbours. If the molecule is sufficiently stable it may return to the ground state by the emission of radiant energy corresponding to BE - The energy represented by BE is less than the energy represented by AD, which explains the action of wave shifters. The molecular mean life is of the order of 10^{-8} secs. so that it is important that the energy cannot be dissipated in

3.4 contd.

3.4.3 contd.

other ways. For efficient fluorescence the potential energy curves of the normal and excited electronic states should be well separated, so that the probability of transitions from B to the ground state, other than radiative transitions should be small.

3.5 Electronics of Counting System.

The photomultiplier tubes used were both EMI type 6097B with the venetian-blind dynode structure. This structure has a good efficiency for collecting photoelectrons because of its large effective surface area. The tubes were operated in the conventional manner with cathode at earth potential. Fig.3.6 is a diagram of the type of dynode chain of resistors used with each tube. The photomultiplier tubes were operated in the 1200 volt region which gave a potential drop approximately 90 volts per megohm. The high voltage supply to the photomultiplier tube was passed through an R-C filter in cascade (Fig.3.7) so as to attenuate any high frequency components that might be present. The output signal was fed into a preamplifier and then into a main amplifier and a scaler. The preamplifier used was

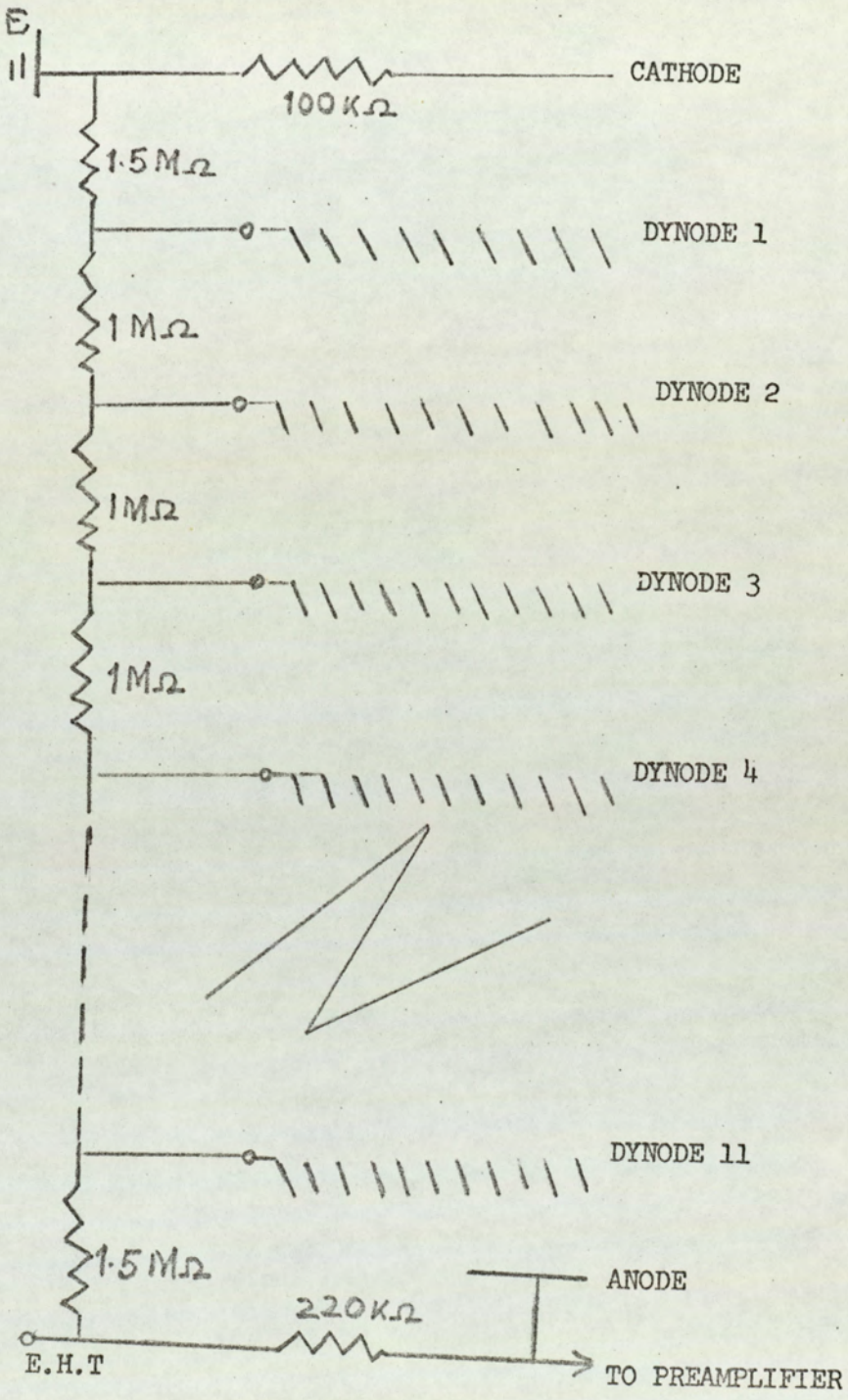

FIG. 3.6 DYNODE CHAIN OF RESISTORS

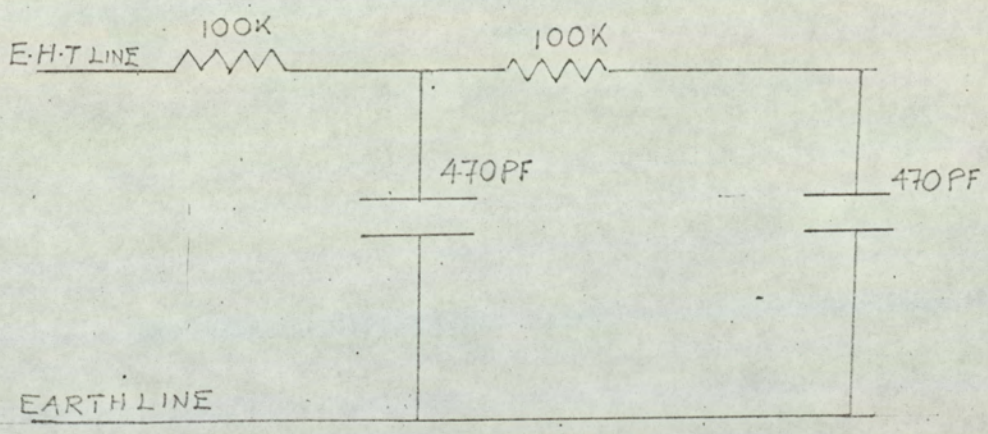

FIG 3.7 R-C FILTER

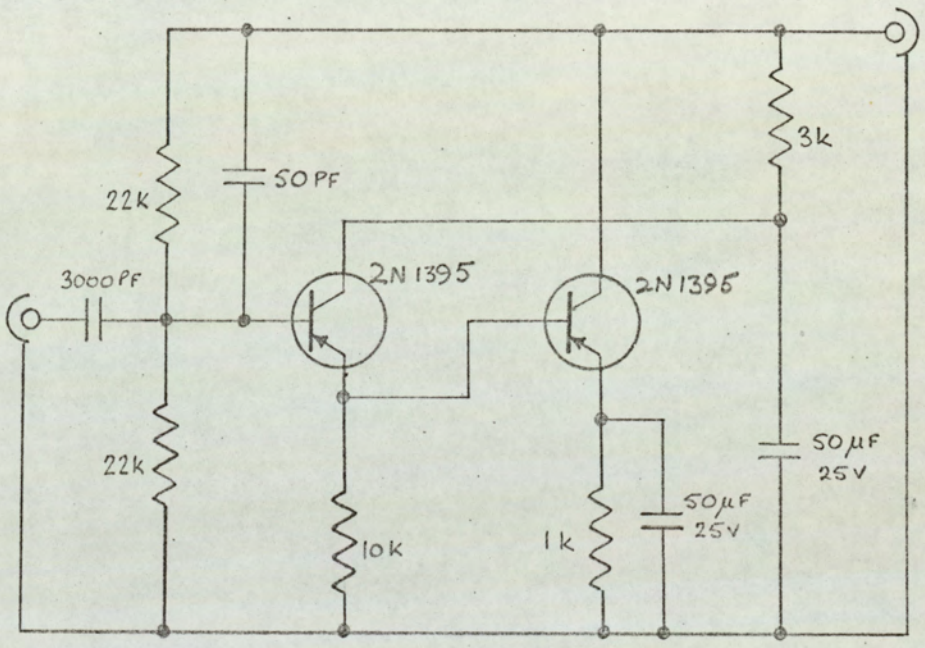

Fig. 3.8

"RIDL" TYPE CHARGE SENSITIVE PREAMPLIFIER

3.5 contd.

a charge-sensitive amplifier to a design by "RIDL". This type of amplifier provides an input signal proportional to the change and independent of the detector capacitance. A circuit diagram of the preamplifier is shown in Fig.3.8.

As the main function of the preamplifier is impedance matching to enable pulses to be conducted through connecting cables with minimum attenuation and reflection it was essential to have the preamplifier wired as close as possible to the photomultiplier tube. The photomultiplier, scintillator and circuitry were mounted as shown in Fig.3.9. The photomultiplier tube and scintillator with associated electronics were enclosed in a light free compartment constructed from brass. Coaxial connectors (type Plessey Mk IV), which are light tight in normal circumstances fed EHT and signal leads through the case. The main amplifier used was a modified form of the 1192A amplifier. A diagram of it is shown in Fig.3.10.

3.6 Foil Counting.

A block diagram of the counters and associated electronics used for the foil counting is given in Fig.3.11. a picture of the whole series of counting installation can also be seen in Fig.3.11. The circuitry of the timing/control

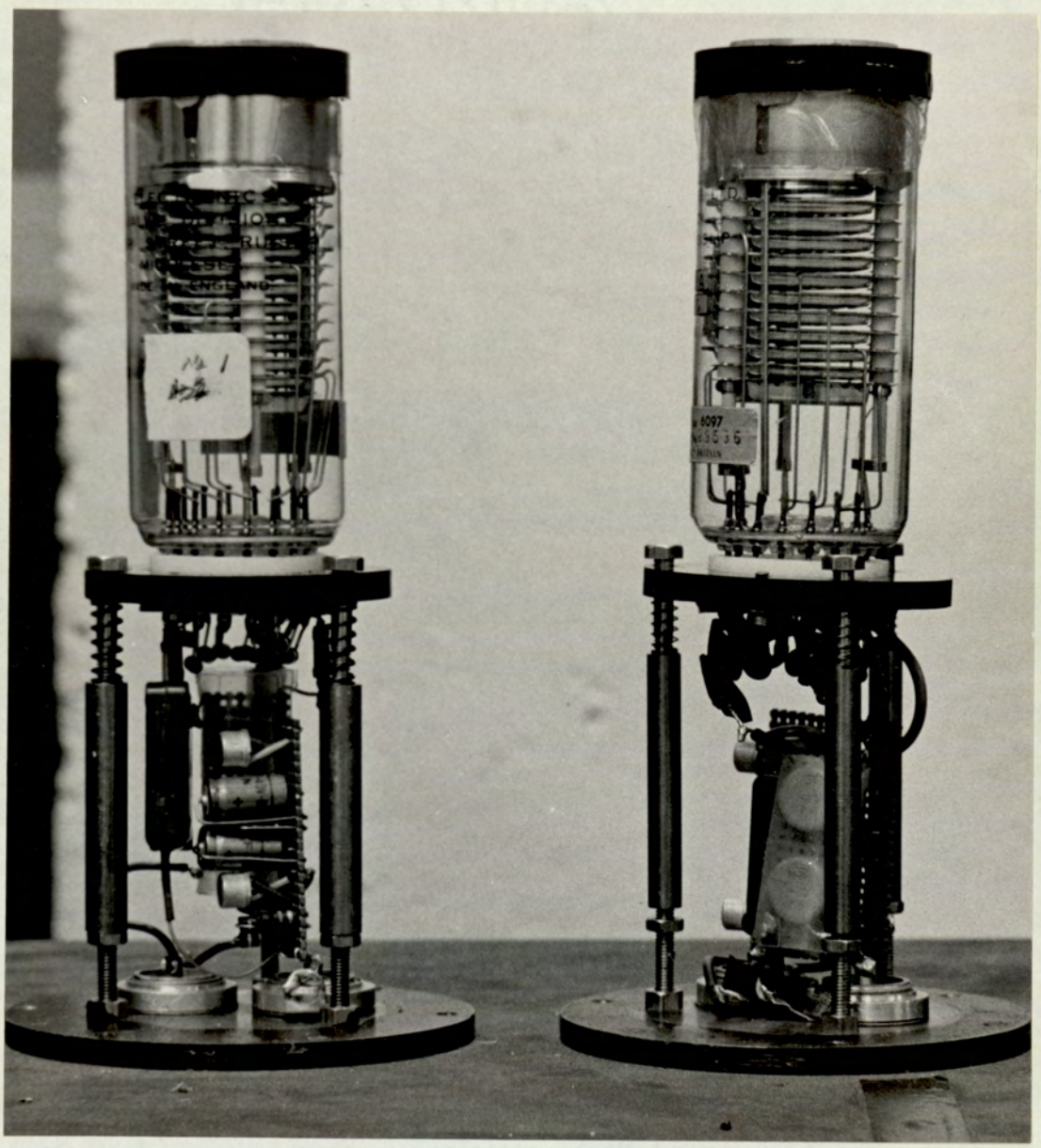

FIG. 39

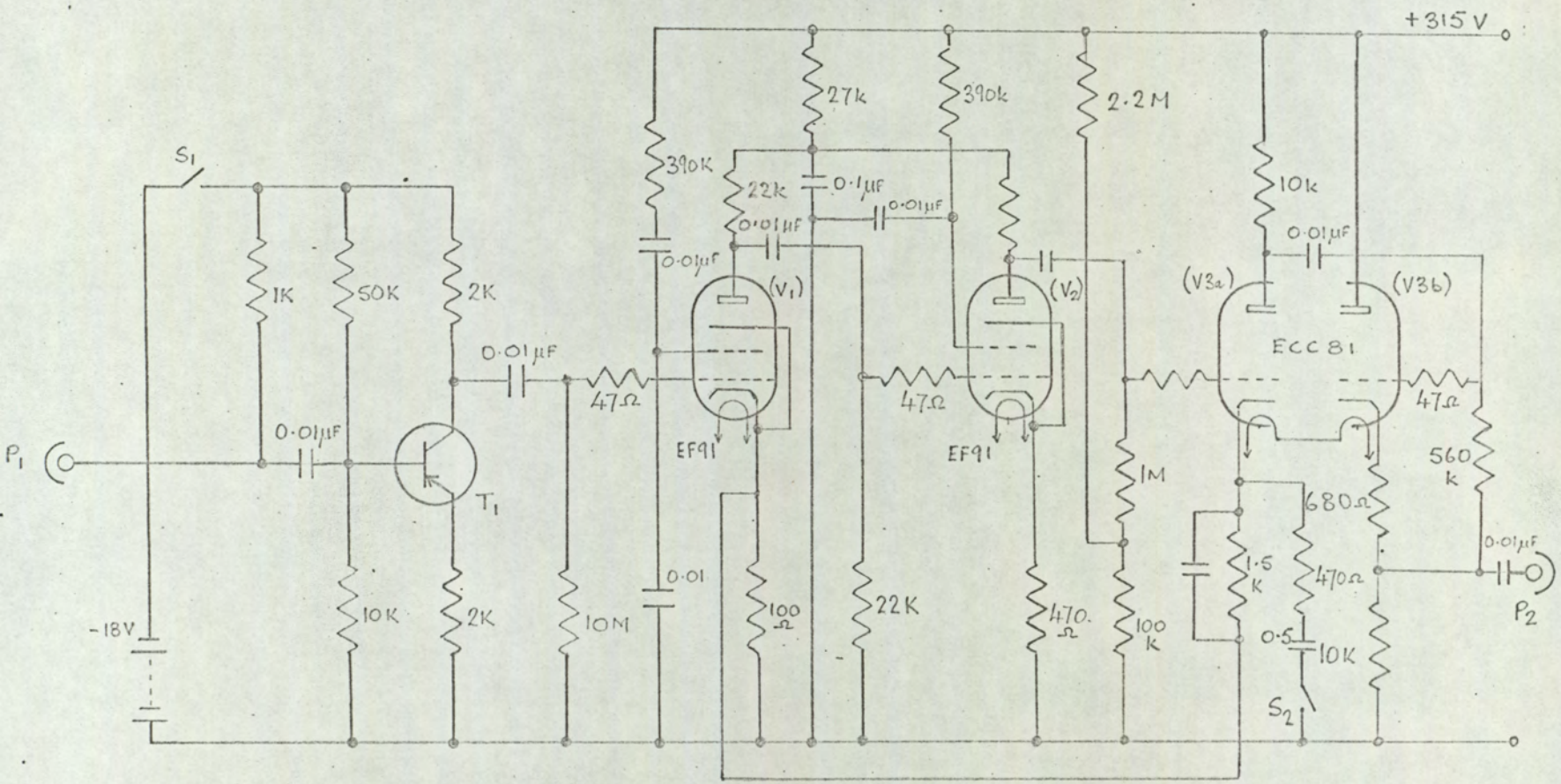

Fig. 3.10

MODIFIED 1192A AMPLIFIER FOR FOIL COUNTING EQUIPMENT

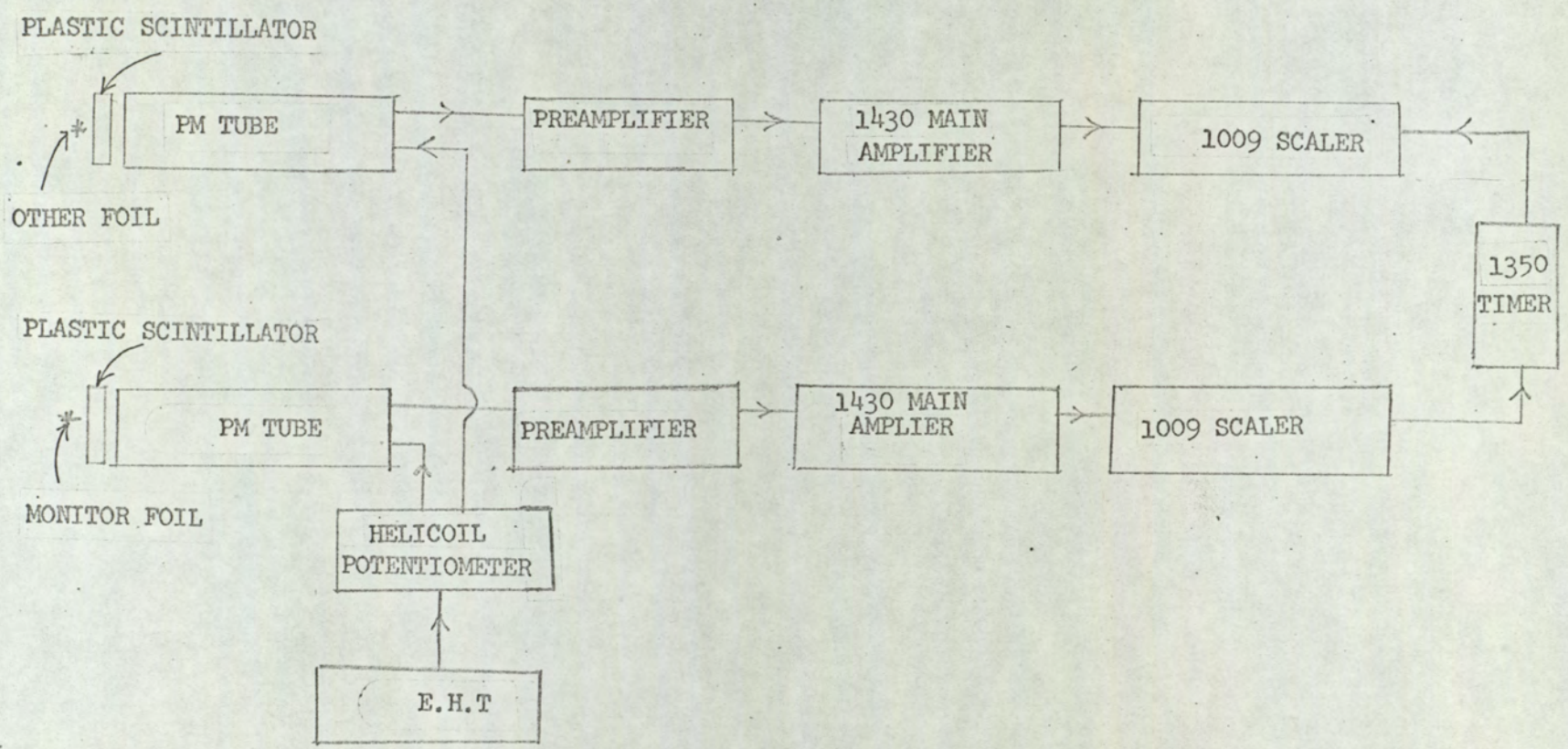

FIG 3.11 BLOCK DIAGRAM OF COUNTING SYSTEM

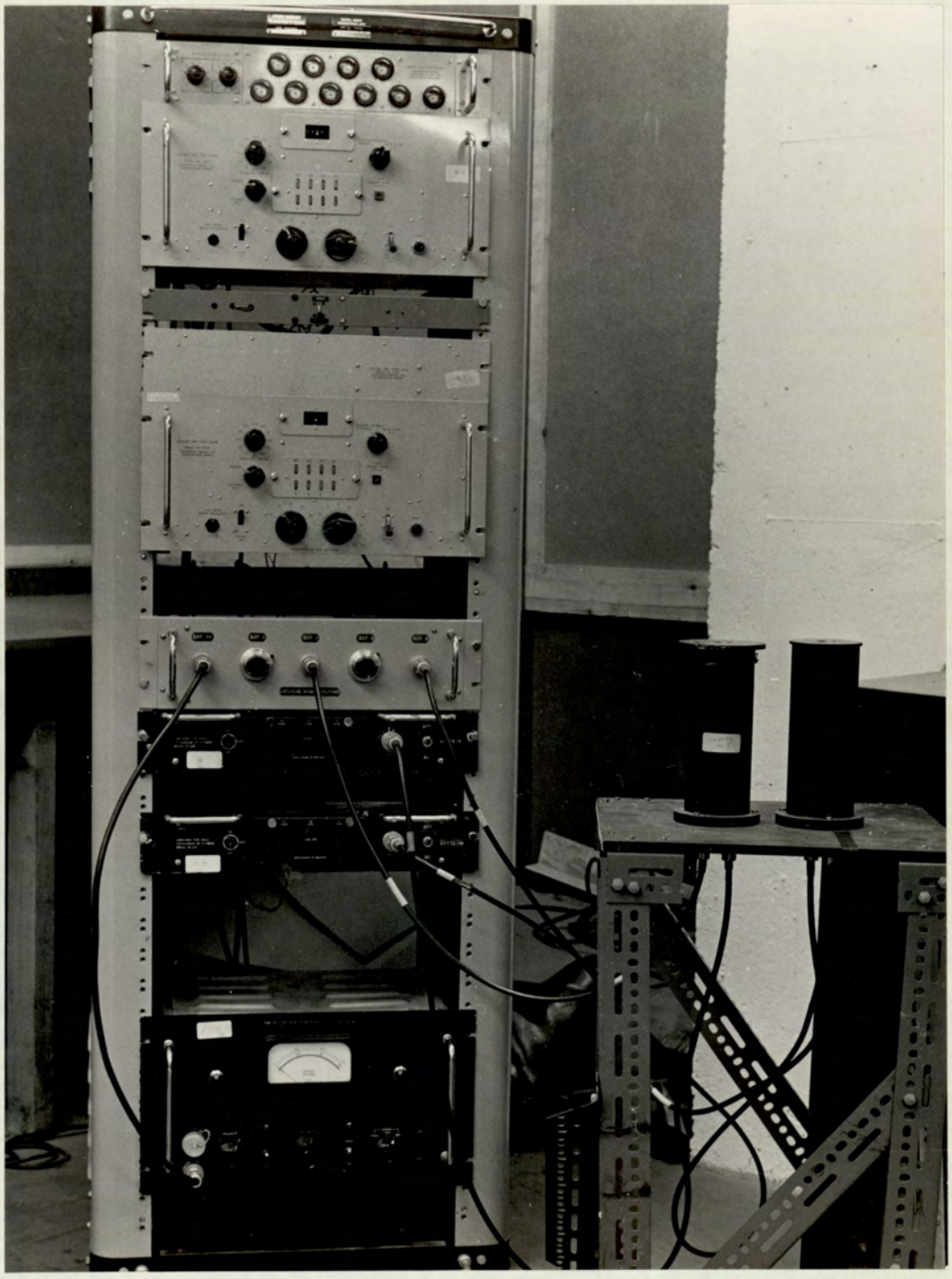

FIG. 3.12

3.6 contd.

unit (type 1340) was modified to operate the two scalers simultaneously.

3.6.1 Counter Suitability for β Detection.

In order to check the response of the scintillation counter to β particles, preliminary investigations with a standard Tℓ-204 β source had to be carried out with each of the counters in turn. For this the 400-Channel "RIDL" Pulse Height Analyser was used in conjunction with the scintillation counters. Thallium-204 emits β particles with a maximum energy of 0.77 Mev. A typical plot of the β spectrum from the Thallium-204 β source is shown in Fig.3.13.

Later some Indium foils were irradiated in the subcritical assembly using D-D neutrons source provided by the accelerator. A spectrum plot of the β particles produced during the decay of Indium-116 was made as before. Fig.3.14 gives a typical β spectrum from Indium-116 as obtained in these preliminary investigations. It can be seen from Fig.3.13 and Fig.3.14 that the shape of the spectra obtained are confirmation of the effectiveness of the plastic scintillation counters constructed for the detection of β particles and hence of their suitability for neutron flux measurements via the activation of Indium foils in the subcritical assembly.

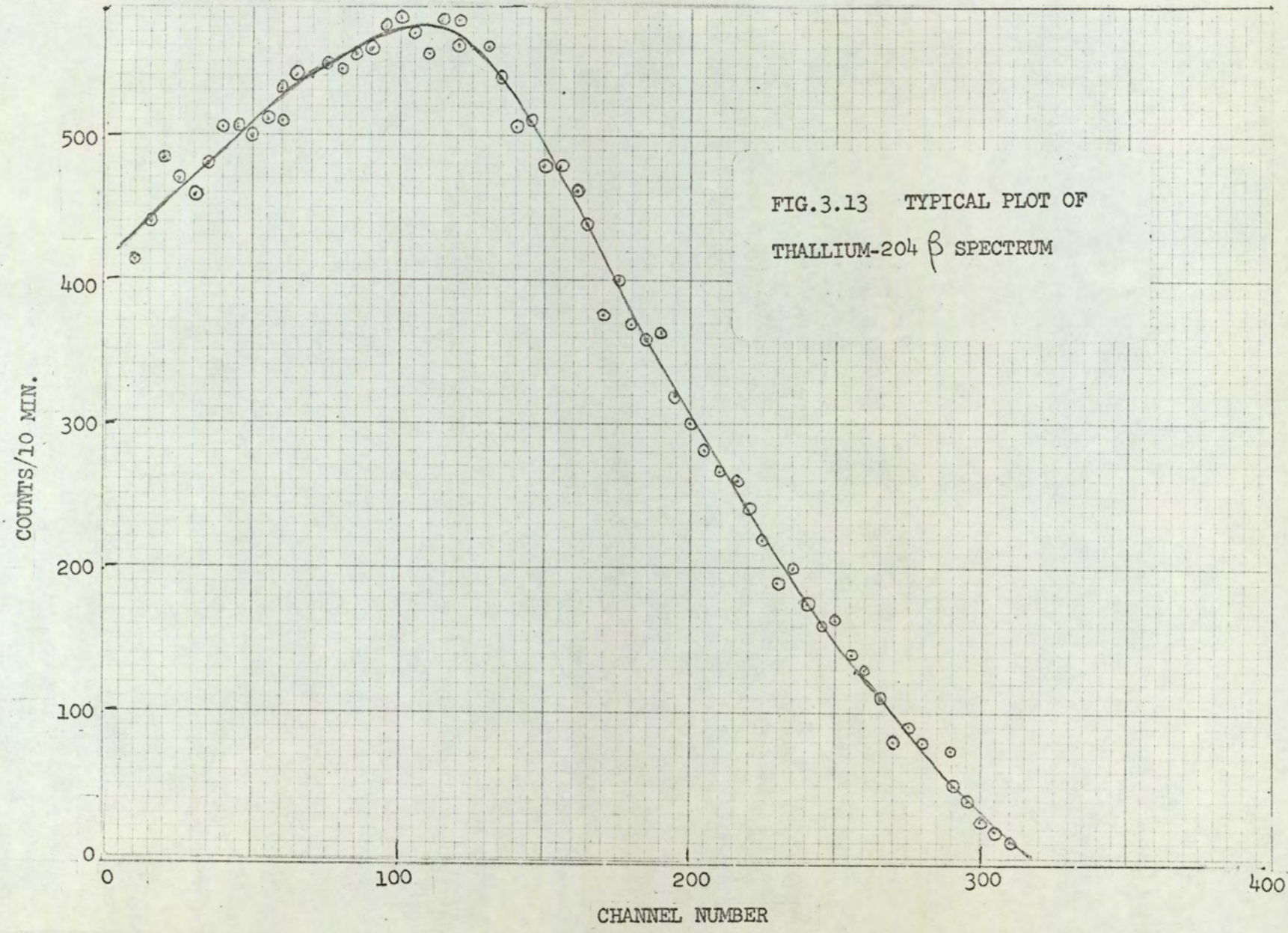

FIG.3.13 TYPICAL PLOT OF THALLIUM-204 β SPECTRUM

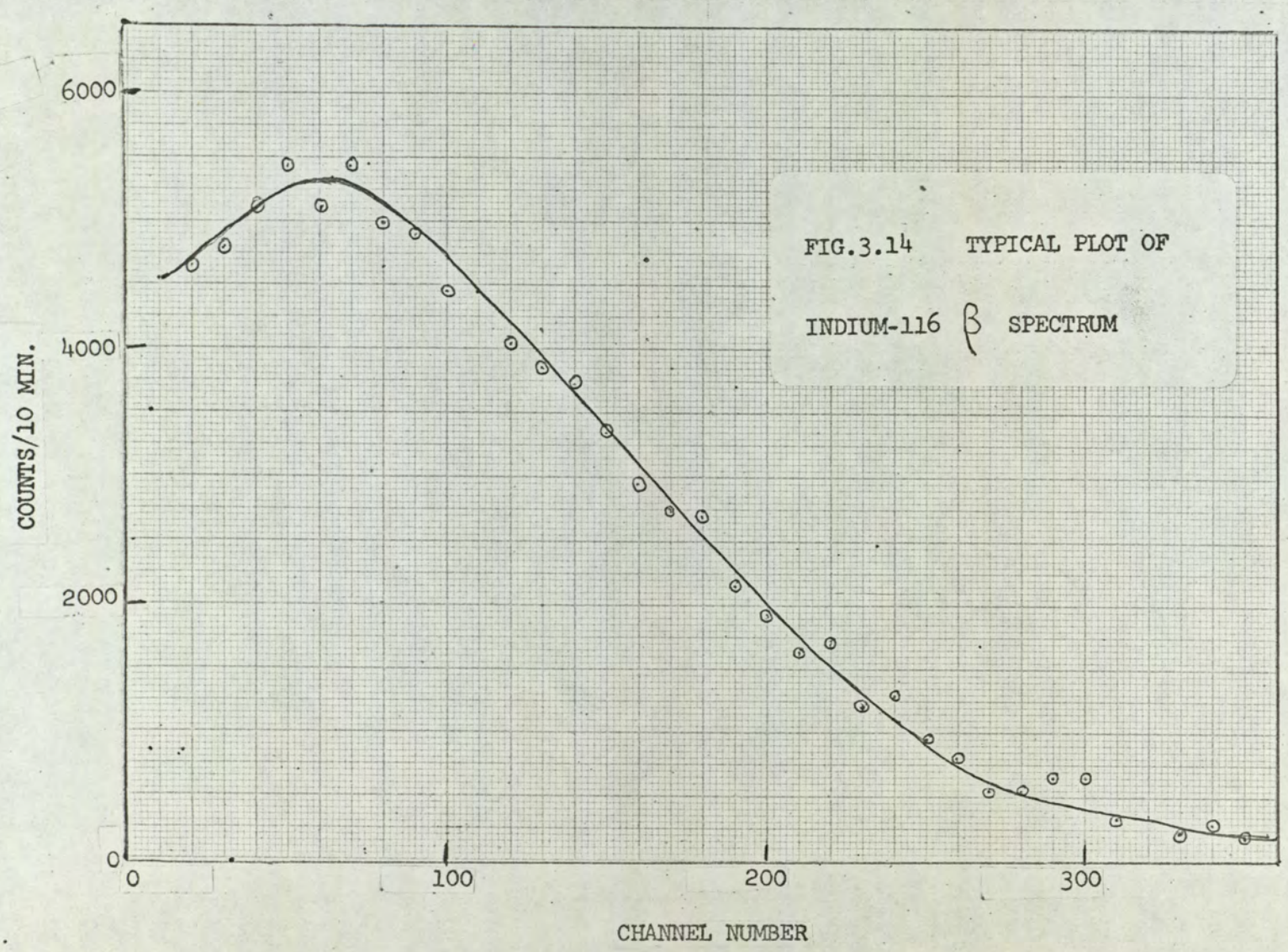

FIG.3.14 TYPICAL PLOT OF INDIUM-116 β SPECTRUM

3.7 Corrections in Foil Irradiations.

It was necessary to apply some corrections to the foil counting rates before using the data in the buckling calculations. The corrections were twofold:

(i) Background

(ii) Thermal flux depression -

This needs elaborating upon and more will be said about it in the next section.

In addition, since the foils used in the measurements were not all of the same mass the counting rates had to be normalized to unit mass of foil.

3.7.1 Thermal Flux Depression.

The problem of flux depression caused by the detecting foils is well reported on[17],[22],[23],[24],[25]. The necessary correction that must be made to the counting rate of a foil after irradiation to obtain a number proportional to the unperturbed flux is the result of two superimposed effects:

(i) Self-shielding of the internal layers of the foil by the outer layers. The correction factor shall be denoted by G where G is given by the following equation:[22]

$$G = \frac{1 - e^{-B}(1-B) - B^2 E_1(B)}{2B} \qquad 3.1$$

3.7 contd.

3.7.1 contd.

(i) contd.

where B is the foil thickness measured in mean free path units and $E_1(B)$ is the exponential integral defined by Equation 3.2

$$E_1(B) = \int_B^\infty \frac{e^{-y}}{y}\, dy \qquad 3.2$$

(ii) Outer flux depression - The flux in the neighbourhood of the foil is lowered owing to that fraction of available neutrons which are lost by absorption in the foil.

The correction factor is denoted by H. Tittle's[17] modification of Bothe's[22] original expression was used to determine H. This is given in Equation 3.3

$$H = \frac{1}{1 + \frac{\alpha}{2}\left(\frac{3}{2}\frac{R}{\lambda tr}\,\frac{L}{R+L} - 1\right)} \qquad 3.3$$

Equation 3.3 applies to the case when the radius R of the foil is greater than the transport mean free-path, λtr of the medium.

3.7 contd.

3.7.1 contd.

(ii) contd.

Here $\alpha = 1-e^{-B}(1-B) - B^2E_1(B)$

$$L^2 = \frac{\lambda tr\ \lambda a}{3}$$

λa = absorption mean free path in medium around foil, cm.

The flux depression factor, F is the ratio of the average flux measured by the detector to the unperturbed flux and is given by

$$F = GH \qquad 3.4$$

The foils were grouped according to weight and the flux depression factor, F determined for all of them. The results are shown in Table 3.1. The other foil parameters are given in Table A.3.1.

TABLE 3.1

Calculated Flux Depression Factor for Foils.

Foil No.	Flux Depression Factor, F	Foil No.	Flux Depression Factor, F
57	.865	65	.857
67	.864	22	.855
74	.866	14	.857
64	.864	38	.850
70	.864	1	.852
73	.864	4	.852
23	.860	5	.852
47	.860	61	.855
32	.860	62	.853
53	.864	60	.855
57	.860	15	.850
72	.860	17	.851
3	.860	36	.851
19	.861	39	.850
75	.860	48	.851
55	.860	12	.852
58	.860	41	.850
46	.855	45	.850
63	.860	52	.850
9	.857	20	.851
43	.855	35	.851
59	.858	49	.850
69	.857	71	.852
11	.860	68	.850

TABLE 3.1 (contd)

Foil No.	Flux Depression Factor, F	Foil No.	Flux Depression Factor, F.
66	.848	76	.837
27	.847	25	.834
40	.848	16	.833
10	.850	29	.830
21	.844		
50	.847		
51	.848		
33	.844		
34	.847		
30	.850		
18	.843		
6	.844		
2	.840		
7	.842		
26	.842		
37	.840		
13	.840		
44	.840		
8	.840		
31	.840		
56	.843		
24	.837		
28	.836		
42	.834		

3.7 contd.

3.7.2 Analysis of Experimental data.

This is best shown in the manner set out in Table 3.2.

TABLE 3.2

	Monitor Foil	Other Foil
Mass of foil	m_2	m_1
Flux Depression Factor	F_2	F_1
Number of counts including background	C_2	C_1
Background Counts	C_{b_2}	C_{b_1}
Counts correct for background	$C_2 - C_{b_2} = C_{t_2}$	$C_1 - C_{b_1} = C_{t_2}$
Counts per unit mass	C_{t_2}/m_2	C_{t_1}/m_1
Counts corrected for flux depression.	C_{t_2}/F_2	C_{t_1}/F_1
Counts per unit mass with depression correction	$\frac{C_{t_2}}{F_2 m_2} = K_2$	$\frac{C_{t_1}}{F_1 m_1} = K_1$

The activity A_i of each foil relative to the monitor foil will be given by

$$A_i = \frac{K_1}{K_2} \qquad 3.5$$

where $$K_1/K_2 = \frac{C_{t_1}}{F_1 m_1} \Big/ \frac{C_{t_2}}{F_2 m_2} \qquad 3.6$$

3.8 Error Assessment on Experimental Data.

The expression for determining the activity of each foil relative to the monitor foil is given by

3.8 contd.

$$\frac{K_1}{K_2} = \frac{C_{t_1}}{C_{t_2}} \times \frac{F_2 m_2}{F_1 m_1} \qquad \text{(Eqn.3.6)}$$

If we let $\delta\left(\frac{K_1}{K_2}\right)$ represent the error in K_1/K_2 then we can write:

$$\delta\left(\frac{K_1}{K_2}\right) = \frac{K_1}{K_2}\sqrt{\left(\frac{\delta K_1}{K_1}\right)^2 + \left(\frac{\delta K_2}{K_2}\right)^2} \qquad 3.7$$

where δK_1 = error in K_1

δK_2 = error in K_2

Referring to Table 3.2, K_1 and K_2 are defined as:

$$K_1 = \frac{C_{t_1}}{F_1 m_1} \qquad 3.8$$

$$K_2 = \frac{C_{t_2}}{F_2 m_2} \qquad 3.9$$

So that we can say that:

$$\frac{\delta K_1}{K_1} = \frac{\delta C_{t_1}}{C_{t_1}} + \frac{\delta F_1}{F_1} + \frac{\delta m_1}{m_2} \qquad 3.10$$

$$\frac{\delta K_2}{K_2} = \frac{\delta C_{t_2}}{C_{t_2}} + \frac{\delta F_2}{F_2} + \frac{\delta m_2}{m_2} \qquad 3.11$$

where δC_{t_1} = error in C_{t_1}

δm_1 = error in C_{t_2}

where δC_{t_1} = error in C_{t_1}

3.8 contd.

δm_1 = error in C_{t_2}

δF_1 = error in F_1

and likewise for δC_{t_1}, δF_2 and δm_2.

To a first approximation, $\frac{\delta F_1}{F_1}$ is assumed to arise mainly from the error in determining the thickness x_o of the foil. Now x_o is obtained via mass m and diameter D of the foil as is easily seen from the following relationship:

$$m = \frac{\pi D^2}{4} \rho x_o \qquad 3.12$$

where m = mass of foil, gm.

D = Diameter of foil, cm.

x_o = Thickness of foil, cm.

From equation 3.12 it can be seen that x_o varies as m/D^2 so that

$$\frac{\delta x_o}{x_o} = \frac{\delta m}{m} + \frac{2\delta D}{D} \qquad 3.13$$

where δx_o = error in x_o

δm = error in mass of foil

δD = error in diameter of foil.

The Oertling R.20 balance which was used for measuring mass of foil enabled measurements to be made to an accuracy of about 0.5%. The travelling microscope used for measuring the diameter also gave measurements to an accuracy of about 0.5%.

3.8 contd.

So that typically taking a foil of mass 0.0561 gm. and diameter 0.950 cm. we find

$$\frac{\delta x_o}{x_o} = \frac{.0003}{.0561} + \frac{2 \times .005}{.950}$$

which is about 1.5%.

1.5% change in x_o will hardly affect the flux depression factor so that $\frac{\delta F_1}{F_1}$ may be taken as zero. Considering $\frac{\delta F_1}{K_1}$ as a whole we find $\frac{\delta F_1}{F_1}$ is negligible. $\frac{\delta m_1}{m_1}$ is typically around 0.5% which may be neglected in comparison with $\frac{\delta C_{t_1}}{C_{t_1}}$.

From the foregoing $\frac{\delta K_1}{K_1}$ approximates to the following:-

$$\frac{\delta K_1}{K_1} = \frac{\delta C_{t_1}}{C_{t_1}} \qquad 3.14$$

This is also true for $\frac{\delta K_2}{K_2}$ for which we can say:

$$\frac{\delta K_2}{K_2} = \frac{\delta C_{t_2}}{C_{t_2}} \qquad 3.15$$

Combining equations 3.14 and 3.15 with equation 3.7 yields

$$\delta\left(\frac{K_1}{K_2}\right) = \frac{K_1}{K_2}\sqrt{\left(\frac{\delta C_{t_1}}{C_{t_1}}\right)^2 + \left(\frac{\delta C_{t_2}}{C_{t_2}}\right)^2} \qquad 3.16$$

Let us now consider the expression under the square root sign in equation 3.16. It can be shown that:

3.8 contd.

$$(\delta C_{t_1})^2 = C_1 + C_{b_1} \qquad 3.17$$

$$(\delta C_{t_2})^2 = C_2 + C_{b_2} \qquad 3.18$$

From Table 3.2 it can be seen that

$$C_{t_1} = C_1 - C_{b_1} \qquad 3.19$$

$$C_{t_2} = C_2 - C_{b_2} \qquad 3.20$$

Combining equations 3.16–3.20 yields:

$$\delta\left(\frac{K_1}{K_2}\right) = \frac{K_1}{K_2}\sqrt{\frac{C_1 + C_{b_1}}{(C_1 - C_{b_1})^2} + \frac{C_2 + C_{b_2}}{(C_2 - C_{b_2})^2}} \qquad 3.21$$

Equation 3.21 gives the expression for calculating the error in each flux measurement taken relative to the monitor foil.

CHAPTER 4.

MEASUREMENT OF MATERIAL BUCKLING

4.1 Introduction.

Material Buckling is a macroscopic parameter of prime importance to the reactor designer since it shows whether any core arrangement can become critical and also predicts critical size. Its measurement therefore constitutes one of the most useful experiments that may be undertaken in an exponential assembly. It is usually measured from differentiation of the thermal neutron flux distribution.

4.2 Theory.

For a nomogeneous multiplying medium in the form of a rectangular parallelepiped the appropriate form of the diffusion equation which describes the steady state flux distribution in the medium is:

$$\nabla^2\phi(x,y,z) + B_m^2\phi(x,y,z) = 0 \qquad 4.1$$

where B_m^2 is Material Buckling to be determined

ϕ = the flux in the medium.

The solution of Equation 4.1 may be written in this form following standard procedure[1],[26],[27],[28],[29]

$$\phi(x,y,z) = F(x)\,G(y)\,H(z) \qquad 4.2$$

Substitution of this equation into Equation 4.1 yields

$$\frac{F''(x)}{F(x)} + \frac{G''(y)}{G(y)} + \frac{H''(z)}{H(z)} = -B_m^2 \qquad 4.3$$

4.2 contd.

In order for this equation to be satisfied each term must be a constant independent of the variables x,y,z.

Let the constants be ω_1^2, ω_2^2 and K^2 then

$$\frac{F''(x)}{F(x)} = - \omega_1^2 \qquad 4.4$$

$$\frac{G''(y)}{G(y)} = - \omega_2^2 \qquad 4.5$$

$$\frac{H''(z)}{H(z)} = K^2 \qquad 4.6$$

where $B_m^2 = \omega_1^2 + \omega_2^2 - K^2$ 4.7

and K^2 is a positive number if the system is subcritical, which will be assumed in the following argument. The signs of the constants shown in Equations 4.4 - 4.6 have been chosen to satisfy the boundary conditions of the problem and the anticipated flux distribution in the assembly.

The geometry under consideration is a rectangular parallelepiped with source at one end as shown in Fig.4.1

4.2 contd.

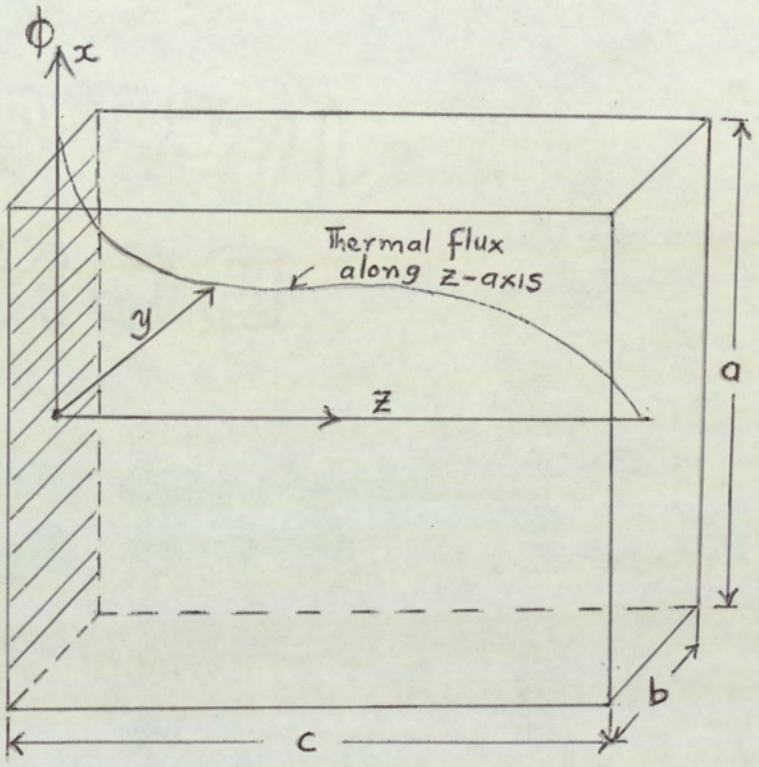

Fig.4.1 Exponential Pile

The boundary conditions are

(i) $\phi = \phi_o$, arbitrary flux level over whole surface plane z = o.

(ii) ϕ = o at planes $x = \pm a/2$, $y = \pm b/2$ z = c where extrapolated distances are included in dimensions.

It can be seen from Equation 4.7 that B_m^2 can be determined if ω_1^2, ω_2^2 and K^2 are known - This is the basis of the experimental measurement of the

4.2 contd.

material buckling B_m^2.

The general solution of Equation 4.1 which satisfies both the requirements of symmetry and conditions of slowing down density for the type of geometry under consideration here is:

$$\phi = A_{mn} \sum_{m=1}^{\infty} \sum_{n=1}^{\infty} \text{Cos}\frac{m\pi}{a}x \ \text{Cos}\frac{n\pi}{b}y \ \text{Sinh}\, K_{mn}(c-z) \qquad 4.8$$

where m, n are odd integers - Central source eliminates even harmonics. A_{mn} is a constant and a,b and c are as shown in Fig.4.1. If the z-dimension of the parallelepiped is long enough then the Sinh component of the flux may be approximated to a simple exponential and Equation 4.8 then becomes

$$\phi = A_{mn} \sum_{m=1}^{\infty} \sum_{n=1}^{\infty} \text{Cos}\frac{m\pi}{a}x \ \text{Cos}\frac{n\pi}{b}y \ e^{-K_{mn}z} \qquad 4.9$$

where A_{mn} now has half its previous value.

Equation 4.9 may be conveniently broken down into simpler expressions. Considering only the first and third harmonics:

$$\phi(x) = A \text{ Cos } \omega_1 x + B \text{ Cos}3 \ \omega_1 x \qquad 4.10$$

$$\phi(y) = A \text{ Cos } \omega_2 y + B \text{ Cos}3 \ \omega_2 y \qquad 4.11$$

4.2 contd.

$$\phi(z) = C \exp(-K_{11}z) - C' \exp(-K_{13}z) - C'' \exp(-K_{31}z) - C''' \exp(-K_{33}z) \quad 4.12$$

The parameters ω_1, ω_2 and K_{11} can be determined from some suitable experimental measurements thus leading to a value for B_m^2. It is to be noted that the other exponential terms will rapidly die out as the distance from the source plane increases and can be neglected except close to the source.

4.3 Experimental Method.

The experimental measurement of the buckling (B_m^2) was found from Indium foil measurements of the spatial thermal neutron flux distribution. Flux measurements were made along the three principal axes i.e. x, y and z of the rectangular assembly by the activation of Indium foils placed in perspex (methyl methacrylate) foil holders inserted between the fuel elements. The observed variation in foil activities after correction for background, flux depression and normalization to monitor foil counts were fitted by least squares computer programmes to the functions given in Equations 4.10-4.12. The details of the measurements and counting procedure are given in Chapter 3. There is one further comment however - During the irradiation process care was taken to ensure that all the foils in any

4.3 contd.

one measurement kept to the same geometry regarding the way they faced the axial flux gradient. The foils were fixed to the holders in such a way that the face with perspex backing was perpendicular to the axial flux gradient. The bare face of the Indium foil was therefore not in direct contact with the lassothene tape used for fixing the foils to the holder which would otherwise damage the foil.

Secondly, the error caused by the difference in activity of the two faces is minimized as the counting was done with the bare face of the foil resting against the scintillator.

4.4 Computer Programmes for Data Analysis.

Least squares fit computer programmes were written in Algol language for the Elliott 803 computer using the assumed flux distributions given in Equations 4.10-4.12. The details of the actual computer programmes identified as Programme P.1 and Programme P.2 have been given in Appendices 1 and 2 respectively. By using Programme P.1 the value of ω_1 could be determined when the input data related to horizontal flux measurements. When the input data related to vertical flux measurements then Programme

4.4 contd.

P.1 gave the value of ω_2. Programme P.2 which was written on the basis of an assumed exponential flux distribution enabled the value of K to be obtained. The value of K could also be obtained from the slope of the semilog plot of the axial flux distribution though the computer would naturally give a more accurate value.

From the values of ω_1 and ω_2 and K obtained from the experimental measurements and the computer calculations the value of the buckling, B_m^2 was calculated using Equation 4.7. Buckling measurements in the manner already described were carried out for various conditions of void in the subcritical assembly. The results were compared with theoretical predictions given in Chapter 5.

4.5 Analysis of Experimental Data.

4.5.1 General Comments.

As has been pointed out earlier, B_m^2 was derived on the basis of a least squares fit computer programme of activation data. The general method adopted for the analysis of foil activities has already been given in Chapter 3. There is, however, one further correction to apply. This is a correction to account for the distortion of the flux in the

4.5 contd.

4.5.1 contd.

vertical direction (y-direction) arising out of the reflection of neutrons from the plinth of concrete at the base of the subcritical assembly. This distortion had the apparent effect of shifting the origin from the mid x-y plane to a point a little further down the bottom of the core. The origin was therefore adjusted to give the best fit.

It is to be noted that there was water in an overhead tank to provide shielding for the top of the assembly. In view of this one would expect that reflection from this water would tend to counter-balance the effect of reflection from the lower plinth of concrete. Perhaps this was so though it did not appear to be enough to completely cancel out the effect due to the concrete at the base of the tank. There was cadmium in the base of the lid tank which would absorb some of the thermal neutrons and so minimize the effect of the reflection from the top. Also the presence of about 4 in. of air gap between the lid tank and the top of the core would contribute towards minimizing the effect of this reflection.

4.5.2 Cosine Flux Fitting.

Apart from giving values of ω_1 and ω_2 computer

4.5 contd.

4.5.2 contd.

programme P.1 gave the other relevant constants so that the fitted cosine flux distribution of the type $\phi_{(x)} = A\,\mathrm{Cos}\omega_1 x + B\,\mathrm{Cos}3\omega_1 x$ could be written more exactly since the constants A,B and ω_1 were known. The points for the graph were calculated and the graphs plotted to show the comparison between the calculated and the experimental points. (Figs.4.3.1-4.4.4).

4.6 Error Assessment.

As given in Equation 4.7, B_m^2 is calculated from the following:

$$B_m^2 = \omega_1^2 + \omega_2^2 - K^2$$

If $\delta\omega_1^2$ = error in ω_1^2

$\delta\omega_2^2$ = error in ω_2^2

δK^2 = error in K^2

δB_m^2 = error in B_m^2

Then it can be shown that

$$\delta B_m^2 = \sqrt{(\delta\omega_1)^2 + (\delta\omega_2)^2 + (\delta K^2)^2} \qquad 4.13$$

The values of ω_1^2 and ω_2^2 and K^2 used in the computation of B_m^2 were the means of several

4.6 contd.

readings. Assume, for example, that n values of ω_1 were obtained from n separate flux measurements. This will yield n separate values of ω_1^2. The mean of all these ω_1^2 values is $\overline{\omega_1^2}$ where $\overline{\omega_1^2}$ is defined by Equation 4.14:

$$\overline{\omega_1^2} = \frac{1}{n} \sum_{i=1}^{n} \omega_{1i}^2 \qquad 4.14$$

The standard deviation on all the different ω_1^2 values is σ_R where σ_R is given by:

$$\sigma_R = \sqrt{\frac{\sum_{i=1}^{n} d_i^2}{n-1}} \qquad 4.15$$

and $$d_i^2 = \overline{\omega_1^2} - \omega_{1i}^2 \qquad 4.16$$

The standard error on the mean is σ_m where σ_m is given by:

$$\sigma_m = \frac{\sigma_R}{\sqrt{n}} \qquad 4.17$$

The value of σ_m as calculated from Equation 4.17 gives the error on $\overline{\omega_1^2}$ i.e. $\overline{\delta\omega_1^2}$.

The errors in $\overline{\omega_2^2}$ and $\overline{K_2^2}$ are then worked out in the manner described for $\overline{\omega_1^2}$.

Knowing $\overline{\delta\omega_1^2}$, $\overline{\delta\omega_2^2}$ and $\overline{\delta K^2}$ the error on the buckling i.e. $\overline{\delta B_m^2}$ can be evaluated by using equation

4.6 contd.

similar to Equation 4.13.

4.7 Experimental Results.

Tables 4.1.1, 4.1.2 and 4.1.3 list the values of ω_1^2, ω_2^2 and K^2 obtained from several flux measurements when there were no bubbles in the assembly, i.e. condition of zero per cent void fraction. Tables 4.2.1, 4.2.2 and 4.2.3 list the corresponding values for 2.5% void fraction in the core of the assembly. The corresponding values for 6.1% void fraction are listed in Tables 4.3.1, 4.3.2 and 4.3.3 while Tables 4.4.1, 4.4.2 and 4.4.3 list the values for 9.1% void fraction. The values of B_m^2 measured for various void fractions are given in Table 4.5. The values of $\overline{\omega_1^2}$, $\overline{\omega_2^2}$ and $\overline{K^2}$ for the various void fractions are also given in this table.

The variation of B_m^2 with void fraction is shown in Fig.4.2. Both the experimental and calculated graphs are given. Typical fitted cosine flux curves for various void fractions with experimental points are shown in Fig.4.3.1 through 4.4.4. Figs.4.5.1-4.5.4 show semilog plots of the axial flux for various void fractions.

The variation of relaxation length with void fraction is given in Fig.4.6.

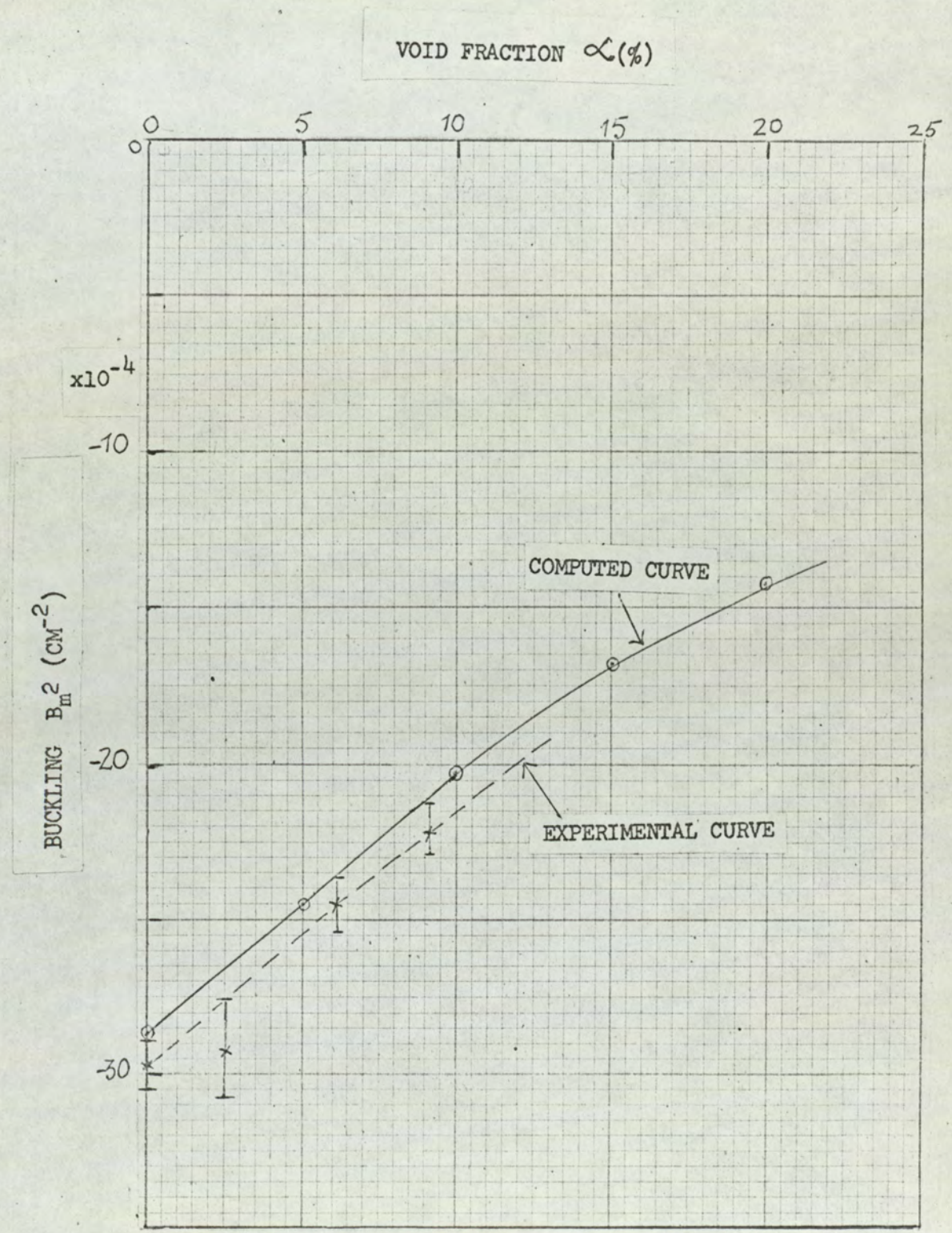

FIG.4.2 VARIATION OF BUCKLING WITH VOID FRACTION

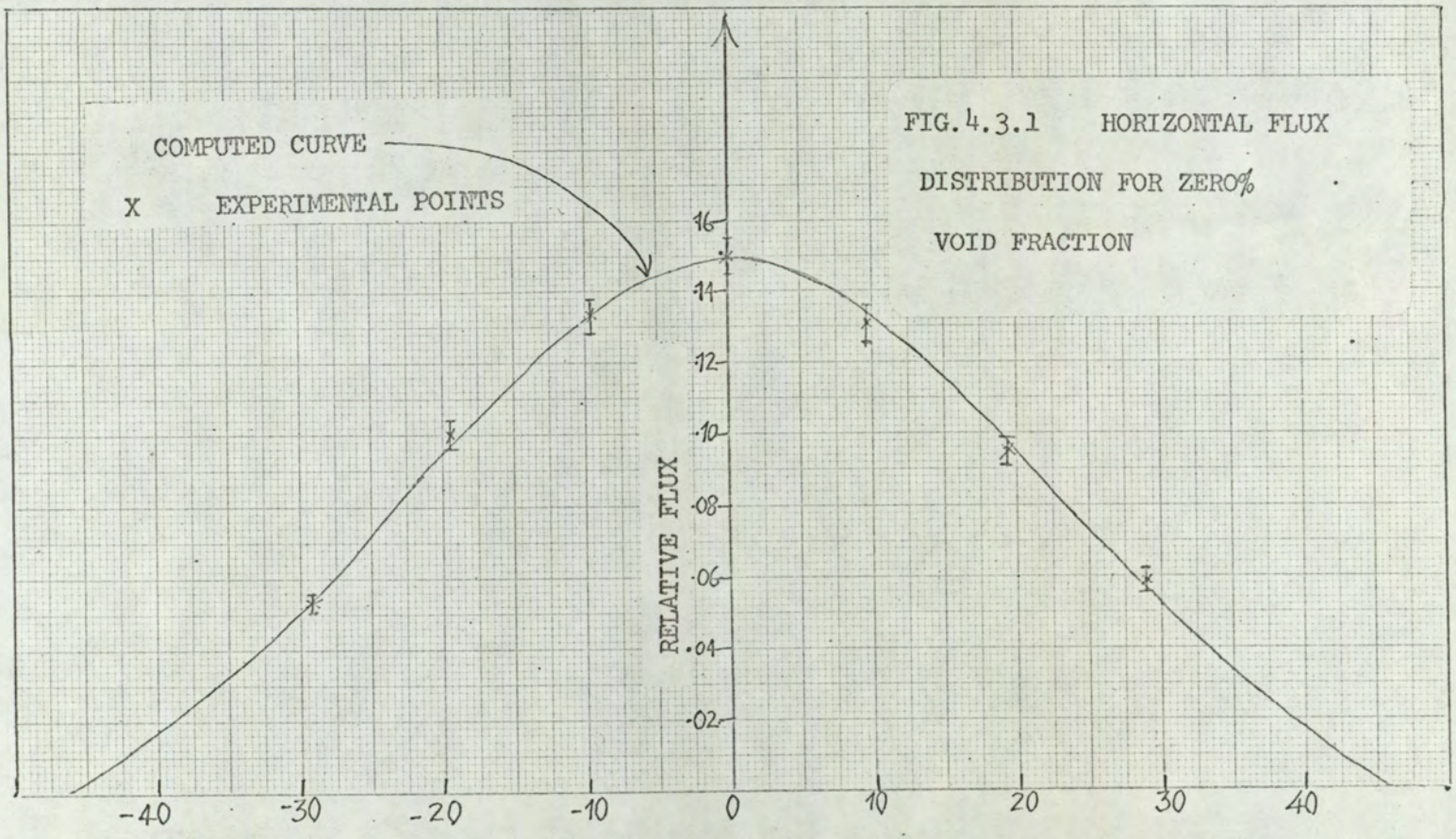

FIG. 4.3.1 HORIZONTAL FLUX DISTRIBUTION FOR ZERO% VOID FRACTION

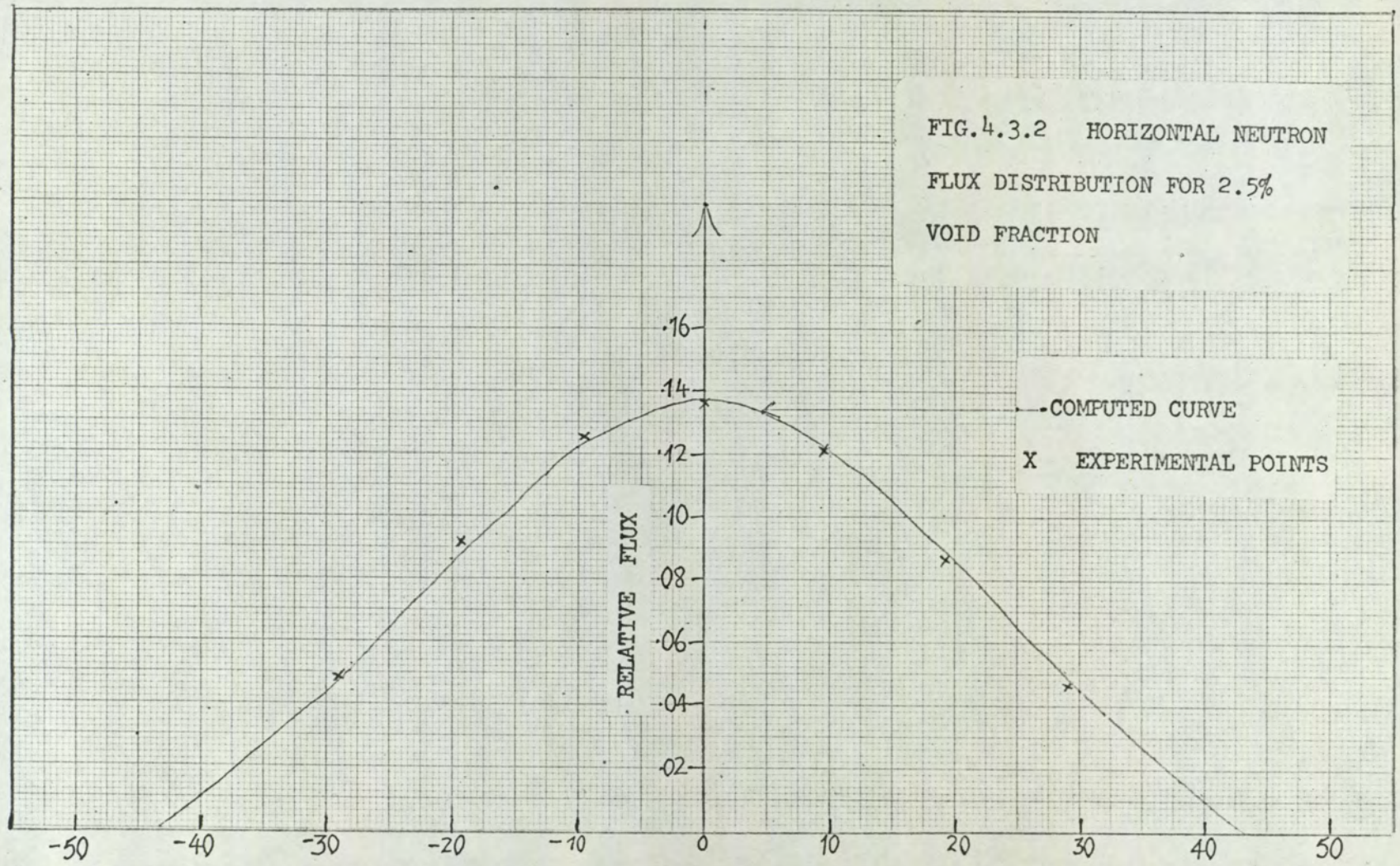
FIG.4.3.2 HORIZONTAL NEUTRON FLUX DISTRIBUTION FOR 2.5% VOID FRACTION
COMPUTED CURVE
X EXPERIMENTAL POINTS
RELATIVE FLUX
·16
·14
·12
·10
·08
·06
·04
·02
-50
-40
-30
-20
-10
0
10
20
30
40
50
DISTANCE FROM CENTRE OF CORE (CMS.)

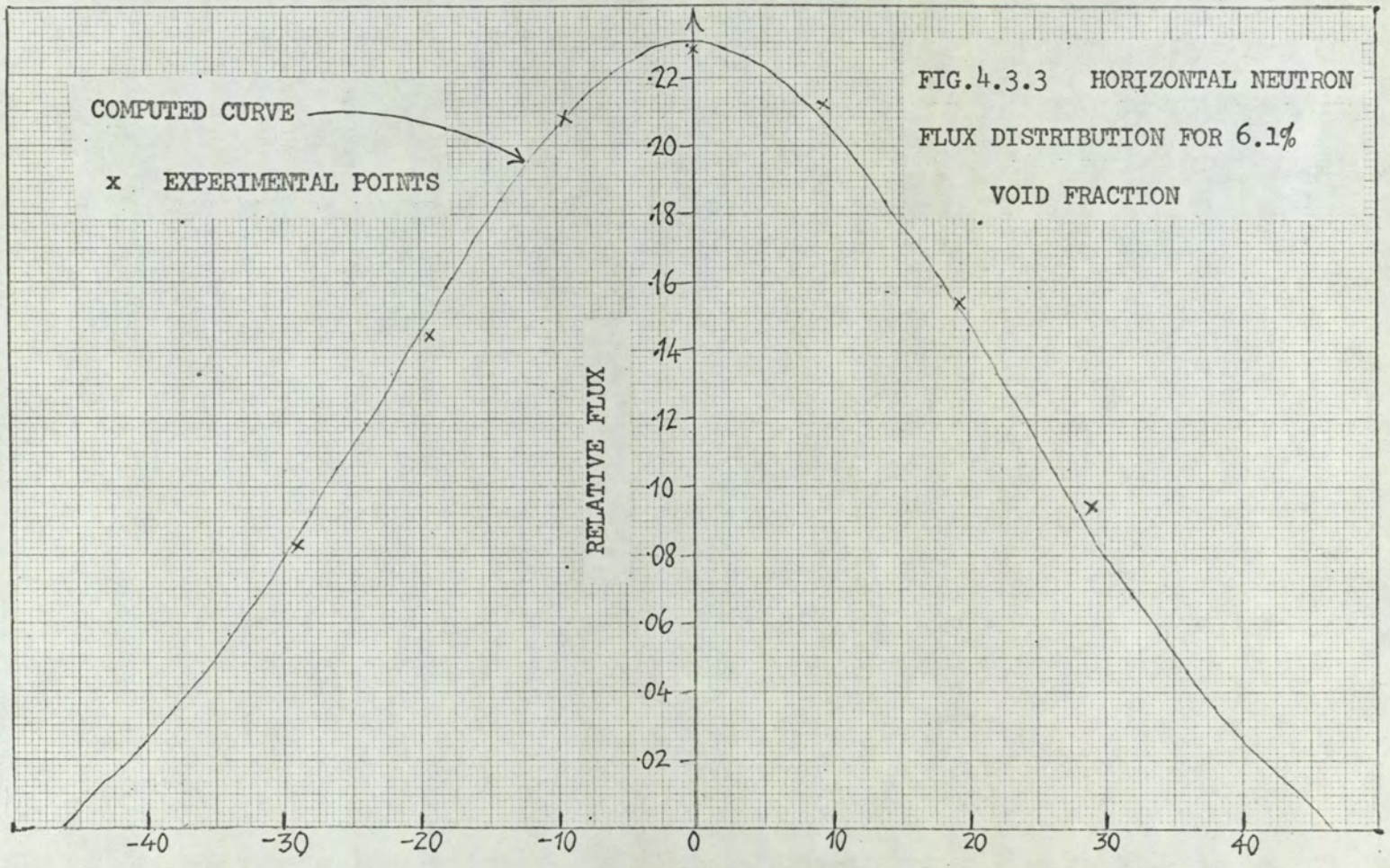

FIG.4.3.3 HORIZONTAL NEUTRON FLUX DISTRIBUTION FOR 6.1% VOID FRACTION

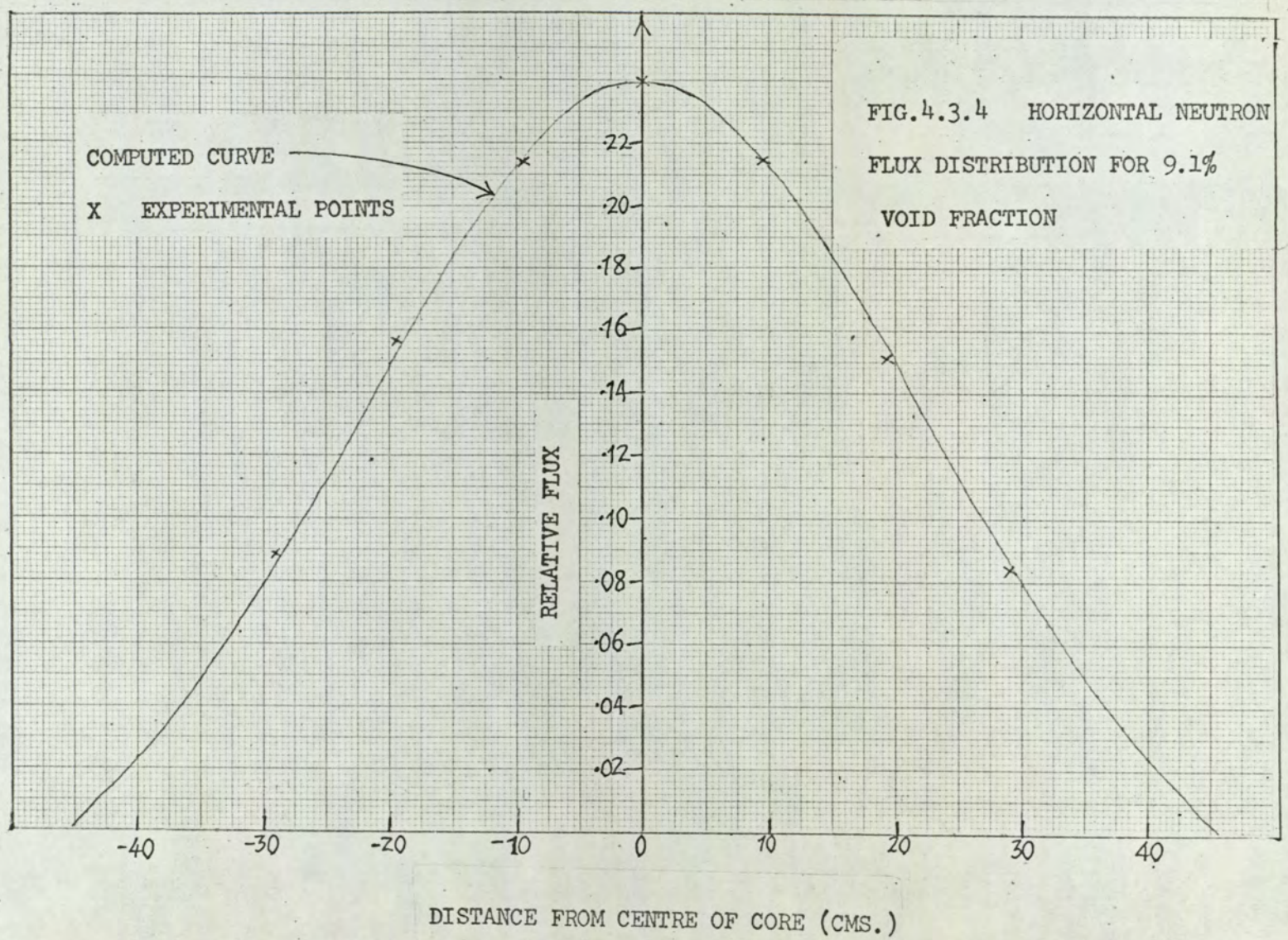

FIG.4.3.4 HORIZONTAL NEUTRON FLUX DISTRIBUTION FOR 9.1% VOID FRACTION

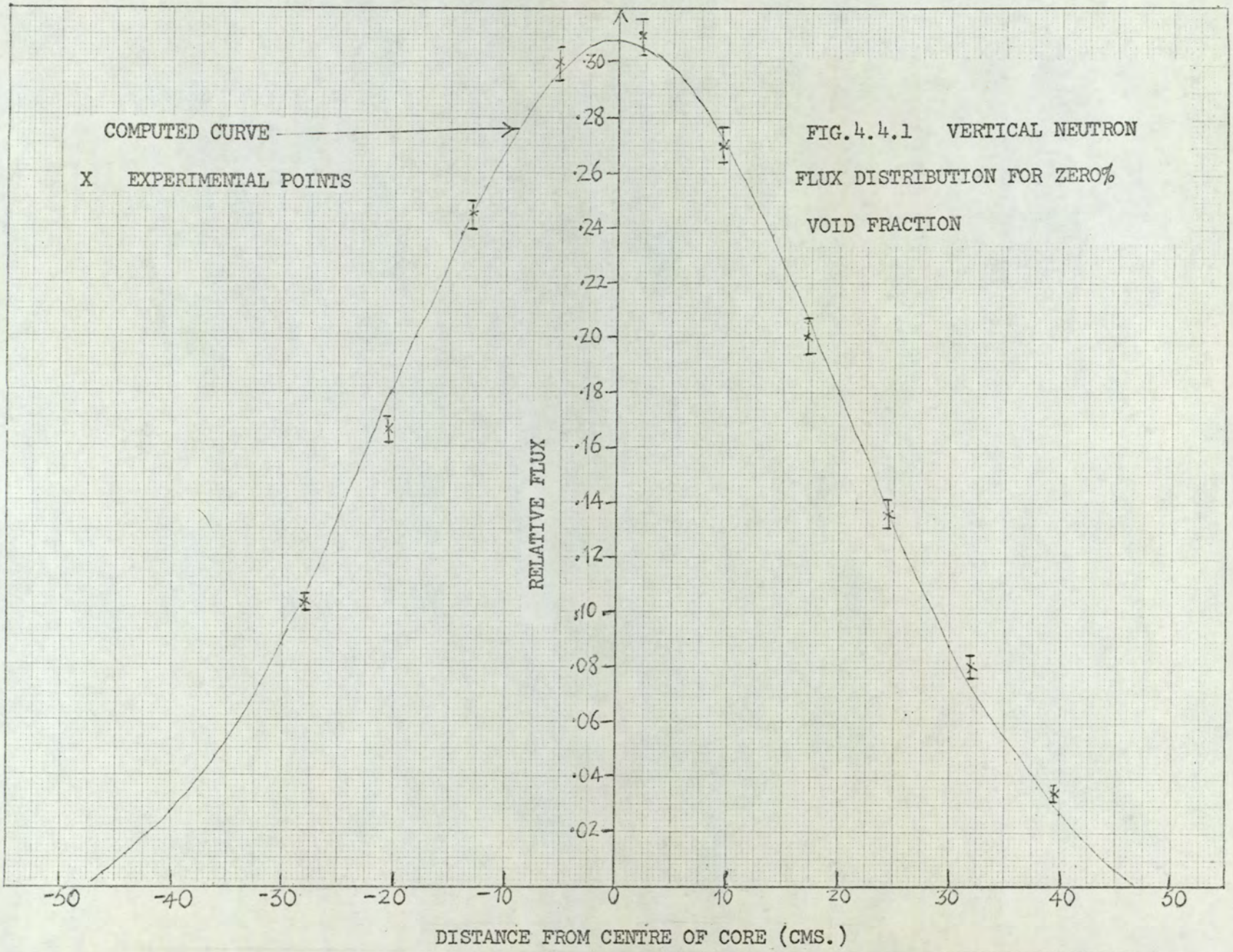

FIG.4.4.1 VERTICAL NEUTRON FLUX DISTRIBUTION FOR ZERO% VOID FRACTION

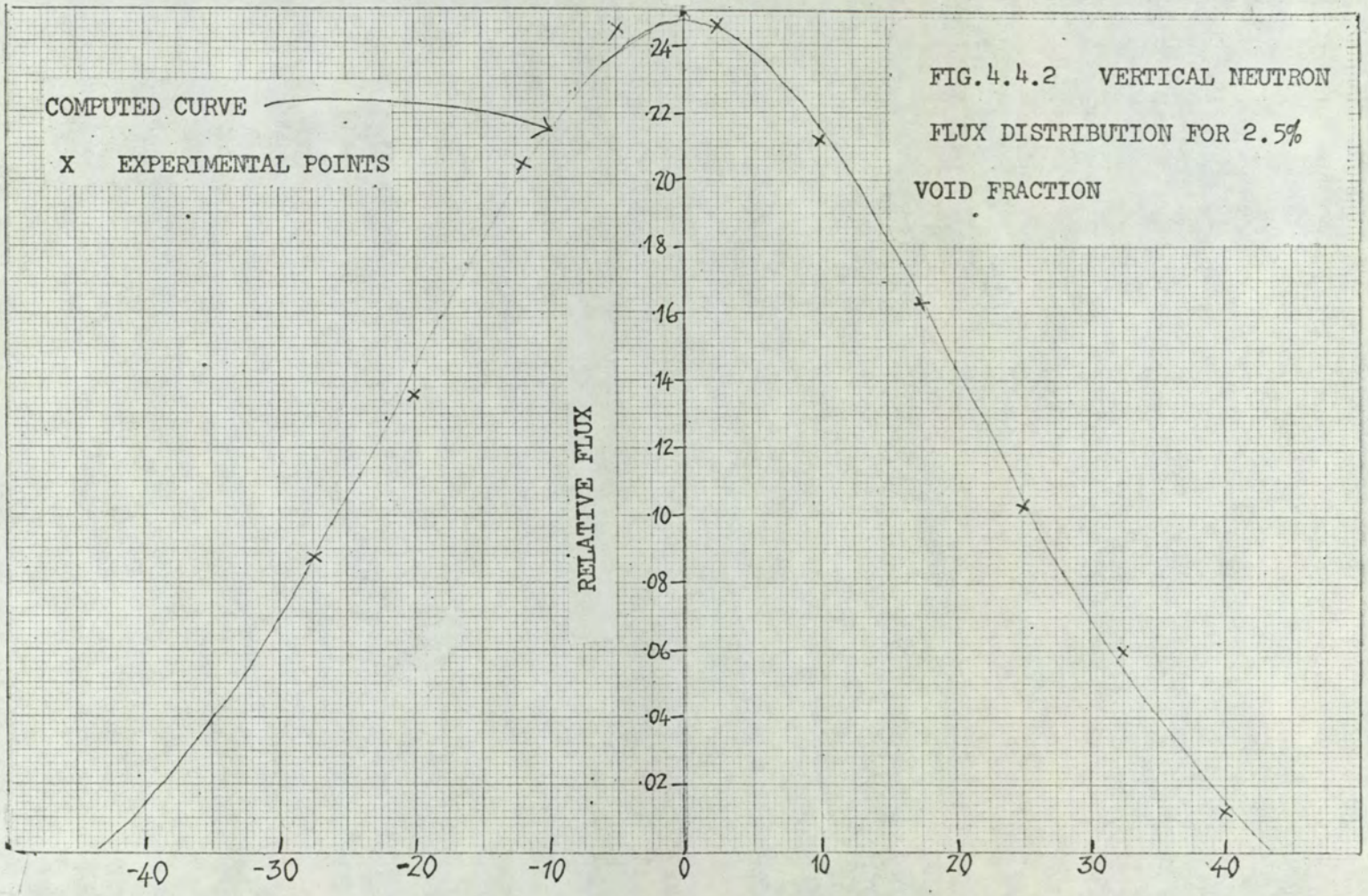

FIG.4.4.2 VERTICAL NEUTRON FLUX DISTRIBUTION FOR 2.5% VOID FRACTION

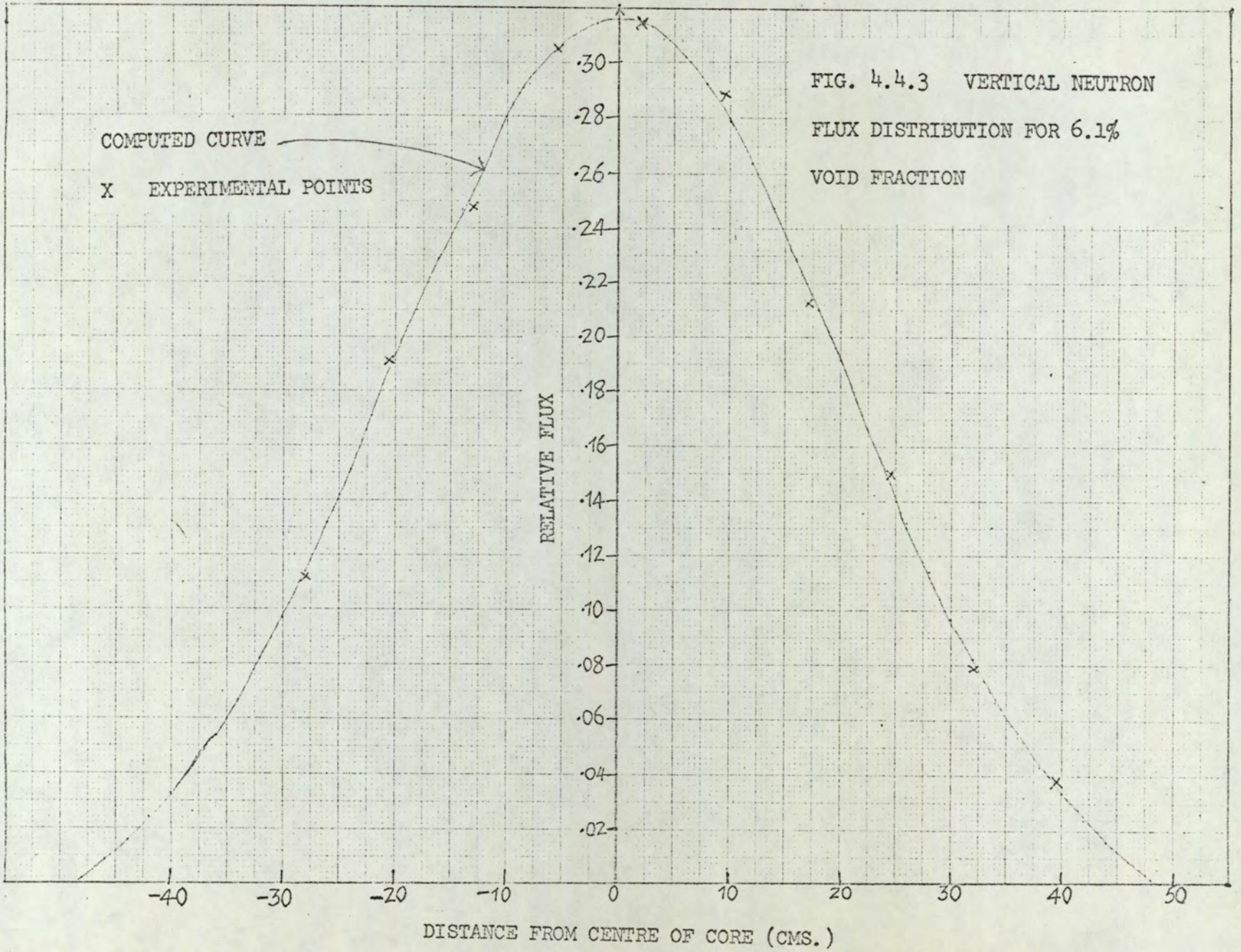

FIG. 4.4.3 VERTICAL NEUTRON FLUX DISTRIBUTION FOR 6.1% VOID FRACTION

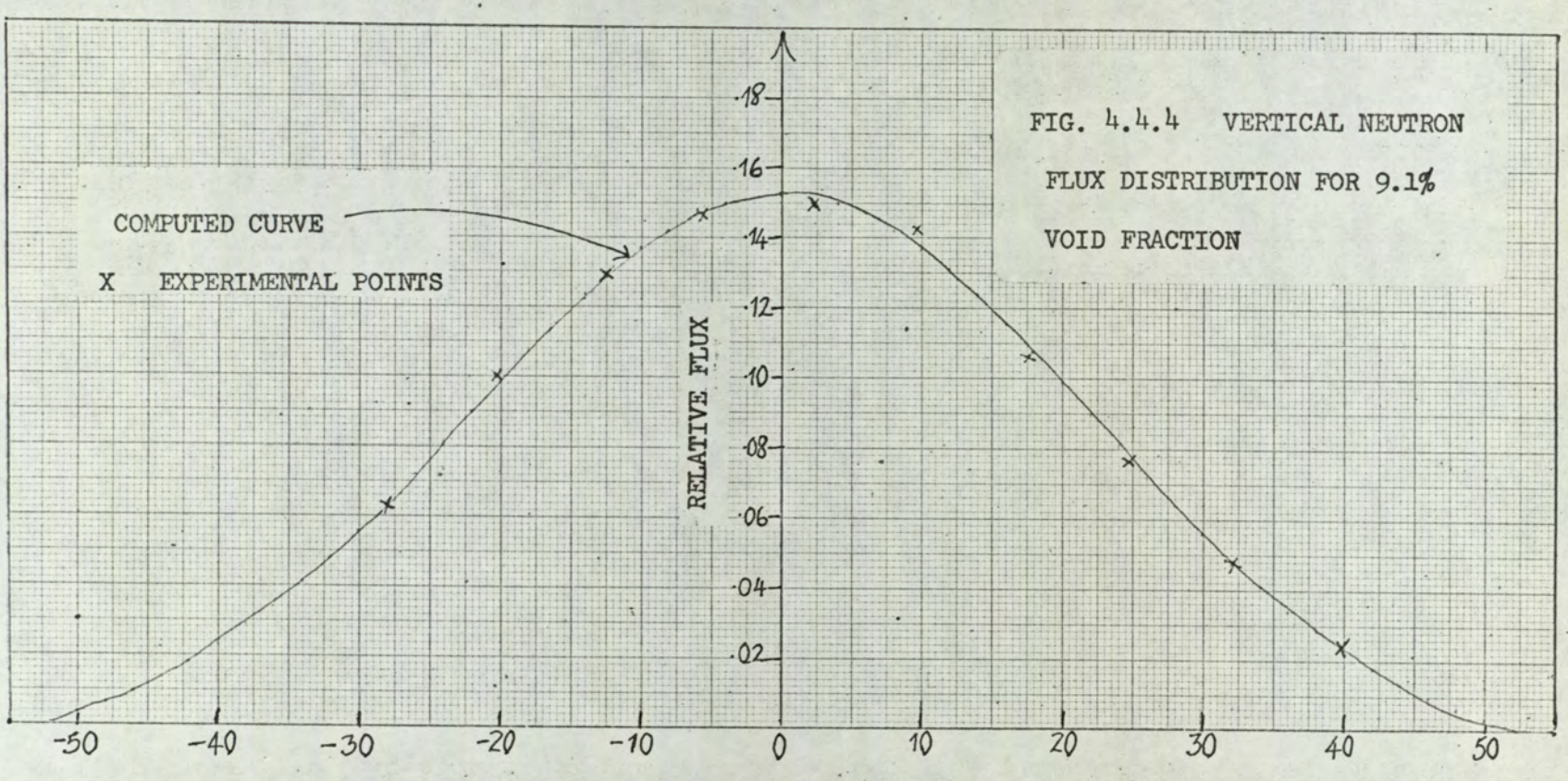

FIG. 4.4.4 VERTICAL NEUTRON FLUX DISTRIBUTION FOR 9.1% VOID FRACTION

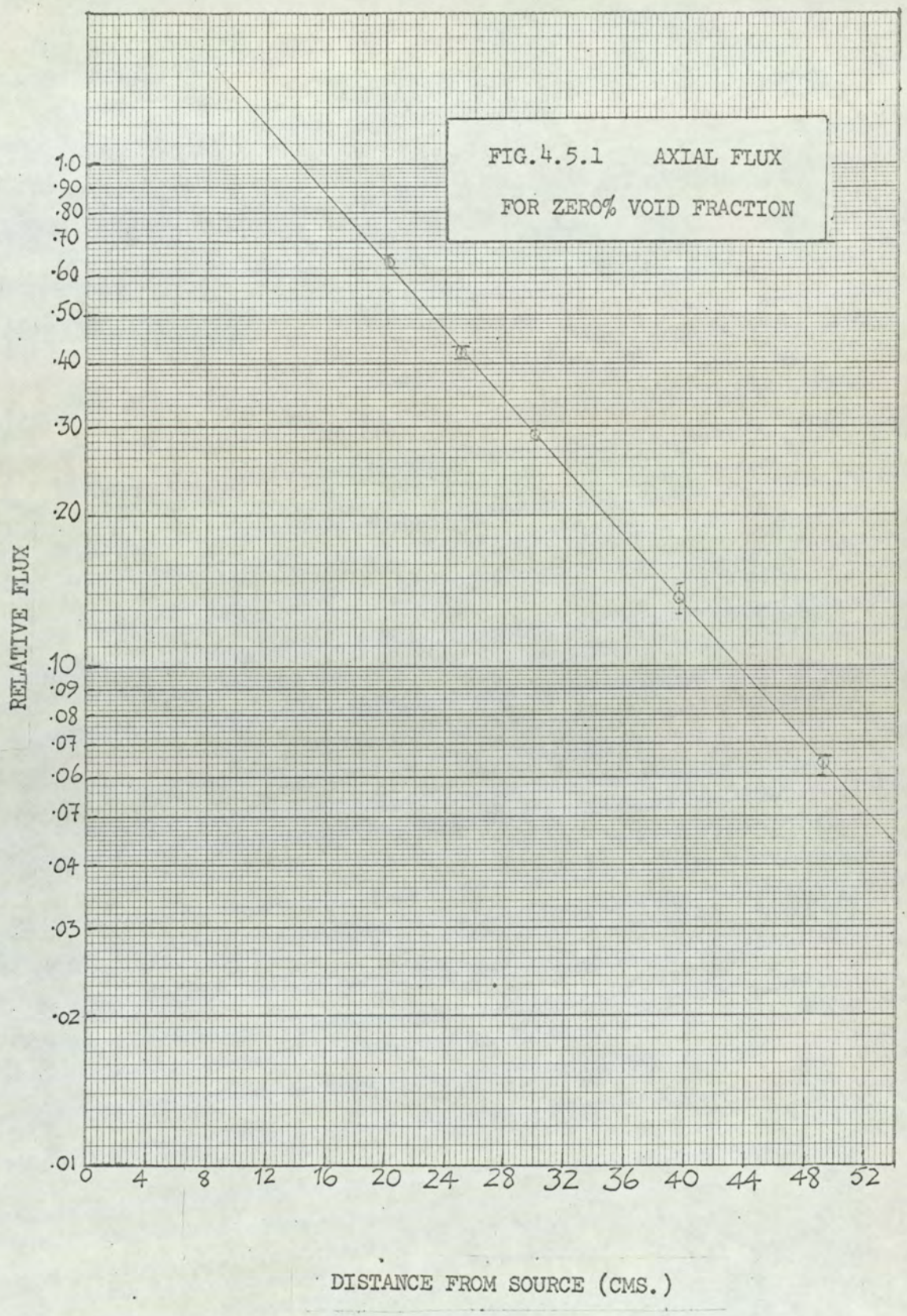
FIG.4.5.1 AXIAL FLUX
FOR ZERO% VOID FRACTION
RELATIVE FLUX
1·0
·90
·80
·70
·60
·50
·40
·30
·20
·10
·09
·08
·07
·06
·07
·04
·03
·02
·01
0
4
8
12
16
20
24
28
32
36
40
44
48
52
DISTANCE FROM SOURCE (CMS.)

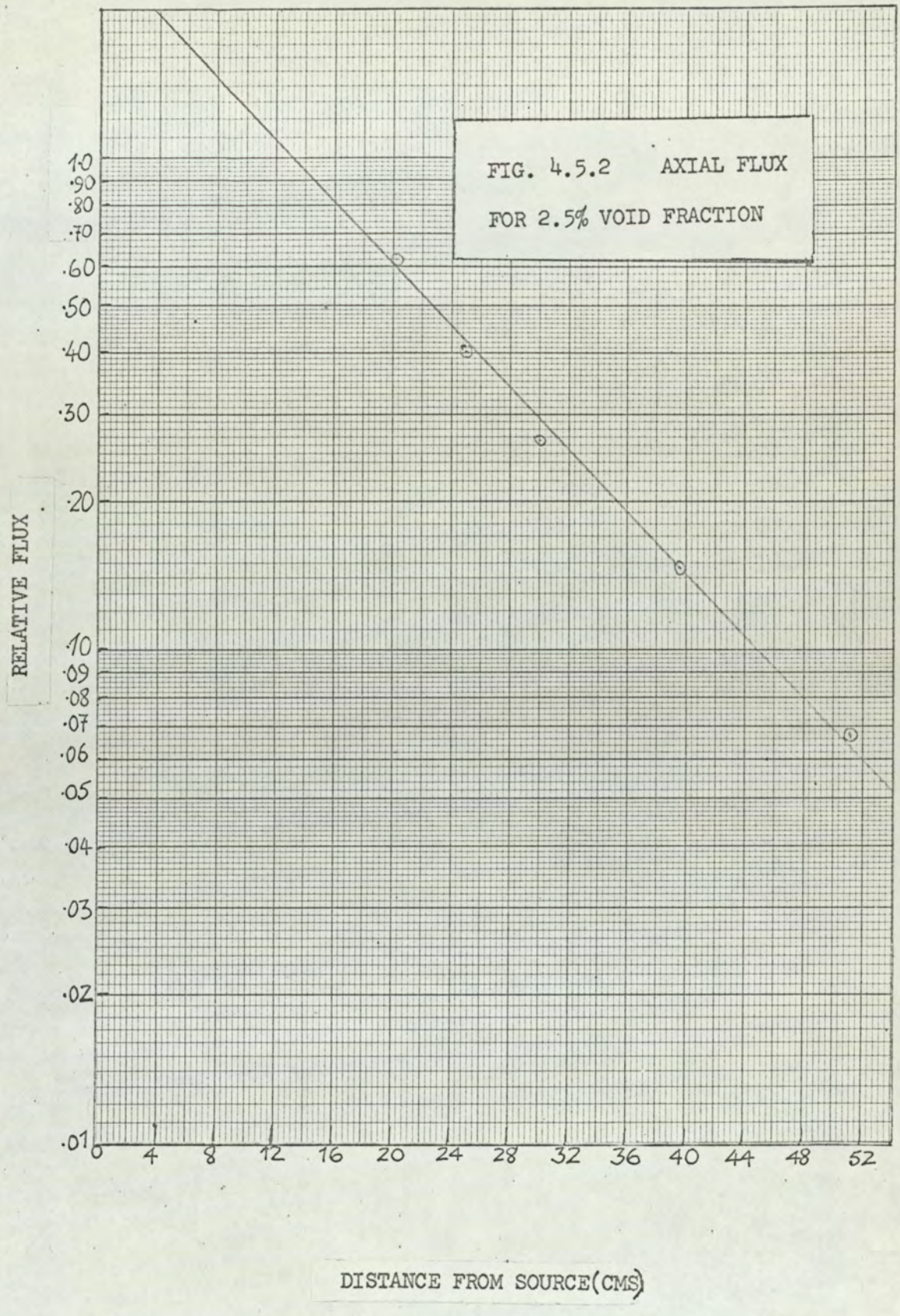
FIG. 4.5.2 AXIAL FLUX
FOR 2.5% VOID FRACTION
RELATIVE FLUX
1·0
·90
·80
·70
·60
·50
·40
·30
·20
·10
·09
·08
·07
·06
·05
·04
·03
·02
·01
0
4
8
12
16
20
24
28
32
36
40
44
48
52
DISTANCE FROM SOURCE(CMS)

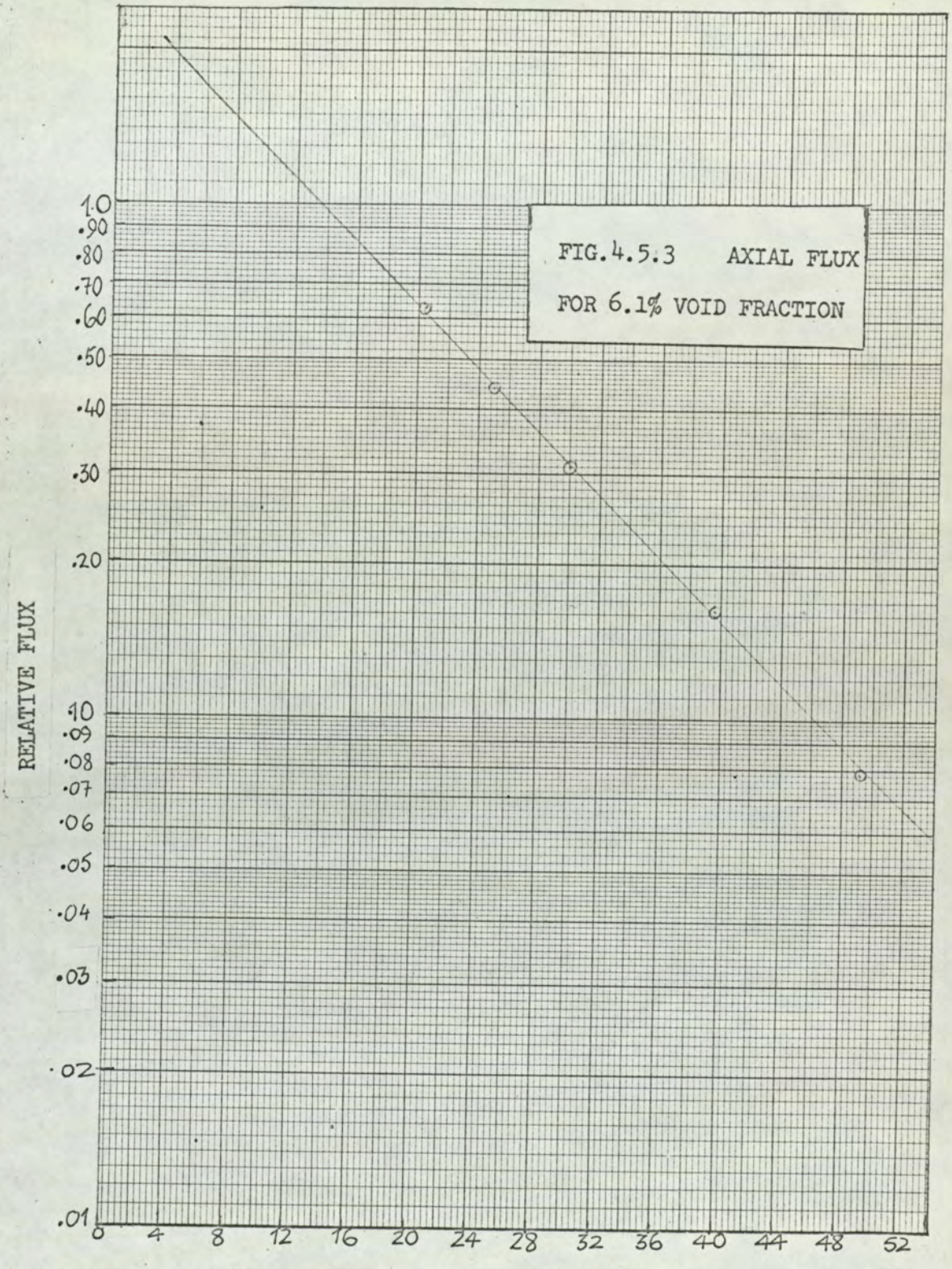
FIG.4.5.3 AXIAL FLUX
FOR 6.1% VOID FRACTION
RELATIVE FLUX
1.0
.90
.80
.70
.60
.50
.40
.30
.20
.10
.09
.08
.07
.06
.05
.04
.03
.02
.01
0
4
8
12
16
20
24
28
32
36
40
44
48
52
DISTANCE FROM SOURCE (CMS.)

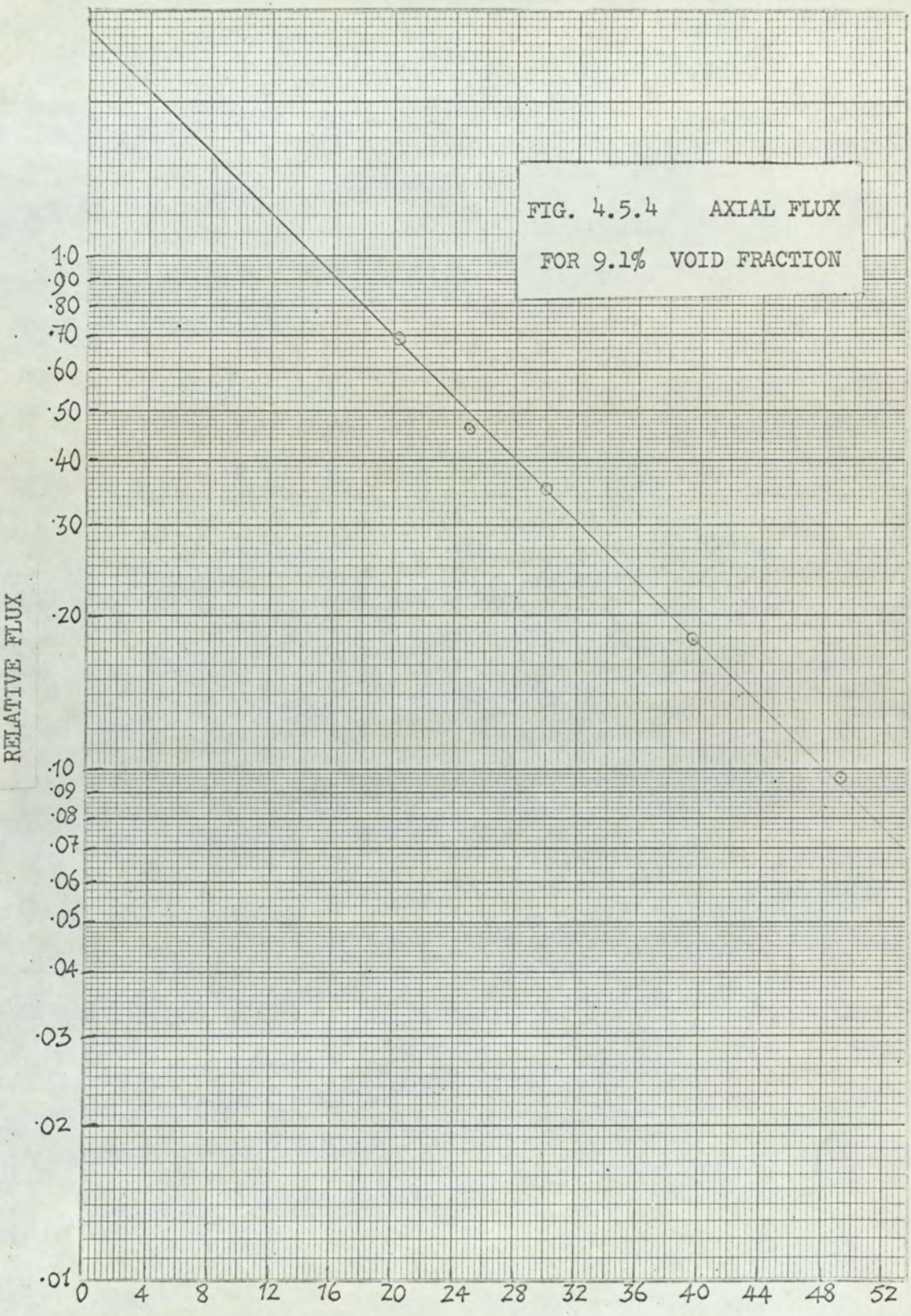
FIG. 4.5.4 AXIAL FLUX
FOR 9.1% VOID FRACTION
RELATIVE FLUX
1·0
·90
·80
·70
·60
·50
·40
·30
·20
·10
·09
·08
·07
·06
·05
·04
·03
·02
·01
0
4
8
12
16
20
24
28
32
36
40
44
48
52
DISTANCE FROM SOURCE (CMS.)

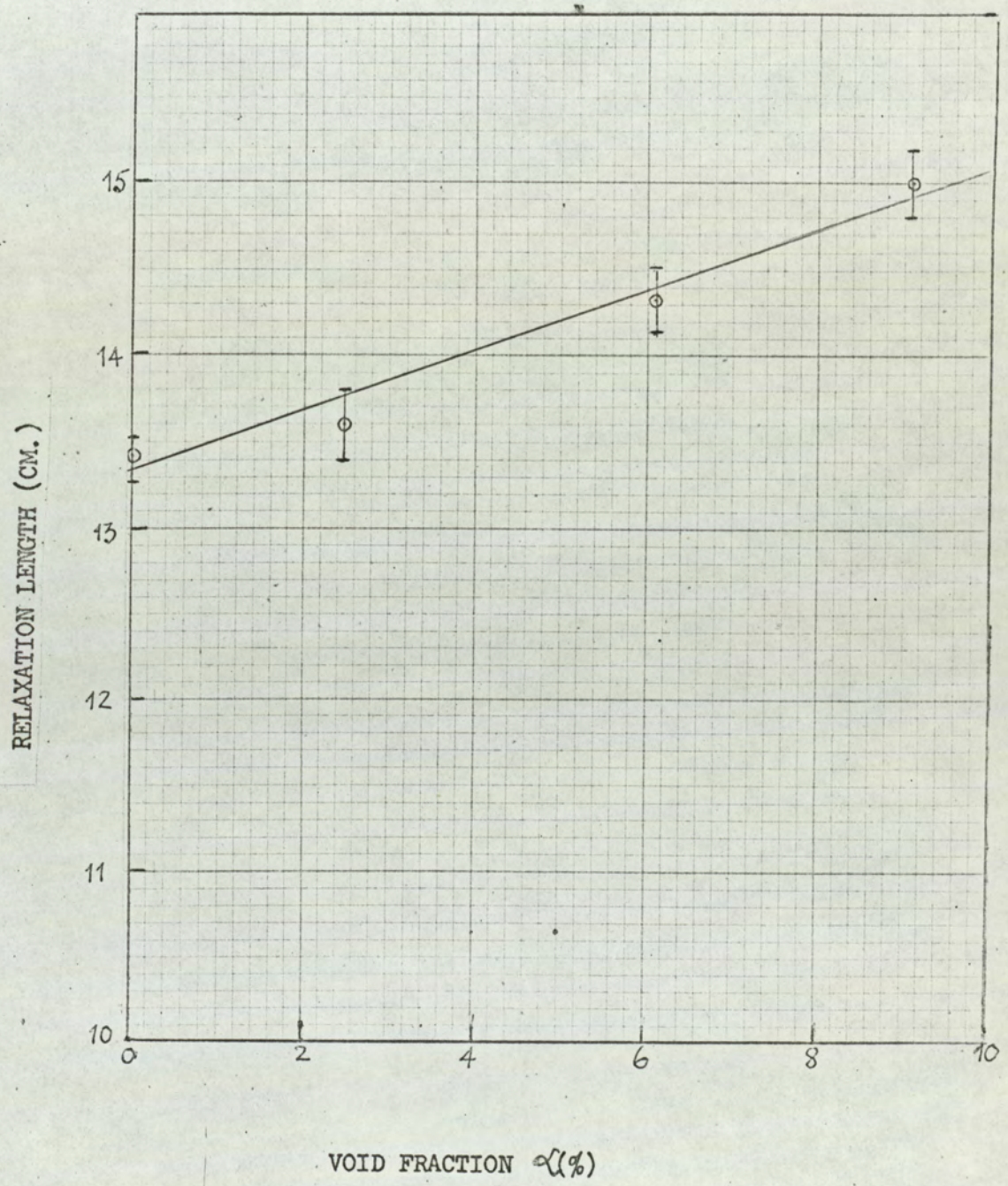

FIG.4.6 VARIATION OF RELAXATION LENGTH WITH VOID FRACTION

4.7 contd.

The uncertainties shown in the experimental points are statistical.

TABLE 4.1.1

Least Squares Values of ω_1 and ω_1^2 for zero % void fraction.

ω_1 cm^{-1}	ω_1^2 $cm^{-2} \times 10^{-4}$
0.03586	12.86
0.04124	17.00
0.03646	13.29
0.03645	13.29
0.03921	15.38
0.04107	16.87
0.04032	16.25
$\overline{\omega_1} = 0.03866$	$\overline{\omega_1^2} = 14.99$
$\sigma_R = 0.00228$	$\sigma_R = 1.81$
$\sigma_m = 0.00087$	$\sigma_m = 0.74$

4.7 contd.

TABLE 4.1.2

Least Squares Values of ω_2 and ω_2^2 for zero % void fraction.

ω_1 cm^{-1}	ω_1^2 $cm^{-2} \times 10^{-4}$
0.03333	11.06
0.03303	10.91
0.03288	10.81
0.03369	11.35
0.03439	11.83
0.03210	10.31
0.03341	11.17
0.03351	11.23
$\overline{\omega_2} = 0.03329$	$\overline{\omega_2^2} = 11.08$
$\sigma_R = 0.00066$	$\sigma_R = 0.44$
$\sigma_m = 0.00024$	$\sigma_m = 0.16$

4.7 contd.

TABLE 4.1.3

Least-Squares Values of K and K^2 for zero % Void Fractions.

K cm^{-1}	K^2 $cm^{-2} \times 10^{-4}$
0.07420	55.06
0.07442	55.38
0.07583	57.50
0.07410	55.56
0.07440	55.35
$\bar{K}$ = 0.07459	$\bar{K^2}$ = 55.77
σ_R = 0.00071	σ_R = .98
σ_m = 0.00032	σ_m = .44

TABLE 4.2.1

Least-Squares Values of ω_1 and ω_1^2 for 2.5% Void Fraction.

ω_1 cm^{-1}	ω_1^2 $cm^{-2} \times 10^{-4}$
0.03470	12.04
0.03553	12.62
0.03641	13.26
0.03768	14.20
$\bar{\omega}_1$ = 0.03608	$\bar{\omega_1^2}$ = 13.03
σ_R = 0.00128	σ_R = 0.92
σ_m = 0.00064	σ_m = 0.46

4.7 contd.

TABLE 4.2.2

Least-Squares Values of ω_2 and ω_2^2 for 2.5% Void Fraction.

ω_2 cm^{-1}	ω_2^2 $cm^{-2} \times 10^{-4}$
0.03374	11.38
0.03624	13.13
0.03366	11.33
0.03347	12.00
$\bar{\omega}_2 = 0.03428$	$\overline{\omega_2^2} = 11.96$
$\sigma_R = 0.00131$	$\sigma_R = 0.84$
$\sigma_m = 0.00066$	$\sigma_m = 0.42$

TABLE 4.2.3

Least-Squares Values of K and K^2 for 2.5% Void Fraction.

K cm^{-1}	K^2 $cm^{-2} \times 10^{-4}$
0.074811	55.97
0.07170	51.41
0.07446	55.44
$\bar{K} = 0.07366$	$\bar{K}^2 = 54.27$
$\sigma_R = 0.00170$	$\sigma_R = 2.49$
$\sigma_m = 0.00098$	$\sigma_m = 1.44$

4.7 contd.

TABLE 4.3.1

Least-Squares Values of ω_1 and ω_1^2 for 6.1% Void Fraction

ω_1 cm^{-1}	ω_1^2 $cm^{-2} \times 10^{-4}$
0.03590	12.89
0.03554	12.63
0.03607	13.01
0.03860	14.90
0.03780	14.29
0.03391	11.50
$\bar{\omega}_1 = 0.03630$	$\overline{\omega_1^2} = 13.20$
$\sigma_R = 0.00168$	$\sigma_R = 1.22$
$\sigma_m = 0.00068$	$\sigma_m = 0.50$

TABLE 4.3.2

Least-Squares Values of ω_2 and ω_2^2 for 6.1% Void Fraction.

ω_2 cm^{-1}	ω_2^2 $cm^{-2} \times 10^{-4}$
0.03238	10.49
0.03376	11.40
0.03251	10.57
0.03321	11.03
0.03370	11.36
0.03325	11.06
$\bar{\omega}_2 = 0.03314$	$\overline{\omega_2^2} = 10.99$
$\sigma_R = 0.00057$	$\sigma_R = 0.55$
$\sigma_m = 0.00023$	$\sigma_m = 0.22$

4.7 contd.

TABLE 4.3.3

Least-Squares of K and K^2 for 6.1% Void Fraction.

K cm^{-1}	K^2 $cm^{-2} \times 10^{-4}$
0.07099	50.39
0.06922	47.92
0.06906	47.69
0.06996	48.95
$\overline{K}$ = 0.06981	$\overline{K^2}$ = 48.74
σ_R = 0.00088	σ_R = 1.23
σ_m = 0.00044	σ_m = 0.62

TABLE 4.4.1

Least-Squares Values of ω_1 and ω_1^2 for 9.1% Void Fraction.

ω_1 cm^{-1}	ω_1^2 $cm^{-2} \times 10^{-4}$
0.03472	12.05
0.03439	11.84
0.03484	12.14
0.03314	10.98
0.03461	11.98
0.03379	11.41
$\overline{\omega}$ = 0.03425	$\overline{\omega_1^2}$ = 11.73
σ_R = 0.00066	σ_R = 0.45
σ_m = 0.00027	σ_m = 0.18

4.7 contd.

TABLE 4.4.2

Least-Squares Values of ω_2 and ω_2^2 for 9.1% Void Fraction.

ω_2 cm^{-1}	ω_2^2 $cm^{-2} \times 10^{-4}$
0.03357	11.27
0.03225	10.40
0.03269	10.69
0.02996	8.97
0.03400	11.56
0.03332	11.10
$\bar{\omega}_2$ = 0.03263	$\overline{\omega_2^2}$ = 10.67
σ_R = 0.00145	σ_R = 0.93
σ_m = 0.00059	σ_m = 0.38

TABLE 4.4.3

Least-Squares Values of K and K^2 for 9.1% Void Fraction.

K cm^{-1}	K^2 $cm^{-2} \times 10^{-4}$
0.06586	43.37
0.06713	45.07
0.06749	45.55
0.06623	43.87
$\bar{K}$ = 0.06668	$\bar{K}^2$ = 44.47
σ_R = 0.00076	σ_R = 1.01
σ_m = 0.00038	σ_m = 0.51

TABLE 4.5

Experimental Values of $\overline{\omega_1^2}$, $\overline{\omega_2^2}$, $\overline{K^2}$ and $\overline{B_m^2}$ for Various Void Fractions.

PARAMETER / VOID FRACTION	$\overline{\omega_1^2}$ $cm^{-2} \times 10^{-4}$	$\overline{\omega_2^2}$ $cm^{-2} \times 10^{-4}$	K^2 $cm^{-2} \times 10^{-4}$	$\overline{B_m^2} = (\overline{\omega_1^2} + \overline{\omega_2^2} - \overline{K^2})$ $cm^{-2} \times 10^{-4}$
0%	14.99 ± 0.74	11.08 ± 0.16	55.77 ± 0.44	-29.70 ± 0.87
2.5%	13.03 ± 0.46	11.96 ± 0.42	54.27 ± 1.44	-29.28 ± 1.57
6.1%	13.20 ± 0.50	10.99 ± 0.22	48.74 ± 0.62	-24.55 ± 0.82
9.1%	11.73 ± 0.18	10.67 ± 0.38	44.47 ± 0.51	-22.07 ± 0.66

4.8 Discussion of Experimental Results.

There is good agreement between the cosine flux plots and the experimental points (Figs.4.3.1 - 4.4.4) showing the assumed flux distributions to be acceptable. It has to be pointed out, however, that the theoretical flux distributions assumed are for a thermal source, whereas a fast neutron source was used. This means that the ideal flux shape is not reached close to the source.

The axial flux plots also show that the flux in the z-direction follows a reasonably good exponential distribution. There was no need to apply harmonic and end corrections to the exponential flux measurements. This was in view of the following considerations - Complete neutron thermalization takes place at a distance of about $2\sqrt{\tau} - 3\sqrt{\tau}$ cm. from the source (τ is the age of fission neutrons in water). This is about 12-15 cm. for light water. Secondly, elimination of higher harmonics is achieved if measurements are taken at least two diffusion lengths from the thermal source plane. For light water this is about 6 cm. The measurements reported in this work were made at least 20 cm. from the source and also away from the ends of the boundary thus making the application of harmonic and end corrections to the exponential flux

4.8 contd.

measurements unnecessary.

There is reasonable agreement between the calculated and experimental curves showing the variation of buckling with void fraction (Fig.4.2). The very large error associated with the 2.5% void fraction measurement (about 13%) would make the experimental value of the buckling at this void fraction somewhat uncertain which is reflected in the wide departure of this experimental point from the rest of the points on the curve.

The variation of buckling with void fraction shows that the introduction of voids in the system would tend to give it a positive void coefficient of reactivity, at least for lower void fractions. This is in agreement with the findings of other workers, notably Kouts et al.[18],[30] who measured buckling variations for various moderator-to-fuel volume ratios. As the introduction of bubbles for void simulation removes moderator from the assembly the effects of bubbling is to reduce moderator-to-fuel volume ratio. To a first approximation the measurement of buckling variation with void fraction is equivalent to its measurement for differing moderator-to-fuel volume ratios. The introduction of

4.8 contd.

voids in the assembly could also be taken equivalent to a reduction of the lattice pitch so that the measurements reported here should give similar results to those made with varying moderator-to-fuel volume ratios or varying lattice pitches.

In view of the foregoing if it were possible to obtain results for higher void fractions instead of for only up to 9.1% void fraction it might have been possible to obtain results showing a peak in the curve of B_m^2 versus Void fraction similar to the results of Kouts et al[30][18]. Unfortunately this could not be done in this work as the core volume and compressor output set a limit to the void fraction that could be introduced into the assembly. For this reason, measurements were of necessity confined to the lower void fraction region. This unfortunately cannot give the full picture of what the effect of voids in an actual reactor would be as the average void fraction in boiling water reactors is of the order of 40%. It can, however, be said that the measurements have given the general trend in the way voids affect the buckling. The extent to which the reactivity is affected by voids is seen to be dependent on the lattice arrangement. Lower void fractions would give the system a positive void

4.8 contd.

coefficient of reactivity whilst higher void fractions would give it a negative void coefficient of reactivity. A reactor can, therefore, be designed to have the desired degree of void fraction by setting a limit on the void fraction to be tolerated. This would at least be true for natural uranium multiplying systems. The effect varies strongly with the initial water-to-fuel volume ratio and for values of this less than about 1.5 can be negative all the way.

CHAPTER 5.

THEORETICAL CALCULATION OF MATERIAL BUCKLING°

5.1 Introduction.

The neutron energy spectrum in a reactor spreads from about 10 Mev down to zero. This wide range of energies is split into some suitable number of groups for purposes of calculation. Natural uranium/graphite moderated reactors can be handled reasonably by splitting the neutron energy spectrum into two groups, viz:- slowing down and thermal but hydrogen moderated reactors are affected by the relatively high thermal neutron absorption cross section of hydrogen. This lowers the thermal flux relative to the slowing down flux and neutron capture by U^{235} leading to fission during slowing down can be important. (Something of the order of 5% of fission may be due to capture of neutrons during slowing down.) For this reason two groups are unsuitable for describing the neutron cycle in a water moderated reactor. Three groups are the very minimum, viz:-

(i) Fission

(ii) Slowing down neutrons

(iii) Thermal neutrons

In view of the foregoing considerations the Three Group method was adopted for calculating the material buckling of the subcritical assembly. The method takes into account the requirements which any

5.1 contd.

calculation method for a water moderated reactor must satisfy. These may be summarized as follows:

(a) There must be adequate treatment of slowing down by hydrogen as well as for the non-hydrogeneous elements present.

(b) There must be adequate representation of the total number of neutrons trapped in U^{238} resonances. In resonance capture there is self-screening of U^{238} which is dependent mainly on the surface-to-mass ratio but also to some extent on the newness of the surrounding rods. This must also be allowed for in the calculations.

(c) There should be adequate allowance for U^{235} fission in the epithermal region.

(d) There must be good representation of the thermal spectrum. In this regard it must be borne in mind that the flux is no longer Maxwellian due to strong neutron absorption in hydrogen. This necessitates the adoption of a non-Maxwellian form such as the Wigner-Wilkins spectrum[31].

(e) There must be a fast fission factor empirical formula to represent fission of U^{238}.

(f) Thermal flux depression in the fuel rods which will vary significantly with void fraction. This

5.1 contd.

(f) contd.

must be adequately represented in the calculation method.

5.2 Nomenclature.

5.2.1 Subscripts used are as follows:

5	refers to	U^{235}
8	" "	U^{238}
u	" "	uranium
m	" "	material
c	" "	material of fuel cladding
t_r	" "	neutron transport
a	" "	neutron absorption
s	" "	neutron scattering
1	" "	fast group
2	" "	epithermal group
3	" "	thermal group
H	" "	Hydrogen
r	" "	slowing down
f	" "	fuel
eff	" "	effective
t	" "	total
w	" "	moderator (water)

5.2.2 Symbols.

a is the radius of the fuel rod

5.2 contd.

5.2.2 contd.

b	is the radius of the equivalent cell
k_{eff}	is the effective multiplication factor
σ	is the microscopic cross section
σ_o	is the microscopic absorption cross section at 2200 m/sec.
Σ	is the macroscopic cross section
D	is the Diffusion coefficient
L_1^2	is the fast slowing down area
L_2^2	is the epithermal group slowing down area
L_3^2	is the thermal diffusion area
K_2	is the epithermal group infinite multiplication factor.
K_3	is the thermal group infinite multiplication factor.
ϵ	is the fast fission factor
η	is the neutron yield per capture in fissile material
ρ_i	is the density in gm/cm^3 of material i
F_i	is the volume fractiin of material i
V_i	is the volume component i of unit cell
N_i	is the number of atoms per unit volume of material i
ϕ_i	is the flux in material i
Φ_i	is the average flux in material i
ϕ	is the flux in the core
Φ	is the average flux in the core

5.2 contd.

5.2.2 contd.

S_i is the surface area of material i

M_i is the mass of material

$\mathcal{L}$ is the Lethargy

p is the resonance escape probability

N_o is Avogadro's Number

W is the flux weighting factor

B is the Buckling of medium

I is the resonance integral

T is the temperature in degrees K

E is energy.

5.3 Theory of Calculation.

The method of calculation is primarily that described by Cooper[32]. This is supplemented by the cell calculation technique developed by Amouyal, Benoist and Horowitz[34] hereinafter denoted as the ABH method (to use the abbreviation of Lamarsh[35]).

5.3.1 The Three-Group Diffusion Equation.

For a just critical system the following equations apply:

$$D_1\nabla^2\phi_1 - \Sigma_{r_1}\phi_1 + \eta_2\epsilon\Sigma_{a_{52}} + \eta_3\epsilon\Sigma_{a_{53}} = 0 \qquad 5.1$$

$$D_2\nabla^2\phi_2 - (\Sigma_{r_2} + \Sigma_{a_2})\phi_2 + \Sigma_{r_1}\phi_1 = 0 \qquad 5.2$$

$$D_3\nabla^2\phi_3 - \Sigma_{a_3}\phi_3 + \Sigma_{r_2}\phi_2 = 0 \qquad 5.3$$

5.3 contd.

5.3.1 contd.

It is necessary to make some substitutions in the three coupled Diffusion equations 5.1, 5.2 and 5.3 to make them more tractable. The substitutions in question are as follows:

$$L_1^2 = D_1 \Big/ \Sigma_{r_1} \qquad 5.4$$

$$L_2^2 = \frac{D_2}{(\Sigma_{r_2} + \Sigma_{a_2})} \qquad 5.5$$

$$L_3^2 = \frac{D_3}{\Sigma_{a_3}} \qquad 5.6$$

$$K_2 = \frac{\eta_2 \epsilon \Sigma_{a_{52}}}{(\Sigma_{r_2} + \Sigma_{a_2})} \qquad 5.7$$

$$p = \frac{\Sigma_{r_2}}{\Sigma_{a_2} + \Sigma_{r_2}} \qquad 5.8$$

$$K_3 = \frac{\eta_3 \epsilon p \Sigma_{a_{53}}}{\Sigma_{a_3}} \qquad 5.9$$

By making use of the substitutions given in Equations 5.4 - 5.9 the Diffusion Equations 5.1 - 5.3 can be rewritten as follows:

5.3 contd.

5.3.1 contd.

$$(L_1^2\nabla^2 - 1)\phi_1 + \frac{K_2 D_2 L_1^2}{D_1 L_1^2}\phi_2 + \frac{K_3 D_3 L_1^2}{D_1 L_3^2}\phi_3 = 0 \qquad 5.10$$

$$(L_2^2\nabla^2 - 1)\phi_2 + \frac{D_1 L_2^2}{D_2 L_1^2}\phi_1 = 0 \qquad 5.11$$

$$(L_3^2\nabla^2 - 1)\phi_3 + \frac{pD_2 L_3^2}{D_3 L_2^2}\phi_2 = 0 \qquad 5.12$$

If a further substitution of the form $\nabla^2\phi = -B_m^2\phi$ is made, the following equation is obtained by elimination of ϕ_1, ϕ_2 and ϕ_3:

$$1 = \frac{K_2(1 + B_m^2 L_3^2) + K_3}{(1+B_m^2 L_1^2)(1+B_m^2 L_2^2)(1+B_m^2 L_3^2)} \qquad 5.13$$

This is the equation for a just critical system. More generally Equation 5.13 may be rewritten as follows:

$$K_{eff} = \frac{K_2(1 + B_m^2 L_3^2) + K_3}{(1+B_m^2 L_1^2)(1+B_m^2 L_2^2)(1+B_m^2 L_3^2)} \qquad 5.14$$

5.3.2 Neutron Energy Groups.

For the Three Group Calculation method the neutron spectrum is divided into three bands. In this calculation the bands correspond to the following energy groups:

5.3 contd.

5.3.2 contd.

Group 1 10 Mev - 180 Kev (fission spectrum)

Group 2 180 Kev - 0.625 ev ($^1/E$ spectrum)

Group 3 0.625 ev - 0 (Wigner-Wilkins spectrum).

5.3.3 Number Density of Components.

In order to evaluate the macroscopic cross sections for the system the average number of atoms N_i of each component per unit volume must be found. If F_i is the volume fraction of the i^{th} component then N_i is defined as follows:

$$N_i = \frac{N_o \rho_i F_i}{A_i} \qquad 5.15$$

5.4 Group-Three Cross Sections.

5.4.1 Microscopic Cross Sections.

Amster[31] has calculated average cross-sections over Wigner-Wilkins spectra for homogeneous mixtures of hydrogen, U^{235} and a $^1/v$ absorber for a range of temperatures. A tabulation of these cross sections calculated for a range of temperatures (293°K - 600°K) is given by Amster[31]. The cross section data corresponding to 293°K which approximates to the temperature at which measurements reported in this work were carried out and hence the data pertinent

5.4 contd.

5.4.1 contd.

to this calculation are listed in Table A.4.1

As stated earlier the cross section data strictly apply to a homogeneous system. Since the subcritical assembly is by no means homogeneous it becomes necessary to define the effective U^{235}-to-hydrogen ratio and also that of the $^1/v$ absorber to hydrogen. The definitions are given in Equations 5.16 and 5.17.

$$\left(\frac{N_5}{N_H}\right)_{eff} = \frac{N_5 \times W_f}{N_H \times W_w} \qquad 5.16$$

$$\left(\frac{\sigma_o(^1/v)}{N_H}\right)_{eff} = \frac{N_s \sigma_{os} W_f + N_H \sigma_{oH} W_w + N_c \sigma_{oc} W_c}{N_H E W_w} \qquad 5.17$$

The flux weighting factor W_i in medium i is defined as:

$$W_i = \frac{\Phi_i}{\Phi} \qquad 5.18$$

To find the cross sections from Table A.4.1 a two-stage interpolation is made between the values of $(N_5/N_H)_{eff}$ and $(\sigma_o(^1/v)/N_H)_{eff}$ computed from Equation 5.16 and Equation 5.17 respectively. This interpolation gives the thermal absorption cross section value for U^{235} i.e.

5.4 contd.

5.4.1 contd.

$\sigma_{a_{53}}$ directly. For all other absorbers which are assumed to be $^1/v$ in the thermal region the interpolated value obtained for unit $^1/v$ absorber is multiplied by the appropriate value of the microscopic absorption cross-section at 2200 m/sec. i.e. σ_o which is given in Table A.4.2. Transport cross sections with the exception of hydrogen are constant and are also taken from Table A.4.2. (Table A.4.2 has been adapted from Deutch[33], Cooper[32,(46)].

5.4.2 Macroscopic Cross Sections.

Both the macroscopic transport cross section Σ_{tr_3} and the macroscopic absorption cross-section Σ_{a_3} are calculated from the following general formula:

$$\Sigma_3 = \sum N_i \sigma_i w_i \qquad 5.19$$

using the appropriate microscopic cross sections.

The thermal diffusion coefficient is defined as follows:

$$D_3 = \frac{1}{3(\Sigma_{a_3} + \Sigma_{tr_3})} \qquad 5.20$$

5.5 Flux Weighting Factors.

The thermal flux in a heterogeneous reacting

5.5 contd.

system is non-uniform and to account for this the term flux weighting factor is sometimes introduced in reactor physics calculations.

The procedure adopted for evaluating the flux weighting factors for the system under consideration will now be described. First the assumption is made that the flux across a unit cell is uniform. This amounts to saying that the flux weighting factor is unity for the can, fuel and moderator i.e.

$$W_w = W_c = W_f = 1 \qquad 5.21$$

The assumed values of W_w, W_c and W_f are then used for evaluating $(N_5/N_H)_{eff}$ and $(\sigma_0(^1/v)/N_H)_{eff}$ as defined in Equations 5.16 and 5.17 respectively. The values obtained for $(N_5/N_H)_{eff}$ and $\left(\frac{\sigma_0(^1/v)}{N_H}\right)_{eff}$ are next used for calculating the microscopic cross-sections using Amster's cross section data[31] in the manner outlined in Section 5.4.1. These cross-section values are then employed in the ABH calculation method[34],[35] to obtain the flux weighting factors. By the ABH method values of the average fluxes, Φ_f/Φ i.e. W_f and Φ_w/Φ i.e. W_w can be obtained. The method does not give the value of Φ_c/Φ i.e. W_c directly. W_c is however required for the calculation of the Group Three Macroscopic cross sections

5.5 contd.

for the fuel can as defined in Equation 5.19. It is considered adequate to take a value for W_c which is half-way between W_w and W_c. The error introduced by taking this value for W_c will not be great in view of the fact that absorption by the can is small. The flux weighting factors thus obtained will be more accurate, at least, for the fuel and moderator. The can flux weighting factor, W_c though a pure guess will nevertheless be a more realistic value to use in the calculation than the initially assumed value of unity. Having obtained what is considered more accurate flux weighting factors the next step in the calculations is to recalculate the values of $(N_5/N_H)_{eff}$ and $(\sigma_0(^1/v)/N_H)_{eff}$ using Equations 5.16 and 5.17 as before. The values obtained will be more accurate than those obtained under the assumption of uniform flux across the cell. The macroscopic cross sections are calculated as before and the values used in the ABH method to give what will still be more accurate flux weighting factors. These flux weighting factors are adopted without modification throughout the calculation.

It will be recalled that the flux weighting factors enter into the calculation in Equations 5.16, 5.17 and 5.19 which are used in the evaluation of $(N_5/N_H)_{eff}$, $(\sigma_0(^1/v)/N_H)_{eff}$ and Σ_3 respectively.

5.5 contd.

The method already described for evaluating the flux weighting factors applies in full to the unvoided moderator. When it comes to the question of evaluating the same factors for the voided moderator it is no longer considered necessary to start with the assumption that

$$W_w = W_f = W_c = 1.$$

Instead it is considered better to start with the final flux weighting factors obtained for the unvoided moderator. Using unvoided moderator flux weighting factors the values of $(N_5/N_H)_{eff}$ and $(\sigma_o(1/v)/N_H)_{eff}$ are calculated as before. The macroscopic cross sections are next calculated and used in the ABH method to obtain the final flux weighting factors.

5.6 Group Two Cross Sections.

5.6.1 Microscopic Cross Sections.

Apart from the epithermal absorption cross sections for U^{238} and U^{235} i.e. σ_{a82} and σ_{a52} respectively all the epithermal cross sections used in this calculation are based on the calculations of Deutsch[33], Pomerance and Macklin[36] and Campbell and Freemantle[37]. The cross section data are given in Table A.4.1

5.6 contd.

5.6.1 contd.

It has to be pointed out that the epithermal cross section calculations referred to above make two basic assumptions in the structure of the epithermal flux viz:-

(i) The flux is proportional to $^1/E$ per unit energy interval.

(ii) The flux has no fine or ripple structure.

The average microscopic cross section is defined by the following equation:

$$\sigma_2 = \frac{\int_{.625}^{1.8 \times 10^5} \sigma \frac{dE}{E}}{\int_{.625}^{1.8 \times 10^5} \frac{dE}{E}} \qquad 5.22$$

5.6.1.1 U^{235} Epithermal Absorption Cross Section

The average epithermal absorption cross section for U^{235} came from the following equation:

$$\sigma_{a_{52}} = \sigma_{05} \left[2g \sqrt{\frac{E_o}{E_\ell}} + S \sqrt{\frac{\pi T_o}{4T}} \right] \times \frac{1}{\Delta \mathcal{L}} \qquad 5.23$$

Here $E_o = .0253$ ev, $E_\ell = .625$ ev, $T_o = T = 293°K$. and $\Delta \mathcal{L} = 12.57$.

5.6 contd.

5.6.1 contd.

5.6.1.1 contd.

The 'g' and 's' values which appear in Equation 5.23 were taken from Campbell and Freemantle[37]. The value adopted for σ_{05} was 698 barns - the same as the value adopted by Campbell and Grant[38] among others. This leads to a value of 22.2 barns for $\sigma_{a_{52}}$.

5.6.1.2 <u>U^{238} Epithermal Absorption Cross Section</u>.

The evaluation of the average epithermal absorption cross section for U^{238} i.e. $\sigma_{a_{82}}$ was carried out on the basis of the following equation:-

$$\sigma_{a_{82}} = I_{eff}/\Delta\mathcal{L} \qquad 5.24$$

It is evident from Equation 5.24 that $\sigma_{a_{82}}$ is easily calculated when the values of I_{eff} and $\Delta\mathcal{L}$ are known.

Several formulae exist for the evaluation of the effective resonance integral, I_{eff}[1],[3],[27],[28],[39-44]. For this calculation the 300°K values of the effective resonance integral for various S_f/M_f values

5.6 contd.

5.6.1 contd.

5.6.1.2 contd.

given in ANL-5800[3] were adopted. The values adopted are listed in Table A.8.1. Using these values a graph of the effective resonance integral versus the surface-to-mass ratio of the fuel was plotted. This is shown in Fig.A.8.1. The surface-to-mass ratio was determined for the type of fuel used in the subcritical assembly. The Dancoff and Ginsberg correction was applied to account for the reduction in resonance absorption caused by the geometric shadowing of the fuel lump by its neighbours[45]. From the graph I_{eff} versus S_f/M_f (Fig.A.8.1) the values of I_{eff} corresponding to the S_f/M_f value of our system was read off. This was found to be 10.4 barns. The value of I_{eff} obtained in this way is the effective resonance integral with no $1/v$ contribution. It therefore remains to increase the value of I_{eff} by the $1/v$ contribution, $I_{(1/v)}$ which is defined as follows:

$$I_{(1/v)} = \int_{E_\ell}^{\infty} \sigma_{os} \sqrt{\frac{E_o}{E}} \frac{dE}{E} \qquad 5.25$$

Here E_o = .0253 ev and E_ℓ = .625 ev.

5.6 contd.

5.6.1 contd.

5.6.1.2 contd.

Equation 5.25 simplifies to:

$$I_{(1/v)} = 2\sigma_{os}\sqrt{\frac{E_o}{E_\ell}} \qquad 5.26$$

The value of σ_{os} adopted is 2.72 barns (Table A.4.1). Putting in the values of σ_{os}, E_o and E_ℓ into Equation 5.26, $I_{(1/v)}$ is found to be 1.1 barns. The value of I_{eff} with $1/v$ contribution is therefore 11.5 barns. The values of $\Delta\mathcal{L}$ is determined from the following equation:

$$\Delta\mathcal{L} = -\Delta \ell n\, E \qquad 5.27$$

Using the values of E_ℓ and E_o given before $\Delta\mathcal{L}$ is found to be 12.57. With values I_{eff} and $\Delta\mathcal{L}$ now known $\sigma_{a_{s2}}$ is easily calculated from Equation 5.24. This gives the value of $\sigma_{a_{s2}}$ as 0.915 barns.

5.6.2 Macroscopic Cross Section.

The macroscopic slowing down cross section Σ_{r_2}, the macroscopic absorption cross section Σ_{a_2} and the macroscopic transport cross section Σ_{tr_2} are all calculated from the general formula:

5.6 contd.

5.6.2 contd.

$$\Sigma_2 = \sum N_i \sigma_i \qquad 5.28$$

using the appropriate microscopic cross sections.

The epithermal diffusion coefficient is defined by:

$$D_2 = \frac{1}{3\Sigma_{tr_2}} \qquad 5.29$$

5.7 Group One Cross Sections.

5.7.1 Microscopic Cross Sections.

All the necessary transport and slowing down cross sections adopted are based on the work of Deutsch[33]. Deutsch[33] gives the transport cross sections as averages over the fission spectrum while the slowing down cross sections are obtained from age calculations combined with transport cross sections.

5.7.2 Macroscopic Cross Sections.

The macroscopic slowing down cross section, Σ_{r_1} and the macroscopic cross section Σ_{tr_1} are calculated from the general form

$$\Sigma_1 = \sum N_i \sigma_i \qquad 5.30$$

using the appropriate microscopic cross sections.

The fast diffusion coefficient D_1 is defined

5.7 contd.

5.7.2 contd.

as follows:-

$$D_1 = \frac{1}{3\Sigma_{tr_1}} \qquad 5.31$$

5.8 Fast Fission Factor ϵ.

To evaluate the fast fission factor the following experimental data[32],[3a] giving the values of ϵ for various N_H/N_f values were adopted:

$\frac{N_H}{N_f}$	1	2	3	4	5	6	7
ϵ	1.110	1.076	1.057	1.046	1.038	1.033	1.028

A graph of N_H/N_f was plotted against ϵ. This is shown in Fig.A.9.1 From this graph the value of ϵ corresponding to the value of N_H/N_f for the subcritical assembly was read off. The value of ϵ is different for each condition of voided moderator as the ratio of hydrogen atoms to uranium atoms i.e. N_H/N_f decreases with increasing voids in the system.

5.9 Solution of B_m^2 from Criticality Equation.

The Three Group criticality equation given in Equation 5.14 is a cubic in B_m^2. Rearrangement of Equation 5.14 yields:

5.9 contd.

$$(B_m^2)^3+(B_m^2)^2\left[\frac{1}{L_1^2}+\frac{1}{L_2^2}+\frac{1}{L_3^2}\right]+B_m^2\left[L_1^2+L_2^2+L_3^2\left(1-\frac{K_2}{K_{eff}}\right)\right]\Big/L_1^2L_2^2L_3^2$$

$$+\left[1-\frac{K_2+K_3}{K_{eff}}\right]\Big/L_1^2L_2^2L_3^2=0 \qquad 5.32$$

The equation has 3 roots, one of which the smallest negative value (for a subcritical seembly) is equivalent to the measured value of B_m^2.

The root of equation 5.32 was extracted by numerical techniques.

5.10 Result of Calculation.

The most important results of this calculation are listed in Table 5.1. Comparison between the calculated and measured values of the material buckling has already been given in Chapter 4.

TABLE 5.1

Calculated Parameters for Different Void Fractions.

PARAMETER	VOID FRACTION %				
	0%	5%	10%	15%	20%
D_1 cm.	1.271	1.304	1.340	1.377	1.416
D_2 cm.	0.678	0.703	0.731	0.762	0.796
D_3 cm.	0.168	0.177	0.187	0.198	0.212
L_1^2 cm^2	27.105	29.267	31.711	34.487	37.663
L_2^2 cm^2	9.628	10.416	11.305	12.514	13.461
L_3^2 cm^2	2.733	2.897	3.086	3.283	3.488
M^2 cm^2 *	39.466	42.580	46.102	50.284	54.612
p	0.7896	0.7812	0.7722	0.7583	0.7514
K_2	0.0581	0.0606	0.0633	0.0675	0.0697
K_3	0.8324	0.8380	0.8464	0.8499	0.8545
K_∞	.890	0.899	0.910	0.917	0.924
K_{eff}	.757	0.756	0.755	0.750	0.744
ϵ	1.053	1.055	1.057	1.060	1.062
f **	0.7634	0.7746	0.7887	0.8000	0.8166
W_w	1.186	1.183	1.178	1.176	1.166
W_f	0.566	0.574	0.585	0.593	0.614
W_c	0.876	0.879	0.882	0.885	0.890
B_m^2 $cm^{-2} \times 10^{-4}$	-28.61	-24.51	-20.20	-16.86	-14.21

* M^2 = Migration area. cm^2

** f = Thermal utilization factor.

CHAPTER 6.

INDUCED FLUCTUATIONS IN NUETRON POPULATION

6.1 Introduction.

Fluctuations in neutron population affect the stability of the reactor. In boiling water reactors in particular, stability is one of the most important criteria as it influences both the maximum attainable power and operational safety. A simple technique which could give an indication of the possible occurrence of fluctuations inside the reactor should therefore be a useful guide in reactor operation. It was therefore the aim of this experiment to investigate a possible technique for predicting the presence of fluctuations from an analysis of the data on induced fluctuations in a subcritical assembly. The presence of fluctuations in the entire core will naturally show up as fluctuations in the reactor power but local fluctuations could have a negligible effect on total power yet might lead to more serious trouble such as burn out.

It has to be borne in mind that the fluctuations as measured by a counter will depend on a number of factors, notably:-

a) Fluctuations in the number of neutrons per fission

b) The absolute criticality of the reacting system

c) The efficiency of the counter

d) The length of time over which counts are taken i.e. (number of counts in the sample).

6.1 contd.

These factors affect what might be termed "statistical fluctuations in the neutron population" to which considerable attention has been given by a number of authors[47-52]. It is to be appreciated that the statistical fluctuations referred to above will show up on top of any fluctuations that are induced in the experiment.

6.2 Theory of Method.

In principle the method consisted in introducing a steady neutron source in the subcritical assembly and then taking several readings of the neutron counting rate over a reasonable length of time. This was done for steady conditions inside the assembly and also for conditions of induced fluctuations. [The S.A.M.E.S. accelerator was not used in this experiment because of its tendency to produce wider fluctuations in source neutrons. This would make the determination of the fluctuations in the neutron population inside the assembly even more complicated.]

The determination of the variance, mean, standard deviation for each condition studied would yield valuable information on the fluctuations present in the system.

6.3 Materials and Apparatus.

The equipment used in this experiment is shown in Fig.6.1 and Fig.6.2 and includes the following:

(i) Subcritical Assembly - This has been described in Chapter I and for this experiment two fuel rods were removed to make room for the source neutrons and the scintillation counter.

(ii) Compressor for producing bubbles.

(iii) Device to enable periodic introduction of voids in the assembly.

(iv) Scintillation counting system.

(v) 3 Curie Am-Be neutron source.

(vi) 100-Channel pulse height analyser.

(vii) Void fraction measurement apparatus - This was the same as the static pressure void fraction measurement equipment described in Chapter 2.

6.4 Scintillation Counting System.

This was constructed from a 1 in. × 1 mm. Li^6 loaded glass scintillator coupled by a light guide to an EMI photomultiplier tube type EMI 6097S.

The detection of neutrons by Li^6 is according to this reaction:

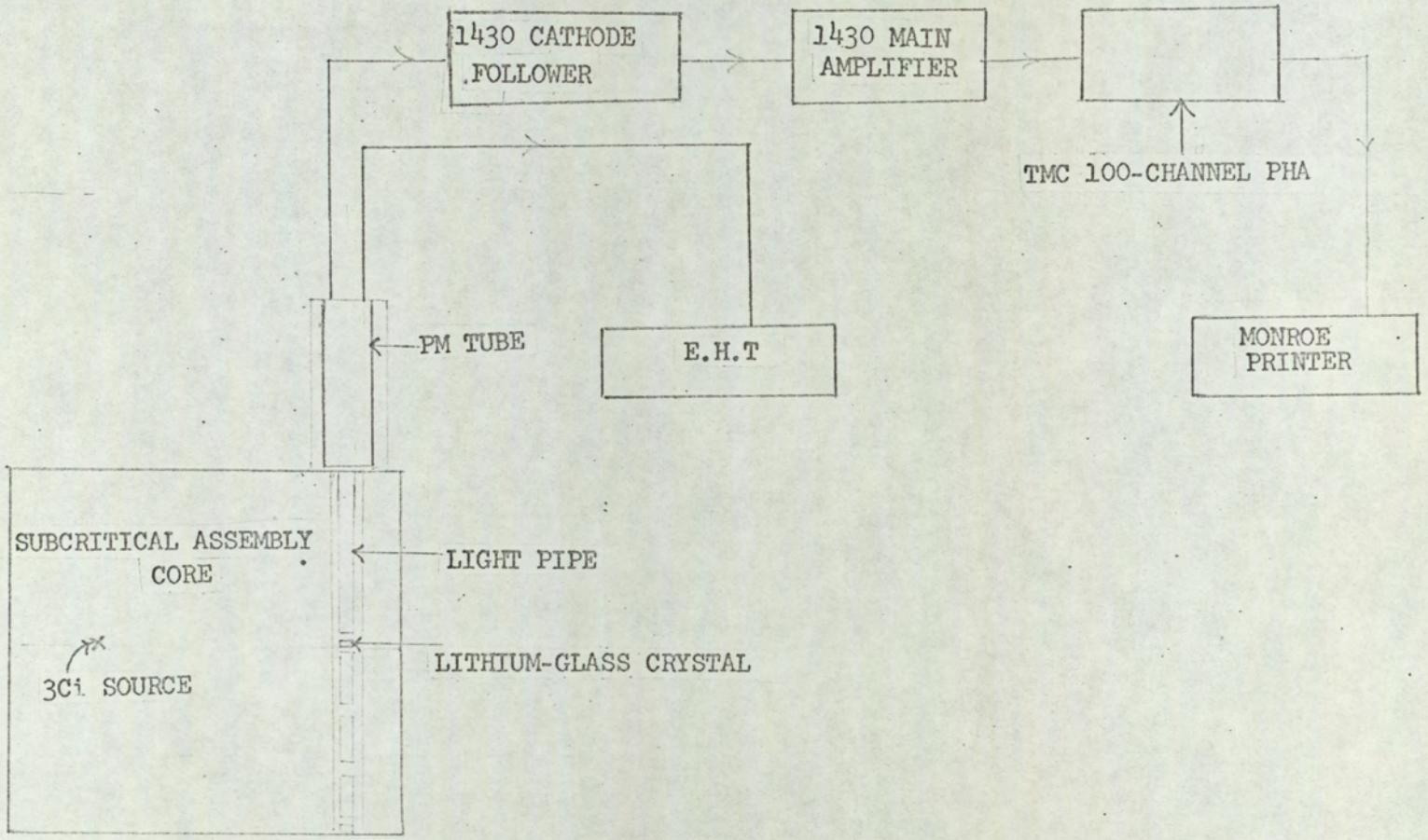

FIG.6.1 EXPERIMENTAL ARRANGEMENT

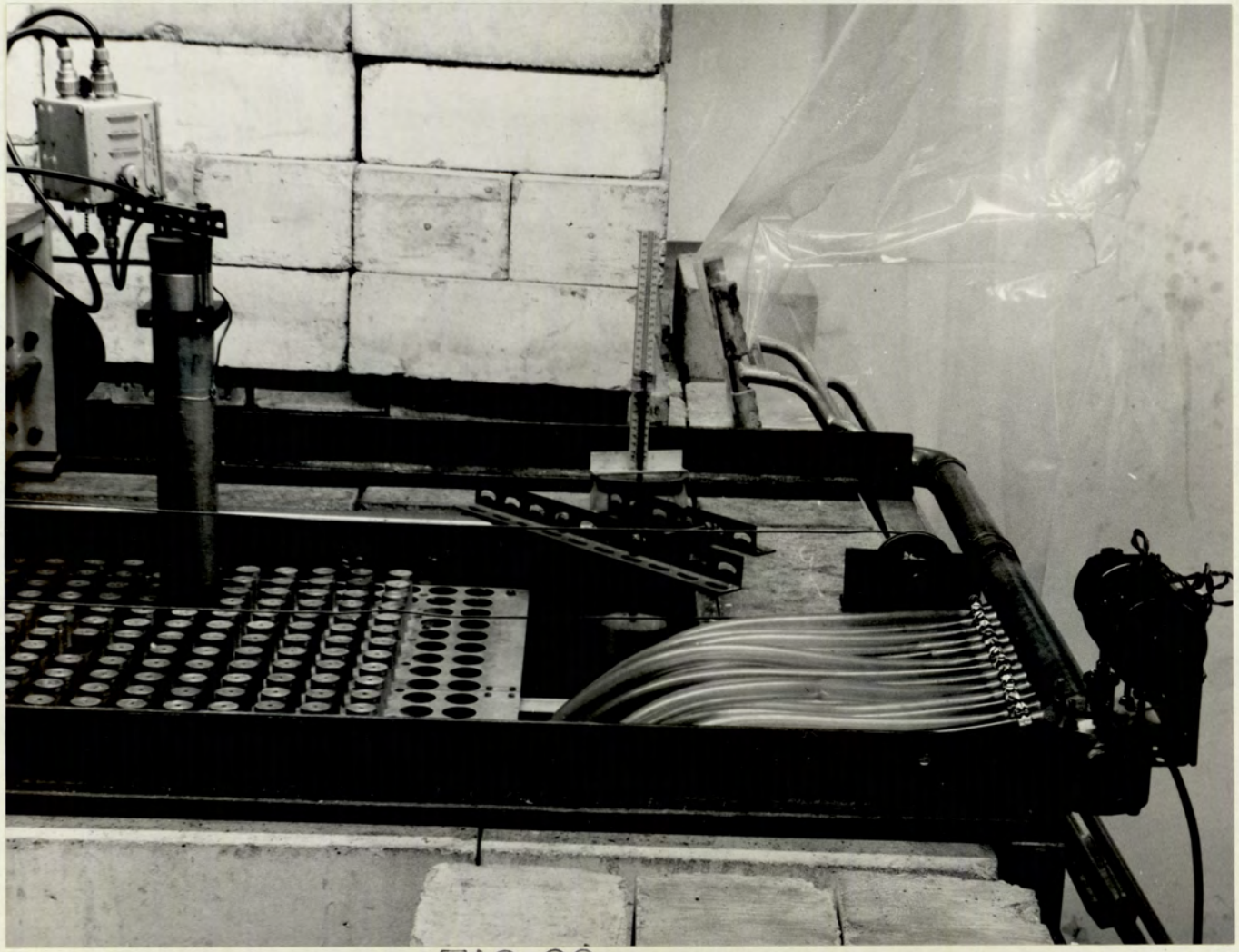

FIG. 62

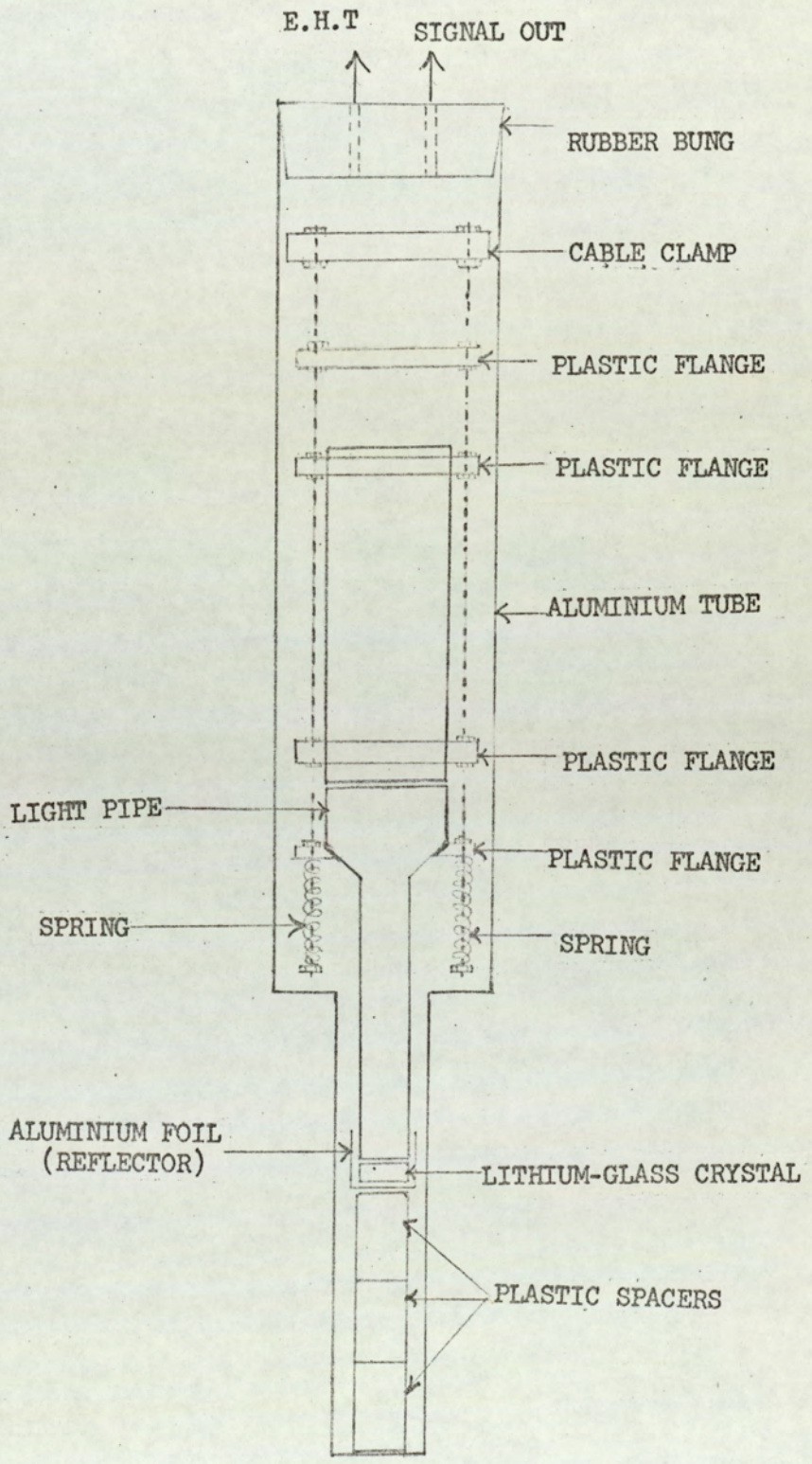

FIG.6.3 LITHIUM-GLASS SCINTILLATION COUNTER MOUNTING

6.4 contd.

$$Li^6 + {}_0n^1 \rightarrow H^3 + He^4 + 4.78 \text{ Mev.}^{(53)}$$

The alpha particle produced in this reaction takes 2.05 Mev and the hydrogen-3 nucleus 2.73 Mev. Both particles cause ionization in the crystal leading to the detected scintillation signals.

The crystal was coupled to the photomultiplier tube by means of a light guide and the assembly was mounted in a light tight aluminium tube which fitted the lattice of the subcritical assembly. A diagram of this is shown in Fig.6.3.

6.5 Method of Inducing Fluctuations.

The device shown in Fig.6.4 consisted of a brass tube with a rotating "butterfly" valve inside it. The tube with valve was fixed at the end of the copper tube through which air was blown from the compressors to the subcritical assembly. The rotating valve was connected to a variac so that the speed of rotation could be varied at will. Rotation of the valve periodically vented the compressed air to the atmosphere thus stopping the production of bubbles in a regular manner. The speed of rotation of the valve could be controlled over a wide range from a period large compared with the time necessary for the bubbles to

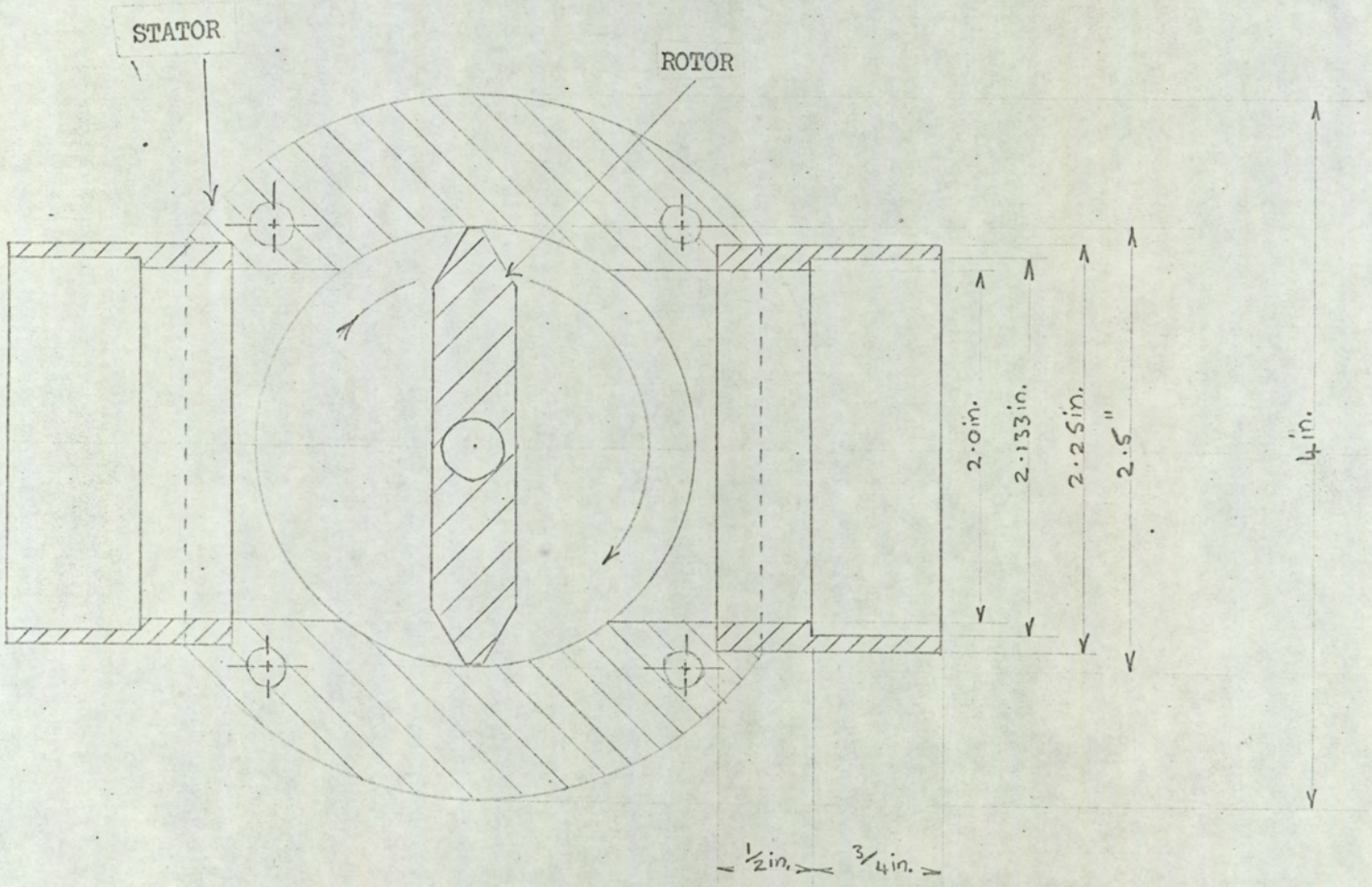

FIG.6.4 APPARATUS FOR INDUCING FLUCTUATIONS

6.5 contd.

clear from the system to a period so short that bubbles were always present in the system. This in effect amounted to inducing fluctuations in the neutron population as the neutron counting rate was related to the amount of voids present in the assembly.

6.6 Preliminary Experiment

In order to check the suitability of the detecting system for the detection of thermal neutrons the Am-Be neutron source was placed in the subcritical assembly and using the arrangement shown in Fig.6.1 a plot of the thermal neutron spectrum was made on the 100-Channel pulse height analyser. Fig.6.5 shows a typical thermal neutron spectrum obtained with the neutron detecting system. The background spectrum is shown in Fig.6.6. From the background spectrum and the thermal neutron spectrum shown it can be concluded that the system was suitable for the detection of thermal neutrons.

6.7 Main Experimental Procedure.

The pulse height analyser was set so that only the peak of the thermal neutron spectrum such as is shown in Fig.6.5 was counted using the pulse

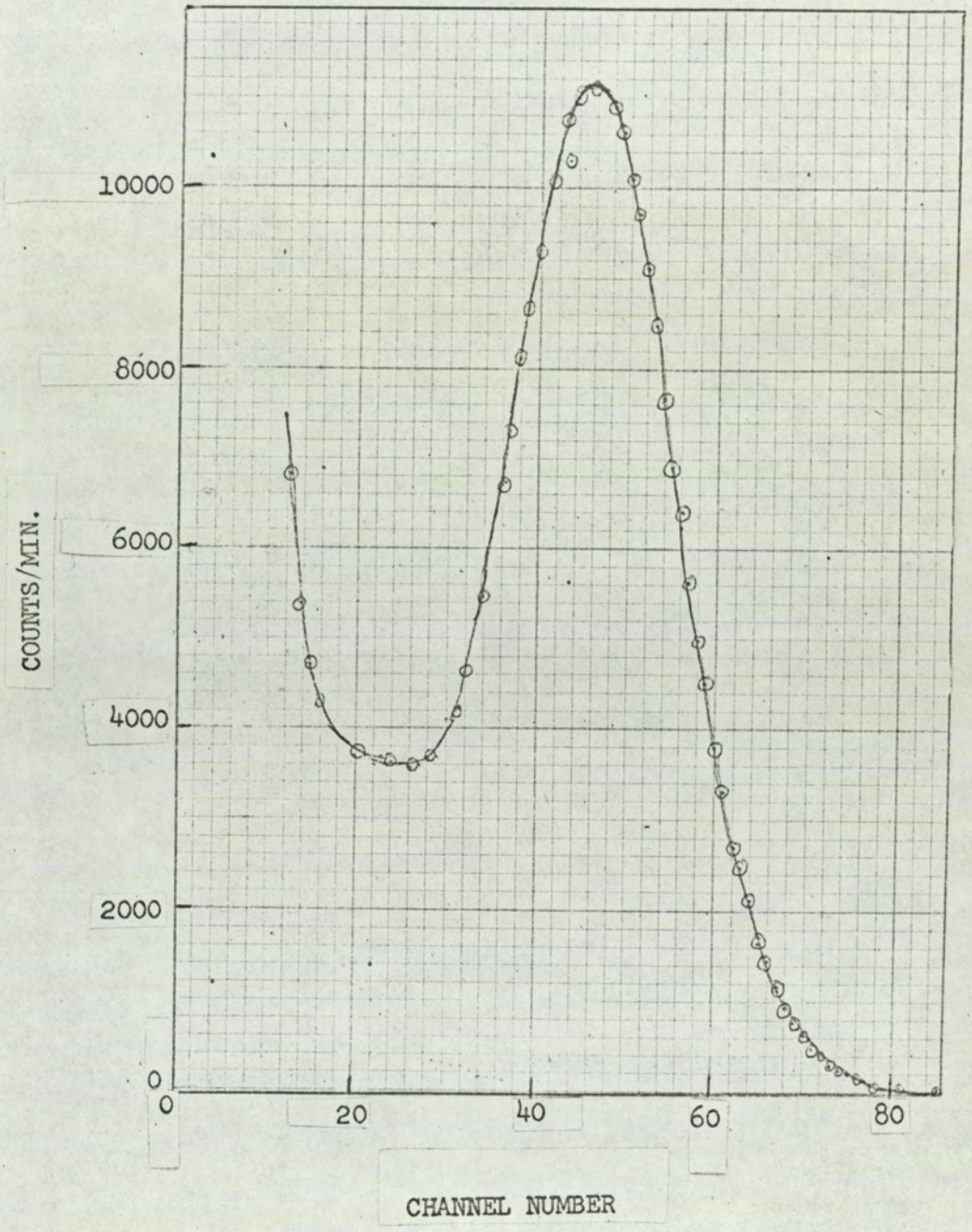

FIG.6.5 TYPICAL PULSE HEIGHT SPECTRUM FROM LITHIUM GLASS SCINTILLATOR IN THERMAL NEUTRON FLUX.

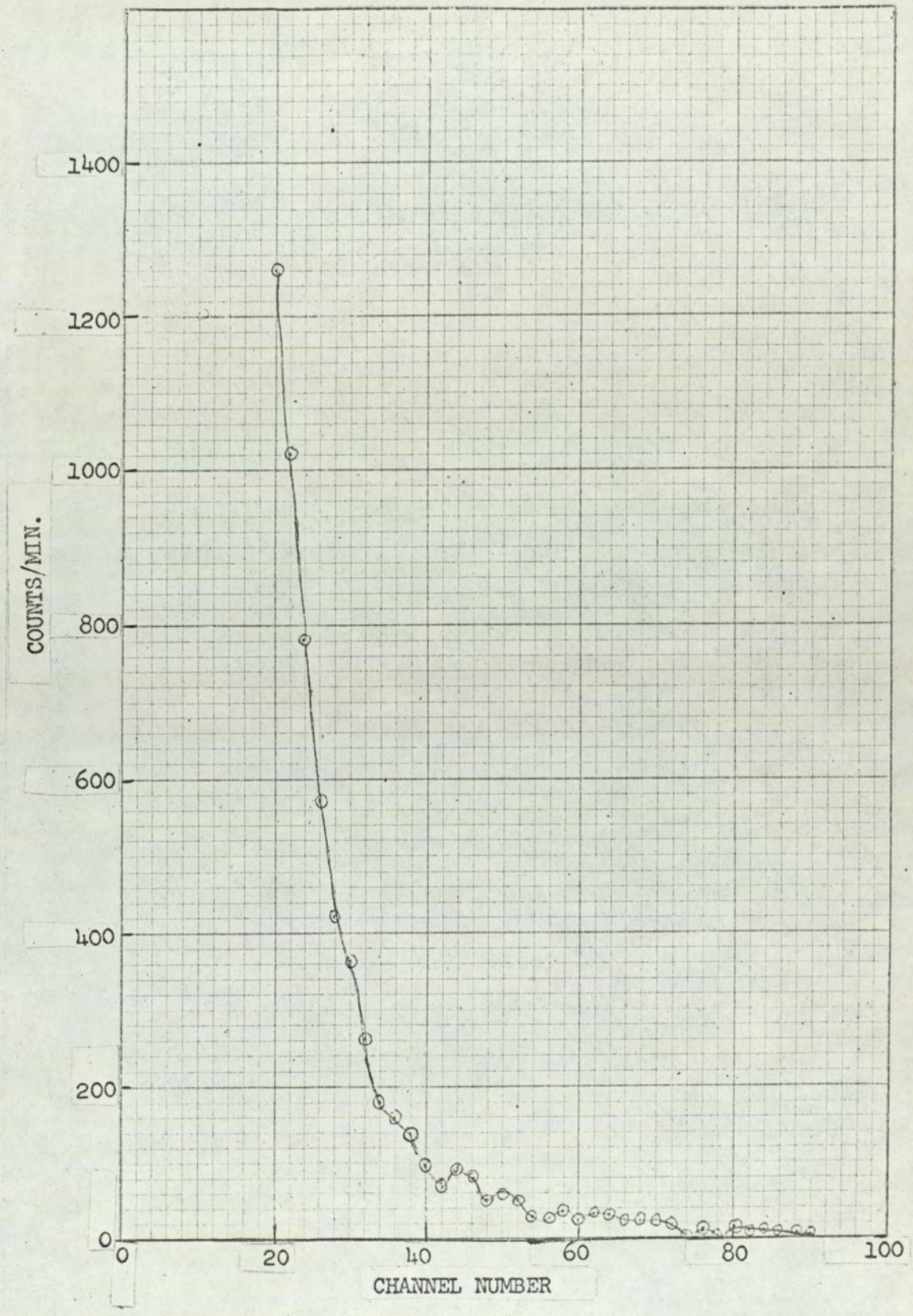

FIG.6.6 TYPICAL BACKGROUND SPECTRUM

6.7 contd.

height analyser in the multiscaling mode.

Four hundred readings of the neutron count were taken with the source and detector in position and with no bubbling taking place in the subcritical assembly. A further 400 readings were taken under the condition of continuous steady bubbling (free bubbling) in the assembly.

Next, fluctuations in the bubbling rate were introduced in the assembly using the rotary valve described in Section 6.5. A series of readings were taken for a range of speeds of rotation. The void fraction associated with each rate of bubbling was measured by the static pressure method described in Chapter 2, modified to have a rapid response time. Minimum and maximum void fractions were determined for each case.

6.8 Analysis of Results and Discussion.

For each set of data obtained in the measurements a histogram was plotted. On the basis of an assumed Gaussian distribution a computer programme was written to give the theoretical curve as well as the variance, mean and the standard deviation. The curves for the no bubbling case and free bubbling case are

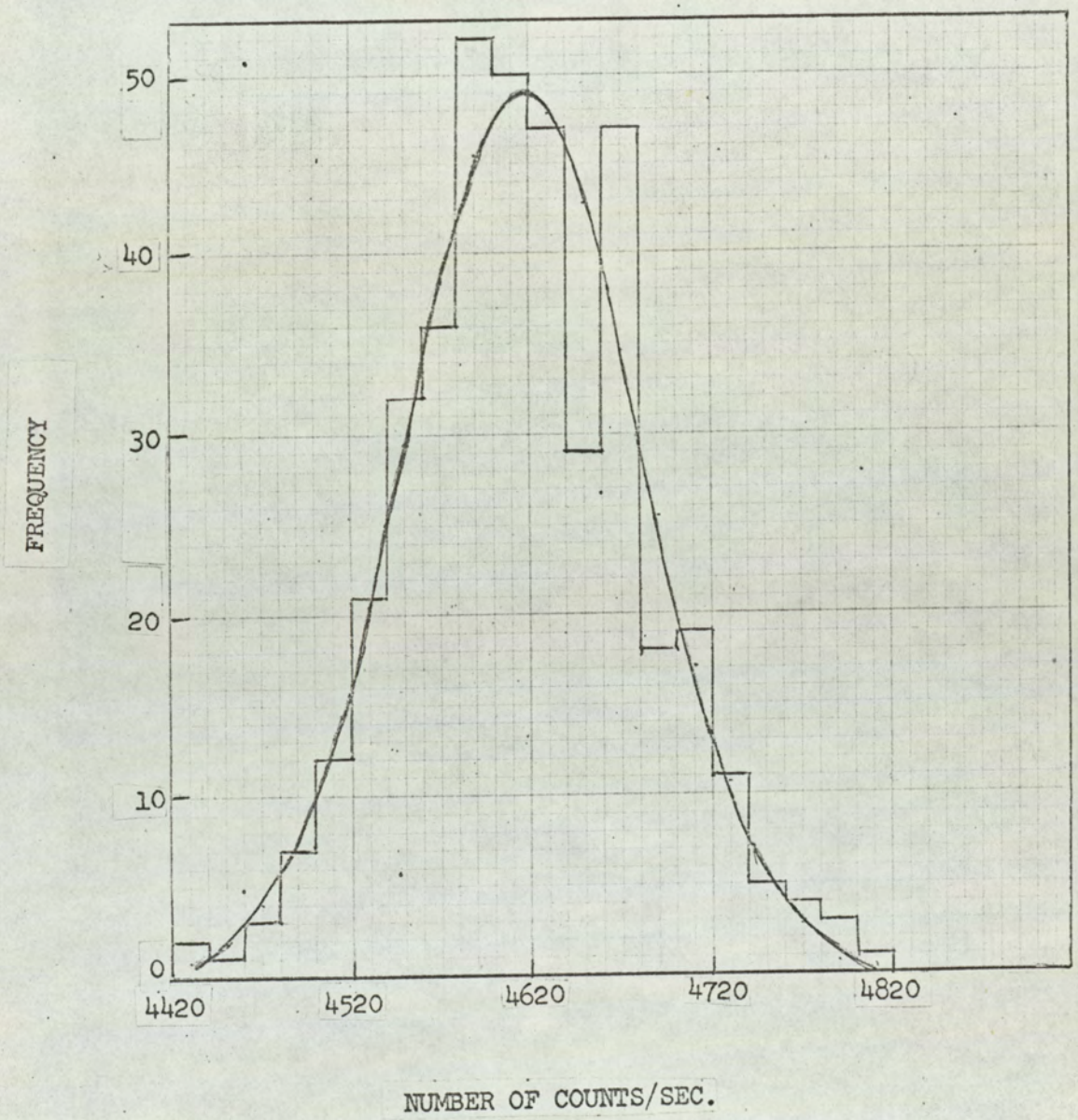

FIG.6.7 HISTOGRAM AND GAUSSIAN FOR NO BUBBLING EXPT.

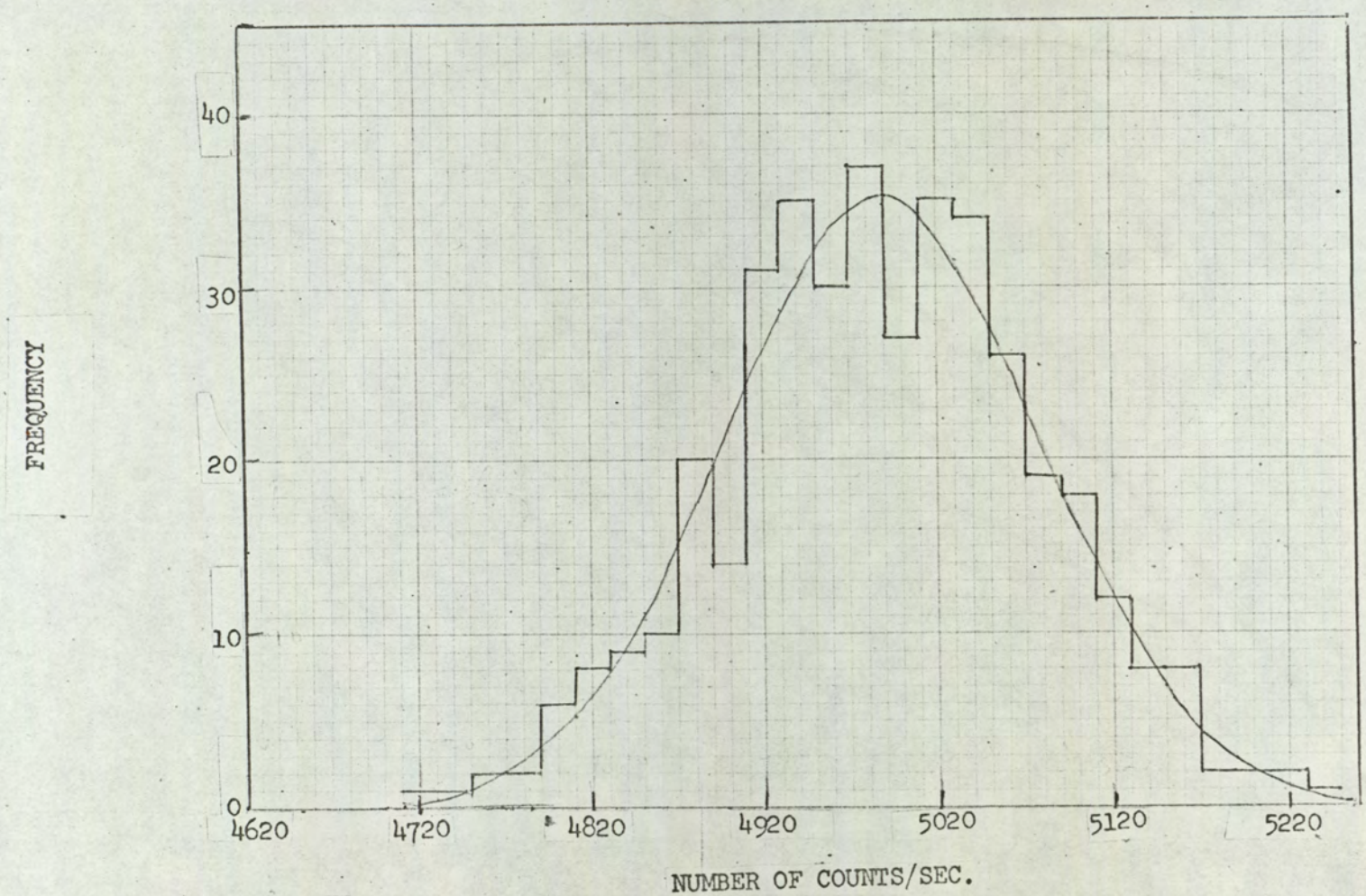

FIG.6.8 HISTOGRAM AND GAUSSIAN FOR FREE BUBBLING EXPERIMENT

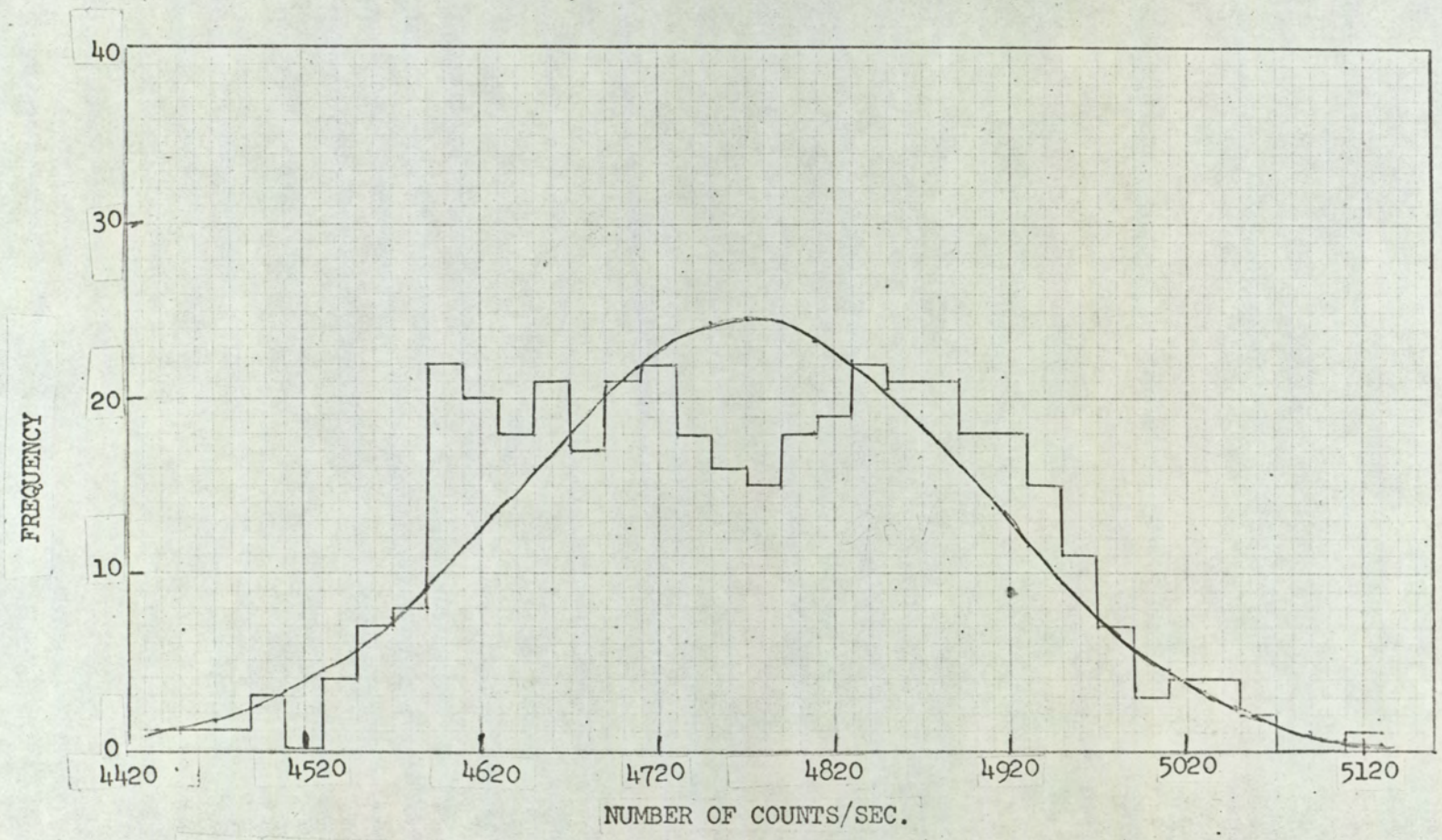

FIG. 6.9 HISTOGRAM AND GAUSSIAN FOR MAXIMUM FLUCTUATIONS

6.8 contd.

shown in Fig.6.7 and Fig.6.8 respectively. The other cases will show wider departures from the Gaussian; the larger the period of the rate of bubbling, the greater will be the fluctuations induced and consequently the wider will be the departure of the curve from a true Gaussian. Fig.6.9 gives the histogram and fitted Gaussian curve for the case with the widest fluctuations in void fraction.The histogram shows two modes as might be expected as the modes for the no bubbling case and free bubbling case would tend to show up separately in the graph.

The more important treatment of experimental data comprised the determination of the quantity $\sigma^2/\bar{c}$ for each set of data. Here σ^2 represents the variance of the readings and $\bar{c}$ the mean. The quantity $\sigma^2/\bar{c}$ is a measure of the fluctuations encountered. A plot of $\sigma^2/\bar{c}$ was then made against the difference between the minimum and maximum void fractions associated with each condition of measurement. The extremes of the void fractions introduced for each condition of measurement constituted the major source of induced fluctuations in the system. In order to obtain the largest change in the void fraction the data obtained for the no bubbling experiment and the free bubbling ex-

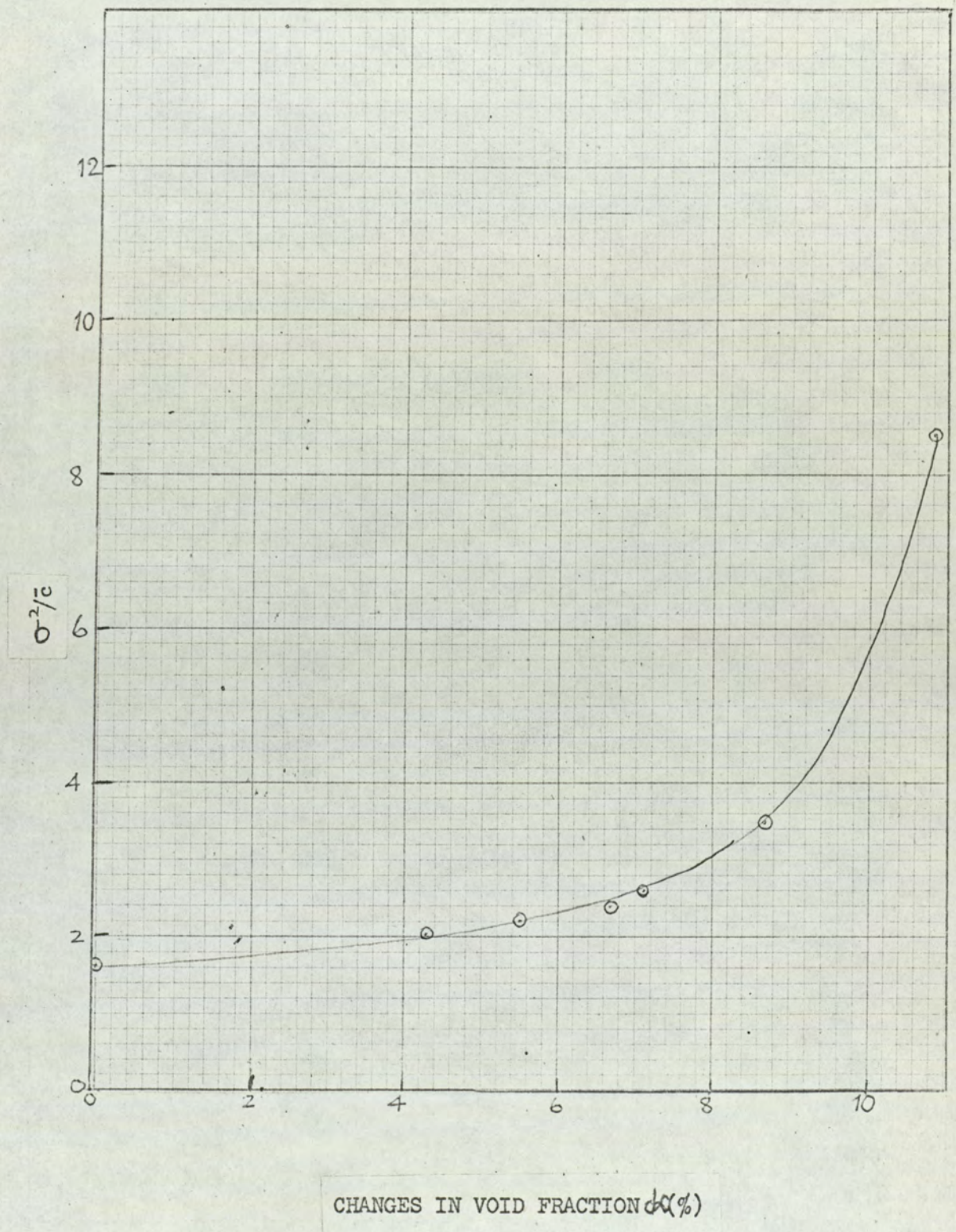

FIG. 6.10 GRAPH OF $\sigma^2/\bar{c}$ AGAINST CHANGES IN VOID FRACTION

6.8 contd.

periment were combined and the value of $\sigma^2/\bar{c}$ determined for the combined data. The free bubbling experiment has, of course, zero change in void fraction.

Fig.6.10 shows the graph of $\sigma^2/\bar{c}$ against the changes in the void fraction. It can be seen from Fig.6.10 that the bigger the fluctuations in the void fraction the bigger the value of $\sigma^2/\bar{c}$. The usefulness of this type of exercise lies in the fact that in an actual reactor centre where an on-line-computer could be installed the computer could be made to compute the quantity $\sigma^2/\bar{c}$ and watch for any sharp increase in the value of the quantity $\sigma^2/\bar{c}$ which would be evidence of the presence of fluctuations in the system.

6.9 Theoretical Explanation of Results.

6.9.1 Assumptions.

The following assumptions are made:

(i) Three Groups of neutrons, viz:-

Group 1 - Fast Neutrons

Group 2 - Epithermal neutrons

Group 3 - Normal neutrons

(ii) Central point source of Group 1 type neutrons only and of strength 4π neutrons/sec.

6.9 contd.

6.9.1 contd.

(iii) A bare spherical core of 50.7 cm. outer radius is assumed. This is equivalent sphere of same volume as rectangular core including reflector savings.

(iv) Counter is at 25.5 cm. radius.

6.9.2 Three Group Subcritical Equations.

The following equations hold:

$$\phi_3 = \frac{A\,\mathrm{Sinh}\mu(R-r)}{r} + \frac{C\,\mathrm{Sinh}\nu(R-r)}{r} + \frac{E\,\mathrm{Sinh}\omega(R-r)}{r} \qquad 6.1$$

$$\phi_2 = \frac{S_1 A\,\mathrm{Sinh}\mu(R-r)}{r} + \frac{S_2 C\,\mathrm{Sinh}\nu(R-r)}{r} + \frac{S_3 E\,\mathrm{Sinh}\omega(R-r)}{r} \qquad 6.2$$

$$\phi_1 = \frac{T_1 A\,\mathrm{Sinh}\mu(R-r)}{r} + \frac{T_2 C\,\mathrm{Sinh}\nu(R-r)}{r} + \frac{T_3 E\,\mathrm{Sinh}\omega(R-r)}{r} \qquad 6.3$$

Here $-\mu^2$, $-\nu^2$, $-\omega^2$ are the roots of the material buckling equation given in Chapter 5. S and T are the coupling coefficients and A,C and E are unknowns (as yet).

ϕ_3 represents the thermal neutron flux

ϕ_2 represents the epithermal neutron flux

ϕ_1 represents the fast neutron flux

R represents the outer radius of the sphere

r represents any radius of the sphere.

6.9 contd.

6.9.3 Solution of Equations.

This is achieved by applying the following boundary conditions at the centre:

(i) Total fast neutron current = source strength

i.e.

$$\frac{Q}{4\pi D_1} = \left[- r^2 \frac{d\phi_1}{dr} \right]_{r=o} \qquad 6.4$$

(ii) Total epithermal neutron current = zero

i.e.

$$0 = \left[- r^2 \frac{d\phi_2}{dr} \right]_{r=o} \qquad 6.5$$

(iii) Total thermal neutron current = zero

i.e.

$$0 = \left[- r^2 \frac{d\phi_3}{dr} \right]_{r=o} \qquad 6.6$$

$$\text{Now, } \frac{d}{dr}\left[\frac{\text{Sinh}\mu(R-r)}{r}\right] = - \frac{\mu r \,\text{Cosh}\mu(R-r) - \text{Sinh}\mu(R-r)}{r^2} \qquad 6.7$$

The total current through a spherical surface of radius $r = -4\pi r^2 D \frac{d\phi}{dr}$ 6.8

$$\underset{r \to o}{\text{Limit}} \; r^2 \frac{d}{dr}\left[\frac{\text{Sinh}\mu(R-r)}{r}\right] = - \text{Sinh}\mu R \qquad 6.9$$

If $Q = 4\pi$ neutrons per second, then the following equations are obtained:

6.9 contd.

6.9.3 contd.

$$T_1 A\,\mathrm{Sinh}\mu R + T_2 C\,\mathrm{Sinh}\nu R + R_3 E\,\mathrm{Sinh}\omega R = {}^1/D_1 \qquad 6.4a$$

$$S_1 A\,\mathrm{Sinh}\mu R + S_2 C\,\mathrm{Sinh}\nu R + S_3 E\,\mathrm{Sinh}\omega R = 0 \qquad 6.5a$$

$$A\,\mathrm{Sinh}\mu R + C\,\mathrm{Sinh}\nu R + E\,\mathrm{Sinh}\omega R = 0 \qquad 6.6a$$

The matrix for the solutions of the three unknowns ($A\,\mathrm{Sinh}\mu R$), ($C\,\mathrm{Sinh}\nu R$) and ($E\,\mathrm{Sinh}\omega R$) is:

$$\begin{pmatrix} T_1 & T_2 & T_3 \\ S_1 & S_2 & S_3 \\ 1 & 1 & 1 \end{pmatrix} \begin{pmatrix} A\mathrm{Sin}\mu R \\ C\mathrm{Sinh}\nu R \\ E\mathrm{Sinh}\omega R \end{pmatrix} = \begin{pmatrix} {}^1/D_1 \\ 0 \\ 0 \end{pmatrix} \qquad 6.10$$

Solving Equation 6.10 yields:

$$a = A\mathrm{Sin}\mu R = \frac{1}{D_1}\left[\frac{S_2 - S_3}{(T_1-T_2)(S_1-S_3)-(T_1-T_3)(S_1-S_2)}\right] \qquad 6.11$$

$$c = C\mathrm{Sinh}\nu R = \frac{1}{D_1}\left[\frac{-(S_1 - S_3)}{(T_1-T_2)(S_1-S_3)-(T_1-T_3)(S_1-S_2)}\right] \qquad 6.12$$

$$e = E\mathrm{Sinh}\omega R = \frac{1}{D_1}\left[\frac{S_1 - S_2}{(T_1-T_2)(S_1-S_3)-(T_1-T_3)(S_1-S_2)}\right] \qquad 6.13$$

and the fluxes become:

$$(\phi_3 r) = \frac{a\mathrm{Sinh}\mu(R-r)}{\mathrm{Sinh}\mu R} + \frac{c\mathrm{Sinh}\nu(R-r)}{\mathrm{Sinh}\nu R} + \frac{e\mathrm{Sinh}\omega(R-r)}{\mathrm{Sinh}\omega R} \qquad 6.14$$

$$(\phi_2 r) = \frac{aS_1\mathrm{Sinh}\mu(R-r)}{\mathrm{Sinh}\mu R} + \frac{cS_2\mathrm{Sinh}\nu(R-r)}{\mathrm{Sinh}\nu R} + \frac{eS_3\mathrm{Sinh}\omega(R-r)}{\mathrm{Sinh}\omega R} \qquad 6.15$$

$$(\phi_1 r) = \frac{aT_1\mathrm{Sinh}\mu(R-r)}{\mathrm{Sinh}\mu R} + \frac{cT_2\mathrm{Sinh}\nu(R-r)}{\mathrm{Sinh}\nu R} + \frac{eT_3\mathrm{Sinh}\omega(R-r)}{\mathrm{Sinh}\omega R} \qquad 6.16$$

6.9 contd.

6.9.4 Results and Discussion.

Table 6.1 lists the values of the more important parameters obtained from solutions of equations discussed in Sections 6.9.2 and 6.9.3. Li^6 glass scintillator is almost "black" to thermal neutrons. This will considerably enhance the response due to epithermal (Group 2) neutrons, which may explain to a large extent the increase in the counting rate. Harmonics have been neglected in these calculations and it is assumed the source neutrons have the same spectrum as Group 1 neutrons which is not true as their mean energy is nearer 5 Mev compared with 2 Mev of fission neutrons.

The results of the calculation have also been used to plot graphs of (ϕr) against r for zero % void fraction for the fast flux, epithermal flux and thermal flux. These are all shown together in Fig.6.11.

Graphs of ($\phi_3 r$) against r and ($\phi_2 r$) against r for the void fractions 0%, 5% and 10% have also been plotted and are shown in Figs.6.12 and 6.13 respectively.

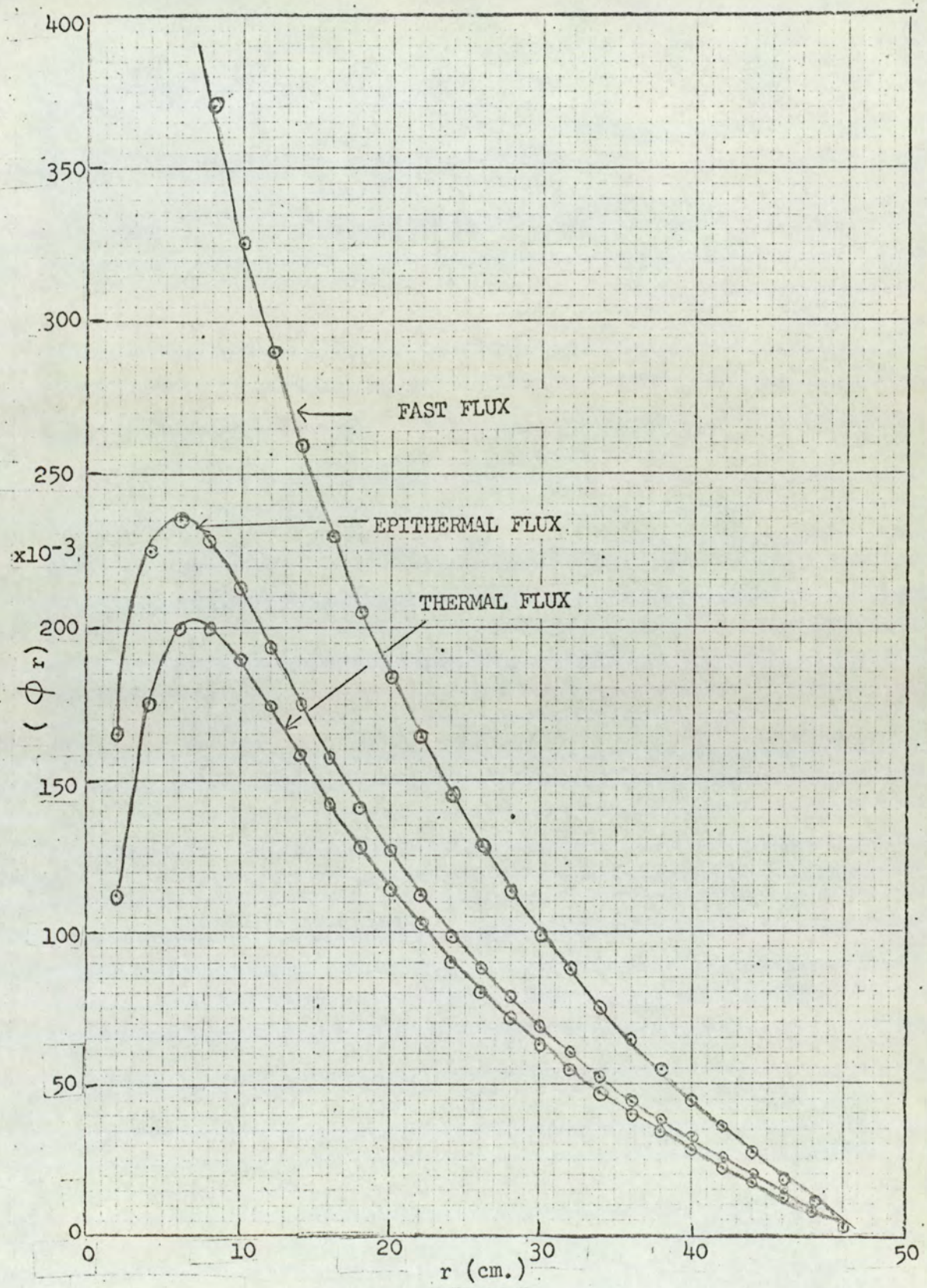

FIG.6.11 GRAPH OF (ϕr) AGAINST r FOR ZERO% VOID FRACTION

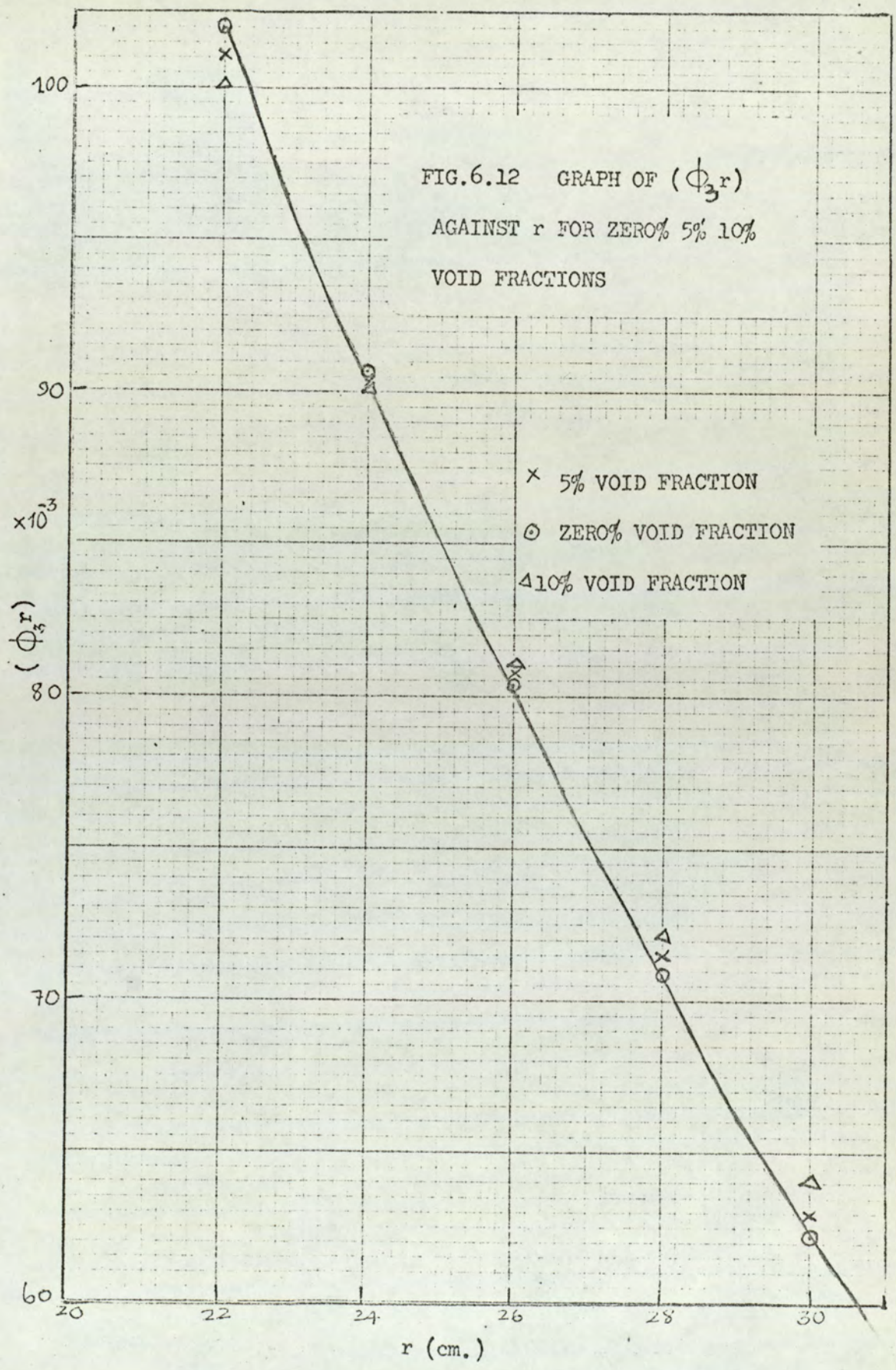

FIG.6.12 GRAPH OF $(\phi_3 r)$ AGAINST r FOR ZERO% 5% 10% VOID FRACTIONS

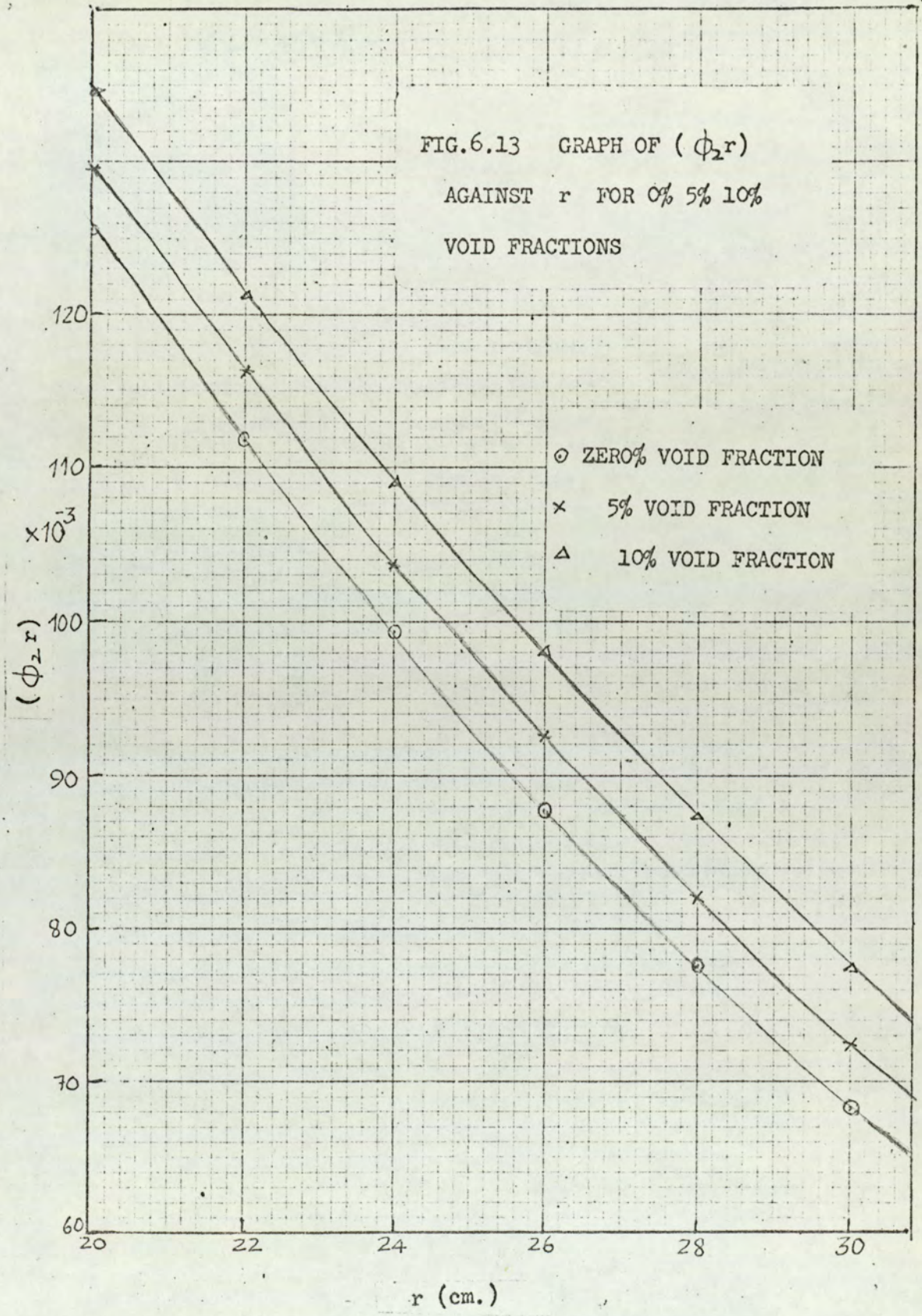
FIG.6.13 GRAPH OF ($\phi_2 r$) AGAINST r FOR 0% 5% 10% VOID FRACTIONS
⊙ ZERO% VOID FRACTION
× 5% VOID FRACTION
△ 10% VOID FRACTION
120
110
100
90
80
70
60
$\times 10^{-3}$
$(\phi_2 r)$
20
22
24
26
28
30
r (cm.)

TABLE 6.1

Calculated Parameters of Subcritical assembly from 3 group calculation.

PARAMETER	VOID FRACTION		
	0%	5%	10%
μ^2 cm^{-2}	0.002861	0.002451	0.002020
ν^2 cm^{-2}	0.152994	0.141296	0.130245
ω^2 cm^{-2}	0.350799	0.331609	0.311787
μ cm^{-1}	0.053488	0.049501	0.044944
ν cm^{-1}	0.391144	0.375894	0.360895
ω cm^{-1}	0.592283	0.575855	0.558379
S_1	+1.095717	+1.147968	+1.207935
S_2	+0.642586	+0.682913	+0.726954
S_3	+0.045572	+0.045469	+0.045977
T_1	+1.597086	+1.694543	+1.807167
T_2	-0.455603	-0.488004	-0.525810
T_3	-0.162399	-0.169025	-0.177725
a	+0.345789	+0.317510	+0.289382
c	-0.608242	-0.549154	-0.493775
e	+0.262452	+0.231643	+0.204393
$\phi_3(25.5)$	0.082771	0.082954	-0.083264
$\phi_2(25.5)$	0.090707	0.095246	0.100602

6.10 Conclusions.

It can be said in conclusion that the results of a simple experiment of the type discussed here could be adapted for use in predicting the presence of local fluctuations in an actual reactor. What is not certain, however, is whether the curve of fluctuations against some parameter such as changes in void fraction which cause fluctuations in the neutron population is easily predictable. The curve for a particular reactor can be easily determined if the source of fluctuations is known. The fluctuations caused by large changes in pressure or void fraction or other factors would present serious stability problems and their prediction by a simple technique such as has been outlined in this discussion will no doubt prove a useful tool to both the reactor operator and the designer. The technique would only enable the reactor operator to know about the presence of local fluctuations inside the reactor a finite time after their onset due to sampling time and the necessity for a large number of samples to be taken. However, with the high neutron fluxes present in reactors the sampling time could be much reduced compared with the experiment that has been described, and the delay could be reduced to perhaps 5 to 10 seconds instead of the 400 second sampling

6.10 contd.

time which was adopted here to reduce normal statistical fluctuations in count rate to a low enough value. Knowledge about the existence of local fluctuations inside the core would, therefore, give sufficient warning to an operator about the possible onset of more extensive fluctuations or other serious phenomenon taking place in the whole core despite the finite delay.

CHAPTER 7.

GENERAL CONCLUSIONS.

The results of the main experiments and calculational methods adopted have been discussed in the relevant chapters. The following general conclusions may be drawn however. Calculation of multiplication changes in a reactor is a long tedious and somewhat uncertain procedure. Reactor neutron energy spectrum spreads from about 10 Mev down to zero which means that for a solution to be possible approximations must be made, e.g. multigroup diffusion theory as used here. More groups should mean higher accuracy but cross section data are more inaccurate for many group theory. For few groups comparison with experiment yields more accurate average cross sections.

It can be said further that comparison between experiment and theory has shown the three group model to be sufficiently accurate to predict the effect of voids provided sufficient care is taken in calculating thermal neutron fine structure. Synthesis of steam voids by air bubbles has been shown to be adequate to simulate bulk boiling conditions and multiplication changes can be measured adequate using a subcritical system.

One further conclusion which could be drawn from this work is that with the help of an on-line computer which might be already present on site it would be possible to predict the presence of local fluctuations in neutron population by quite simple analytical techniques.

A P P E N D I X 1.

COMPUTER PROGRAMME P.1
(TRANSVERSE FLUX FIT.)

```
TRANSVERSE FLUX FIT'
BEGIN
INTEGER K,L,M,N'
REAL D,E,G,H,J,W,W1,W2,A,B,Q,Q1,Q2,SD,P,R,Z'
SWITCH SSS:=REPEAT'
REPEAT:
READ K,L'
PRINT DIGITS(2),ΣΣL2??,K'
BEGIN
REAL ARRAY C1(1:L),C3(1:L),X(1:L),F(1:L),S1(1:L),S3(1:L)'
SWITCH SS:=AGAIN'
READ W'
FOR N:=1 STEP 1 UNTIL L DO
READ X(N),F(N)'
M:=0'
AGAIN:
D:=0'
E:=0'
G:=0'
H:=0'
J:=0'
Q:=0'
P:=0'
FOR N:=1 STEP 1 UNTIL L DO
BEGIN
C1(N):=COS(W*X(N))'
C3(N):=COS(3*W*X(N))'
S1(N):=SIN(W*X(N))'
S3(N):=SIN(3*W*X(N))'
D:=D+F(N)*C1(N)'
E:=E+C1(N)*C3(N)'
G:=G+C1(N)*C1(N)'
H:=H+F(N)*C3(N)'
J:=J+C3(N)*C3(N)'
END'
A:=CHECKR((D*J-H*E)/(G*J-E*E))'
B:=CHECKR((D-A*G)/E)'
Z:=0.01*A*A'
FOR N:=1 STEP 1 UNTIL L DO
BEGIN
R:=(A*A*C1(N)*S1(N)+3*B*B*C3(N)*S3(N)-F(N)*(A*S1(N)+3*B*S3(N))
      +A*B*(S1(N)*C3(N)+3*C1(N)*S3(N)))'
P:=P+R'
Q:=Q+X(N)*R'
END'
M:=M+1'
IF M=1 AND ABS(Q) GREQ Z THEN
```

```
BEGIN
Q1:=CHECKR(Q)'
W1:=CHECKR(W)'
W:=W*0.99'
GOTO AGAIN
END'
IF M=2 AND ABS(Q) GREQ Z THEN
BEGIN
Q2:=CHECKR(Q)'
W2:=CHECKR(W)'
W:=(Q1*W2-Q2*W1)/(Q1-Q2)'
GOTO AGAIN
END'
IF M GREQ 3 AND ABS(Q) GREQ Z THEN
BEGIN
Q1:=Q2'
W1:=W2'
Q2:=CHECKR(Q)'
W2:=CHECKR(W)'
W:=(Q1*W2-Q2*W1)/(Q1-Q2)'
GOTO AGAIN
END'
D:=0'
FOR N:=1 STEP 1 UNTIL L DO
BEGIN
E:=F(N)-A*C1(N)-B*C3(N)'
E:=E*E'
D:=D+E'
END'
SD:=SQRT(D/L)'
PRINT FREEPOINT(6),W,PREFIX(££S1??),A,B,SD,Q,P'
END'
GOTO REPEAT'
END OF PROGRAM'
```

TABLE A.1.1 - Typical Output of Computer Programme

1					
.037869	.555389	.073685	.015995	-.002981	.033947
2					
.035855	.246660	.039201	.005163	-.000214	.004304
3					
.036461	.259969	.036455	.006243	-.000371	.004080
4					
.036450	.249896	.033052	.070376	-.000292	.007405

A P P E N D I X 2.

COMPUTER PROGRAMME P.2

(EXPONENTIAL FLUX FIT)

```
EXPONENTIAL FLUX FIT'
BEGIN
 INTEGER L,M,N'
REAL S1,S2,S3,S4,DY,K,A,D,SD,DK'
SWITCH SS:=REPEAT'
REPEAT:
READ L,M'
PRINT DIGITS(2),L'
BEGIN
REAL ARRAY Z(1:M),F(1:M),Y(1:M)'
FOR N:=1 STEP 1 UNTIL M DO
READ Z(N),F(N)'
S1:=0'
S2:=0'
S3:=0'
S4:=0'
DY:=0'
FOR N:=1 STEP 1 UNTIL M DO
BEGIN
Y(N):=LN(F(N))'
S1:=S1+Z(N)'
S2:=S2+Z(N)*Z(N)'
S3:=S3+Y(N)'
S4:=S4+Y(N)*Z(N)'
END'
K:=(M*S4-S3*S1)/(M*S2-S1*S1)'
A:=(1/M)*(S3-K*S1)'
FOR N:=1 STEP 1 UNTIL M DO
BEGIN
D:=Y(N)-K*Z(N)-A'
D:=D*D'
DY:=DY+D'
END'
SD:=DY/(M-2)'
DK:=(1/K)*SQRT(SD/(S2-S1*S1/M))'
PRINT ALIGNED(1,6),K,PREFIX(££S2??),DK,SD'
END'
GOTO REPEAT'
END OF PROGRAM'
```

TABLE A.2.1 - Typical Output of Computer Programme

1		
-0.074203	-0.040107	0.004786
2		
-0.074416	-0.025471	0.001941
3		
-0.075826	-0.034175	0.003628
4		
-0.074098	-0.027034	0.002168
5		
-0.074396	-0.024003	0.001723

APPENDIX 3.

TABLE A.3.1 Typical Indium Foil Parameters.

Group	Foil No.	Wt.in gm.	Diameter cm.	Lineal Thickness cm $\times 10^{-2}$	Thickness mg.cm^{-2}	Flux Depression Factor.
	57	.0561	.948	1.09	79.48	.865
	67	.0567	.948	1.10	80.33	.864
I	74	.0568	.956	1.08	79.13	.866
	64	.0571	.950	1.11	84.65	.864
	70	.0574	.950	1.11	80.98	.864
	73	.0576	.951	1.15	81.13	.864
	23	.0580	.938	1.15	83.93	.860
	47	.0581	.934	1.16	84.80	.860
	32	.0585	.938	1.16	84.66	.860
	53	.0586	.957	1.11	81.47	.864
	54	.0587	.946	1.14	83.52	.860
	72	.0591	.951	1.14	83.24	.860

APPENDIX 4

CROSS SECTION DATA

TABLE A.4.1 Wigner-Wilkins Cross Sections
(Taken from WAPD-185 (1958)[31]

T°K	$\sigma_o(1/v)$	N_5/N_H	σ(unit $1/v$) barns	σ_s(u-235) barns	σ_{tr}(H) barns
293	0	0	0.8867	589.8	35.63
		0.005	0.7365	481.8	29.49
		0.010	0.6494	419.4	25.92
		0.015	0.5923	378.7	23.57
		0.020	0.5518	349.9	21.90
	2	0	0.7870	578.1	31.5
		0.005	0.6798	441.3	27.16
		0.010	0.6128	393.4	24.41
		0.015	0.5666	360.5	22.51
		0.020	0.5326	336.3	21.10
	4	0	0.7166	467.8	28.67
		0.005	0.6366	410.5	25.39
		0.010	0.5833	372.5	23.20
		0.015	0.5451	345.3	21.62
		0.020	0.5162	324.7	20.42
	6	0	0.6647	430.7	26.54
		0.005	0.6025	386.2	23.99
		0.015	0.5269	332.4	20.87
		0.020	0.5020	314.7	19.83

TABLE A.4.2 Three Group Cross Section Data
(Taken From Deutch[33])

Material	Group 1		Group 2			Above Thermal	Group 3	
	σ_{tr} barns	σ_r barns	σ_{tr} barns	σ_r barns	σ_a barns	σ_s barns	σ_{tr} barns	σ_a barns
H	1.47	0.985	6.40	1.220	0.016	- +	- +	0.330
O	3.09	0.099	3.64	0.0337	0	3.8	3.64	0
Aℓ	3.08	0.118	1.78	0.0088	0.0143	1.4	1.365	0.230
U^{235}	9.0	0.020	9.0	0.0052	- *	10.0	9.97	-++
U^{238}	9.0	0.020	9.0	0.0052	-**	10.0	9.97	2.72

U^{235} $\eta_2 = 1.814$ $\eta_3 = 2.07$

* σ_{a52} value adopted was 22.2 barns (Section 5.6.1.1)

** σ_{as2} value adopted was 0.915 barns (Section 5.6.1.2)

\+ Values adopted are listed in Table A.7.4

++ Values adopted were obtained from Table A.4.1 in manner described in Section 5.5.

APPENDIX 5.

THE CELL CALCULATION METHOD OF AMOUYAL, BENOIST AND HOROWITZ[34]

(ABH METHOD OF CALCULATION)

A.5.1 Assumptions.

The calculations are carried out for the equivalent single cell subject to the following assumptions:

(i) Current is zero at the outer surface of the cell.

(ii) Thermal slowing down density is constant in the moderator and zero in the fuel.

(iii) All thermal neutrons in the cell have the same energy.

(iv) Diffusion theory is not assumed to be valid, at least not in the fuel.

A.5.2 Thermal Utilization factor.

The ABH method enables a calculation of the thermal utilization factor to be made to a good accuracy. The starting point of the calculation is the definition of thermal utilization factor, f given in Equation A.5.1.

$$f = \frac{\Sigma_{af} V_f \Phi_f}{\Sigma_{af} V_f \Phi_f + \Sigma_{am} V_m \Phi_m} \qquad \text{A.5.1}$$

where Σ_{af} = Macroscopic absorption cross section of fuel

Σ_{am} = Macroscopic absorption cross section of moderator

V_f = Volume of fuel in cell

A.5.2 contd.

V_m = Volume of moderator in cell

Φ_f = Average flux in fuel

Φ_m = Average flux in moderator

Rearrangement of Equation A.5.1 yields:

$$\frac{1}{f} = 1 + \frac{\Sigma_{am} V_m \Phi_m}{\Sigma_{af} V_f \Phi_f} \qquad \text{A.5.2}$$

From Equation A.5.2

$$\frac{\Phi_m}{\Phi_f} = \left(\frac{1}{f} - 1\right) \frac{\Sigma_{af} V_f}{\Sigma_{am} V_m} \qquad \text{A.5.3}$$

A.5.3 Flux Weighting Factors.

A.5.3.1 Average Flux in Unit Cell.

The average flux, Φ in the cell may be defined by the following equation:

$$\Phi = \frac{\Phi_m V_m + \Phi_f V_f}{V_m + V_f} \qquad \text{A.5.4}$$

Rearrangement of Equation A.5.4 leads to the following equation :

$$\frac{\Phi_f}{\Phi} = \frac{1 + \frac{V_f}{V_m}}{\Phi_m/\Phi_f + \frac{V_f}{V_m}} \qquad \text{A.5.5}$$

A.5.3.2 Flux Weighting Factor for Fuel.

The flux weighting factor for the fuel W_f is defined as:

A.5.3 contd.

A.5.3.2 contd.

$$W_f = \frac{\Phi_f}{\Phi} \qquad \text{A.5.6}$$

It can be seen from Equation A.5.5 that the evaluation of Φ_f/Φ i.e. W_f depends on the quantities V_f/V_m and Φ_m/Φ_f being known.

Now V_f/V_m is easily determined from the following relationship:-

$$\frac{V_m}{V_f} = \frac{b^2 - a^2}{a^2} \qquad \text{A.5.7}$$

where a = radius of fuel element

b = radius of equivalent cell.

$\frac{\Phi_m}{\Phi_f}$ is obtained from the ABH formulation starting from the following equation

$$\frac{1}{f} - 1 = \frac{1}{p_f} \times \frac{\Sigma_{am} V_m}{\Sigma_{af} V_f} + \frac{1-p_m}{p_m} - \frac{4\Sigma_{am} V_m}{S_f} \qquad \text{A.5.8}$$

where p_f is the probability that neutrons produced uniformly within the fuel lump ultimately escape from the lump without being absorbed.

p_m is the probability that a neutron born uniformly and isotropically in the moderator crosses the surface between the fuel and moderator.

A.5.3 contd.

A.5.3.2 contd.

S_f is the surface area of the fuel.

Combination of Equations A.5.3 and A.5.8 yields:

$$\frac{\Phi_m}{\Phi_f} = \frac{1}{p_f} + \frac{\Sigma_{af} V_f}{\Sigma_{am} V_m}\left[\frac{1 - p_m}{p_m}\right] - \frac{4\Sigma_{af} V_f}{S_f} \qquad \text{A.5.9}$$

p_f is defined as follows:

$$\frac{1}{p_f} = 1 + \frac{\Sigma_{af}}{\Sigma_{tf}}\left\{A\left[1 + \alpha\left(\frac{\Sigma_{sf}}{\Sigma_{tf}}\right) + \beta\left(\frac{\Sigma_{sf}}{\Sigma_{tf}}\right)^2\right] + a\Sigma_{tf}\right\} \qquad \text{A.5.10}$$

where Σ_{sf} = Macroscopic Scattering Cross Section for fuel

Σ_{tf} = Macroscopic Total Cross Section for fuel

A.5.3.3 Calculation of $^1/p_f$

$^1/p_f$ is defined in Equation A.5.10. All the macroscopic cross sections given in this equation are easily calculated. The parameters needing special methods of calculation are A, α and β.

To obtain A, use is made of the values of A listed as a function of $a \times \Sigma_{tf}$ by Amouyal, Benoist and Horowitz[34]. A copy of this is given in Table 4-9 of ANL-5800[3]. Alternatively A is obtained

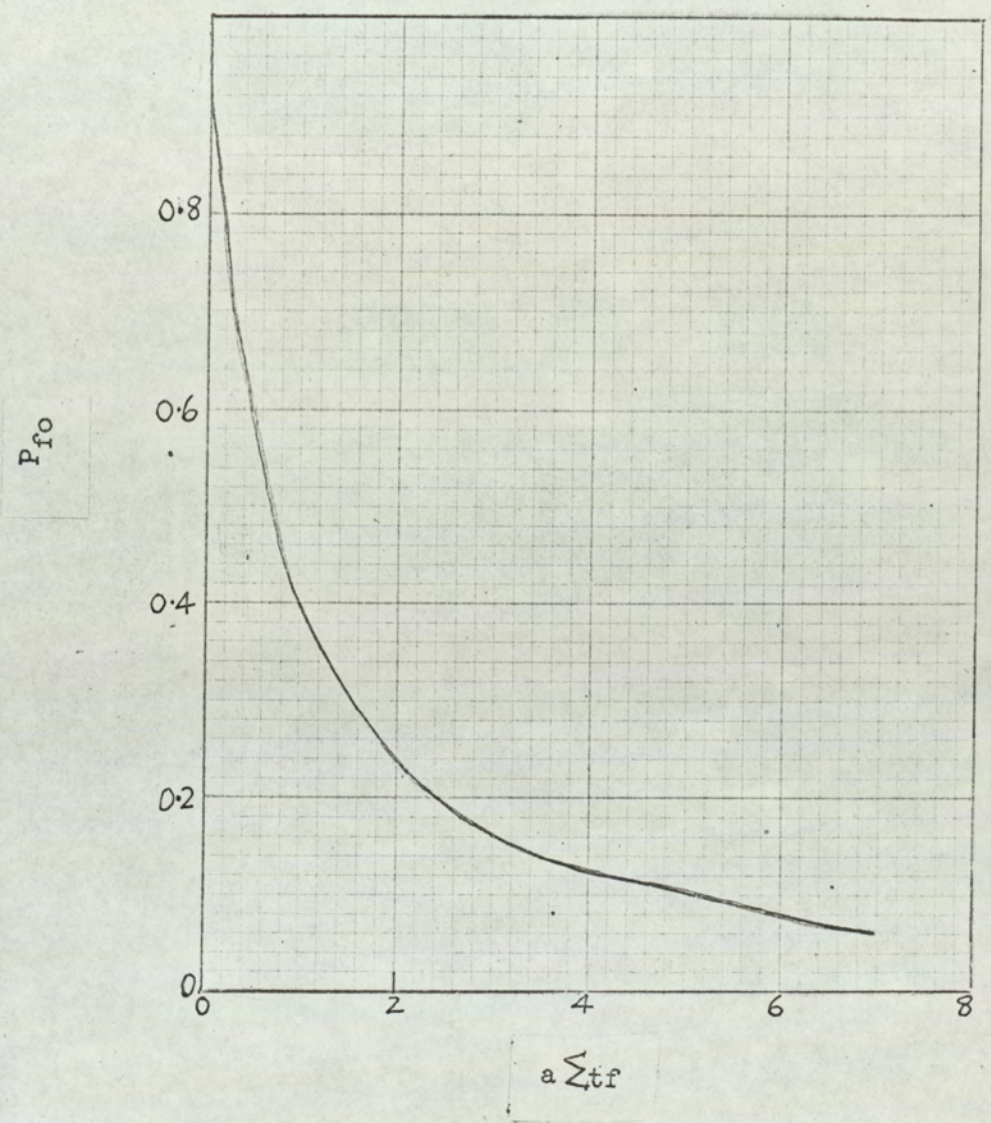

FIG.A.5.1 THE PROBABILITY THAT A NEUTRON ESCAPES FROM AN INFINITE CYLINDER OF RADIUS a AND MACROSCOPIC CROSS SECTION

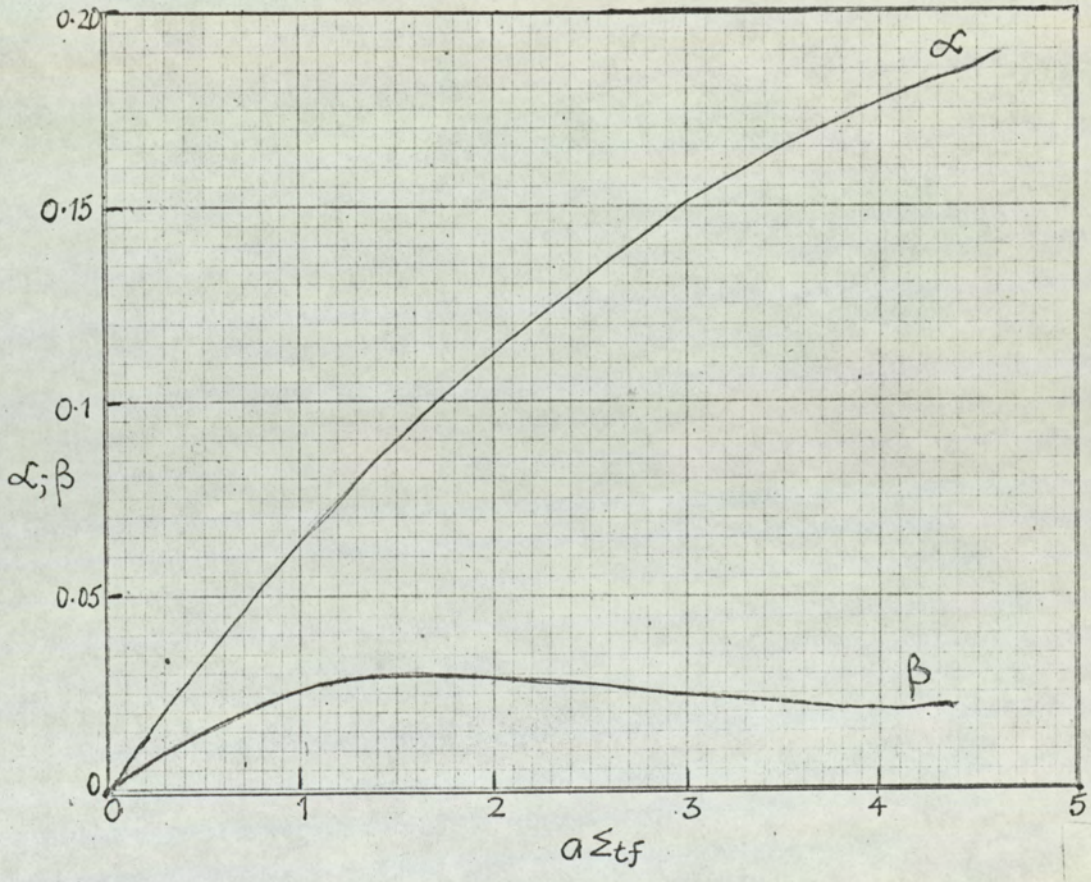

(34)

FIG.A.5.2 THE PARAMETER α AND β AS A FUNCTION OF $a\Sigma_{tf}$

A.5.3 contd.

A.5.3.3 contd.

from this relationship:

$$A = \frac{1 - p_{fo}}{p_{fo}} - \Sigma_{tf} \qquad \text{A.5.11}$$

p_{fo} is the probability of a neutron escaping without collision.

Lamarsh[35] gives a graph of p_{fo} against $a\Sigma_{tf}$ for infinite cylinder of radius a. A copy of this graph is given in Fig.A.5.1. Using this graph and Equation A.5.11 the value of A is easily determined.

To obtain the values of α and β use is made of Fig.A.5.2 which gives values of α and β for various values of $a\Sigma_{tf}$. The graph was taken from Fig.2 of Amouyal,Benoist and Horowitz[34]. Copies of this graph also appear in Lamarsh[35] and ANL-5800[3]

A.5.3.4 Calculation of p_m

p_m is defined as follows:

$$1/p_m = \frac{V_m \, a \, d}{2 F_f L_m^2} + E(K_{ma}, K_{mb}) \qquad \text{A.5.12}$$

where $E(K_{ma}, K_{mb})$ is the lattice function

$$K_m^2 = 1/L_M^2 = 3\Sigma_{tm} \Sigma_{am} \qquad \text{A.5.13}$$

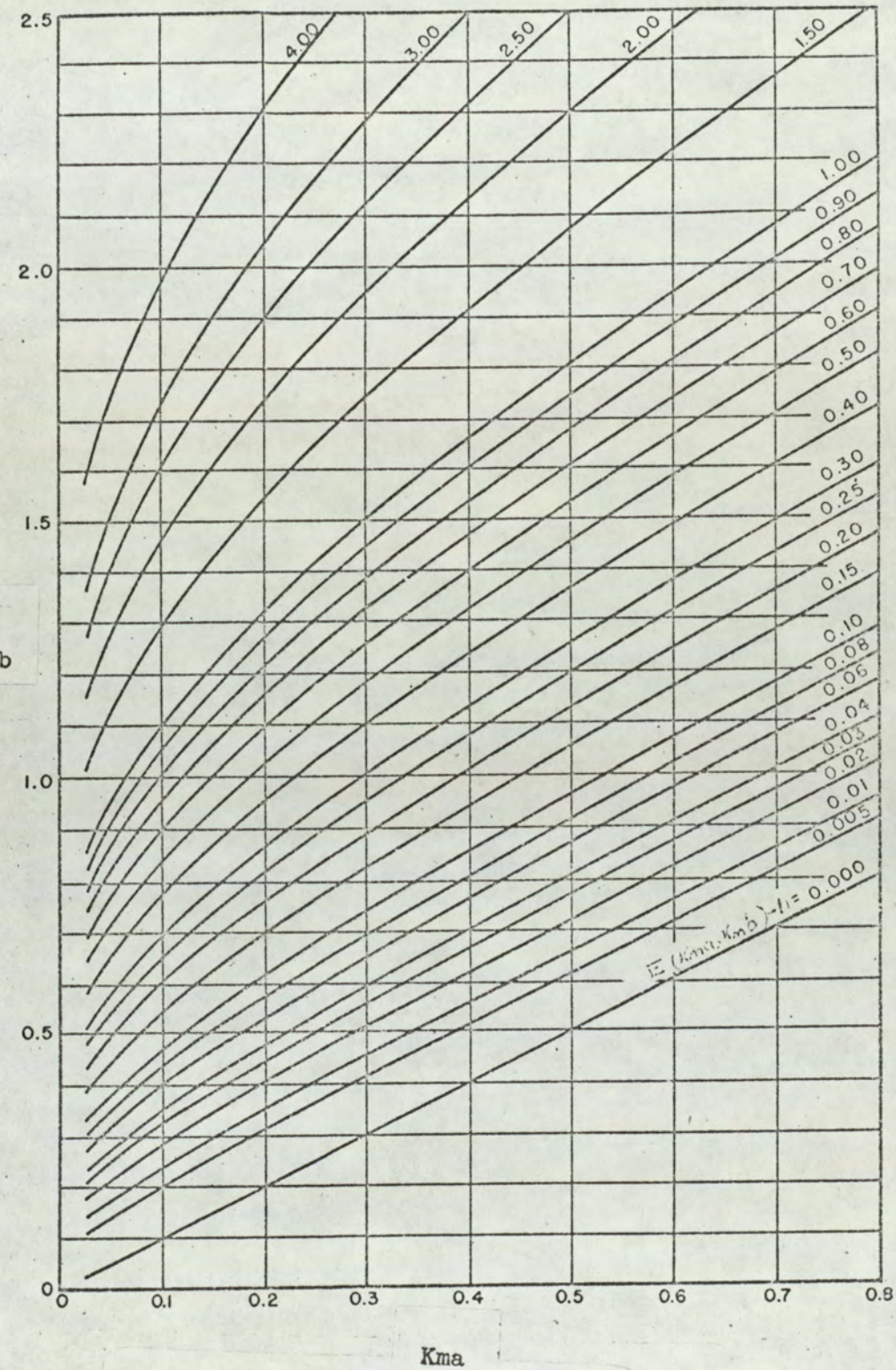

FIG.A.5.3 CONTOURS OF LATTICE FUNCTION E(Kma Kmb) FOR CYLINDRICAL RODS. (54)

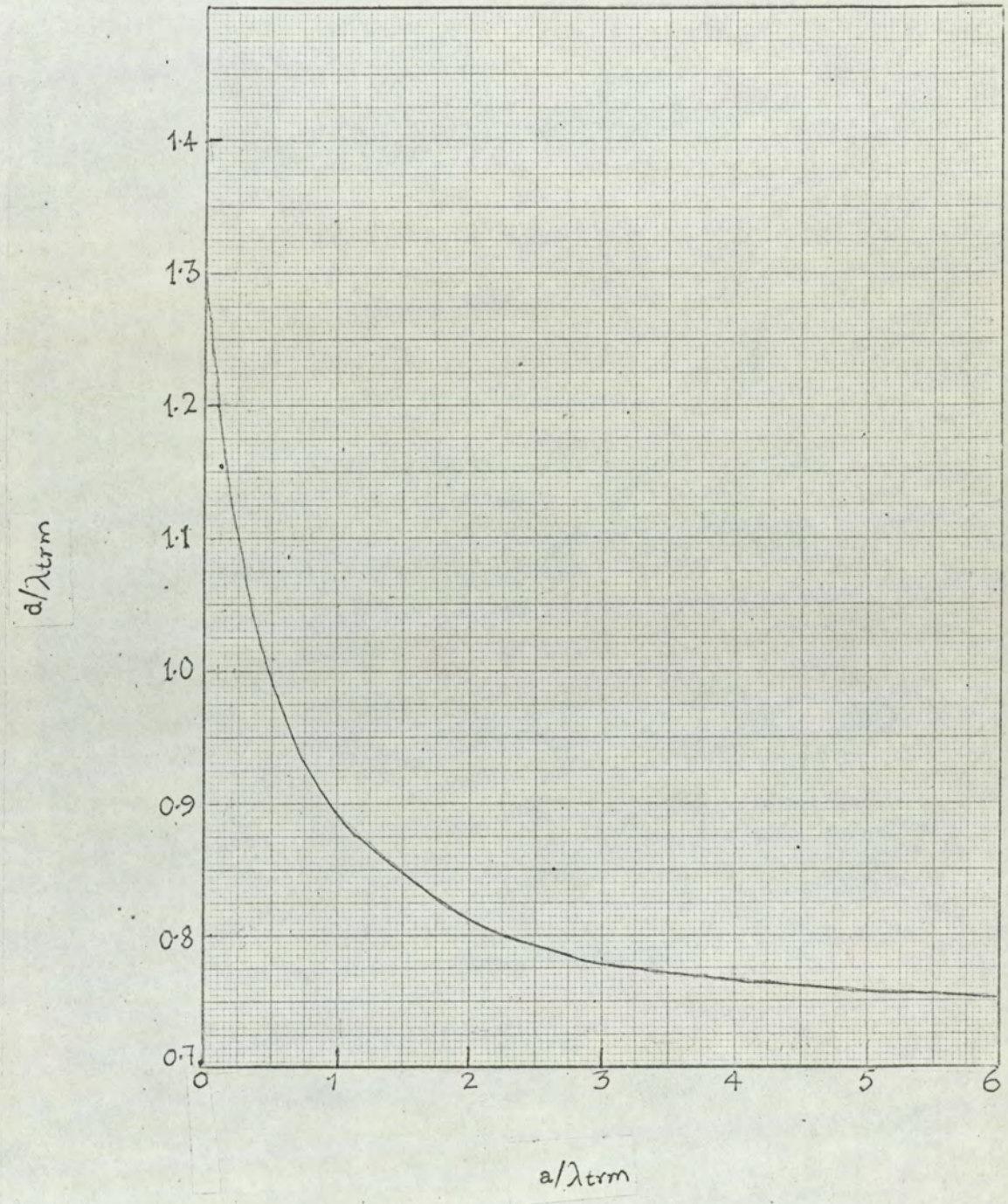

FIG.A.5.4 THE PARAMETER d(IN UNITS OF λ_{trm}) AS A FUNCTION OF THE RADIUS a (ALSO IN UNITS OF λ_{trm}) (35)

A.5.3 contd.

A.5.3.4 contd.

By means of Equation A.5.13 the value of K_m is easily calculated. With the values of a and b known, the values of K_{ma} and K_{mb} are easily calculated. To obtain the value of $E(K_{ma},K_{mb})$ use is made of Fig.A.5.3 which gives contours of the lattice function $E(K_{ma},K_{mb})- 1$ for cylindrical rods. Fig.A.5.3 was taken from USAEC Report AECD-3645[54]. From Fig.A.5.3 the value of $E(K_{ma},K_{mb})- 1$ corresponding to the lattice for the different conditions of voids is determined.

The next parameter to calculate is d which is determined from Fig.A.5.4. This graph gives d/λ_{trm} as a function a/λ_{trm} where λ_{trm} is the transport mean free path of the surrounding medium i.e. of the moderator. Fig.A.5.4 was taken from Lamarsh[35] who based his graph on the work of Davison[55] and Zeretsky[56].

The value of a/λ_{trm} is calculated for each condition of voids in the system and from Fig.A.5.4 the value of d/λ_{trm} is easily determined. As λ_{trm} is known, the value of d is easily calculated.

A.5.3 contd.

A.5.3.4 contd.

The value of p_m is now easily calculated since all the parameters on which p_m depends as given in Equation A.5.12 are known.

With the values of $^1/p_f$ and p_m known $\frac{\Phi_m}{\Phi_f}$ is easily calculated from Equation A.5.9. This means the flux weighting factor for $\frac{\Phi_f}{\Phi}$ i.e. W_f as defined in Equation A.5.5 can now be calculated.

A.5.3.5 Flux Weighting Factor for Moderator.

The flux weighting for the moderator W_m is defined as:

$$W_m = \frac{\Phi_m}{\Phi} \qquad \text{A.5.14}$$

Having already calculated the value of Φ_f/Φ i.e. W_f the value of the flux weighting factor for the moderator is obtained from the following relationship:

$$\frac{\Phi_m}{\Phi} = \frac{\Phi_m}{\Phi_f} \times \frac{\Phi_f}{\Phi} \qquad \text{A.5.15}$$

A.5.3.6 Flux Weighting Factor for Can.

The flux weighting factor W_c for the can does not appear to come out of the ABH

A.5.3 contd.

A.5.3.6 contd.

calculation method. The value adopted in the calculations (Chapter 5) was half-way between W_m and W_f which was not expected to introduce a great error in view of the small absorption by the can.

APPENDIX 6.

THE DANCOFF-GINSBERG CORRECTION FACTOR[45]

A.6.1 Introduction.

In a lattice of rods the presence of one rod depletes the flux at the peak of the resonance which is incident on another rod and thus leads to a reduction of the effective surface. To correct for this the Dancoff-Ginsberg correction factor, C is applied.

It is necessary to obtain the sum

$$C = \Sigma C_i \qquad \text{A.6.1}$$

where C_i is the lump-to-lump Dancoff-Ginsberg factor and the sum is carried out over all lumps in the lattice. The parameters C_i are functions of two variables, a/λ_{tm} and d_i/a where λ_{tm} is the mean free path in the moderator, d_i is the distance to the i^{th} lump and a is the radius of the lump (all lumps assumed to be identical). Extensive tables of C_i have been prepared and are given for example in ANL-5800[3]. As would be expected physically, the value of C_i decreases sharply with increasing d_i/a and it is usually necessary to include only a few terms in Equation A.6.1. It can be shown that to a good approximation the effect of the interaction between fuel lumps in a closely packed lattice is equivalent to a reduction in the surface area of a single lump by a factor 1-C.

A.6.2 Determination of the Dancoff-Ginsberg Factor for the Subcritical Assembly.

This is best done by considering the diagram shown in Fig.A.6.1

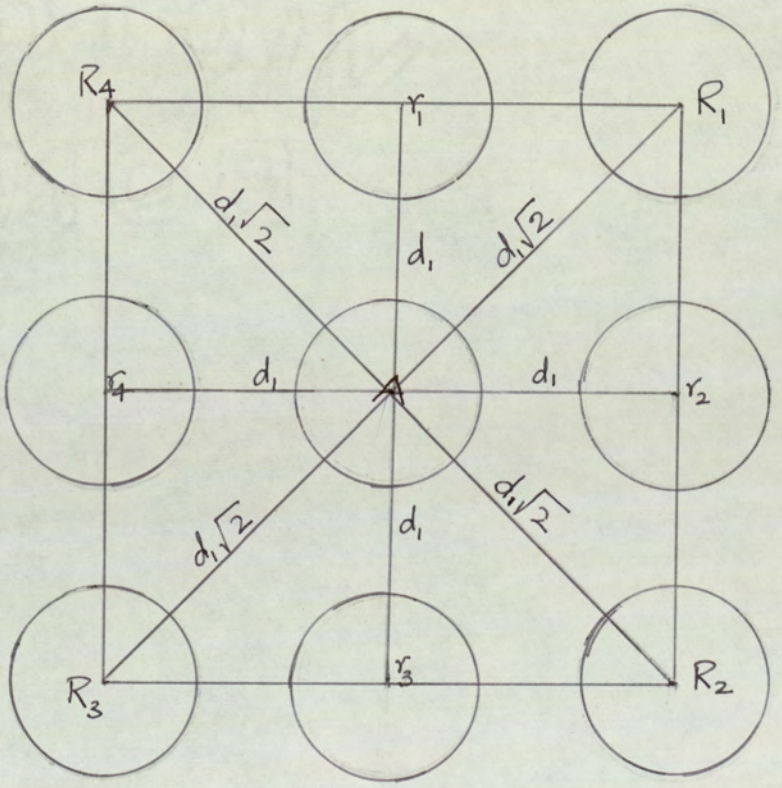

Fig.A.6.1 Dancoff factor for Subcritical Assembly.

Consider a bar of uranium in position A shown in Fig.A.6.1. The rods in positions r_1, r_2, r_3 and r_4 are each at a distance of d_1 from the centre of A and d_1 in this case is the lattice pitch. The rods in positions R_1, R_2, R_3, R_4 are each at a distance

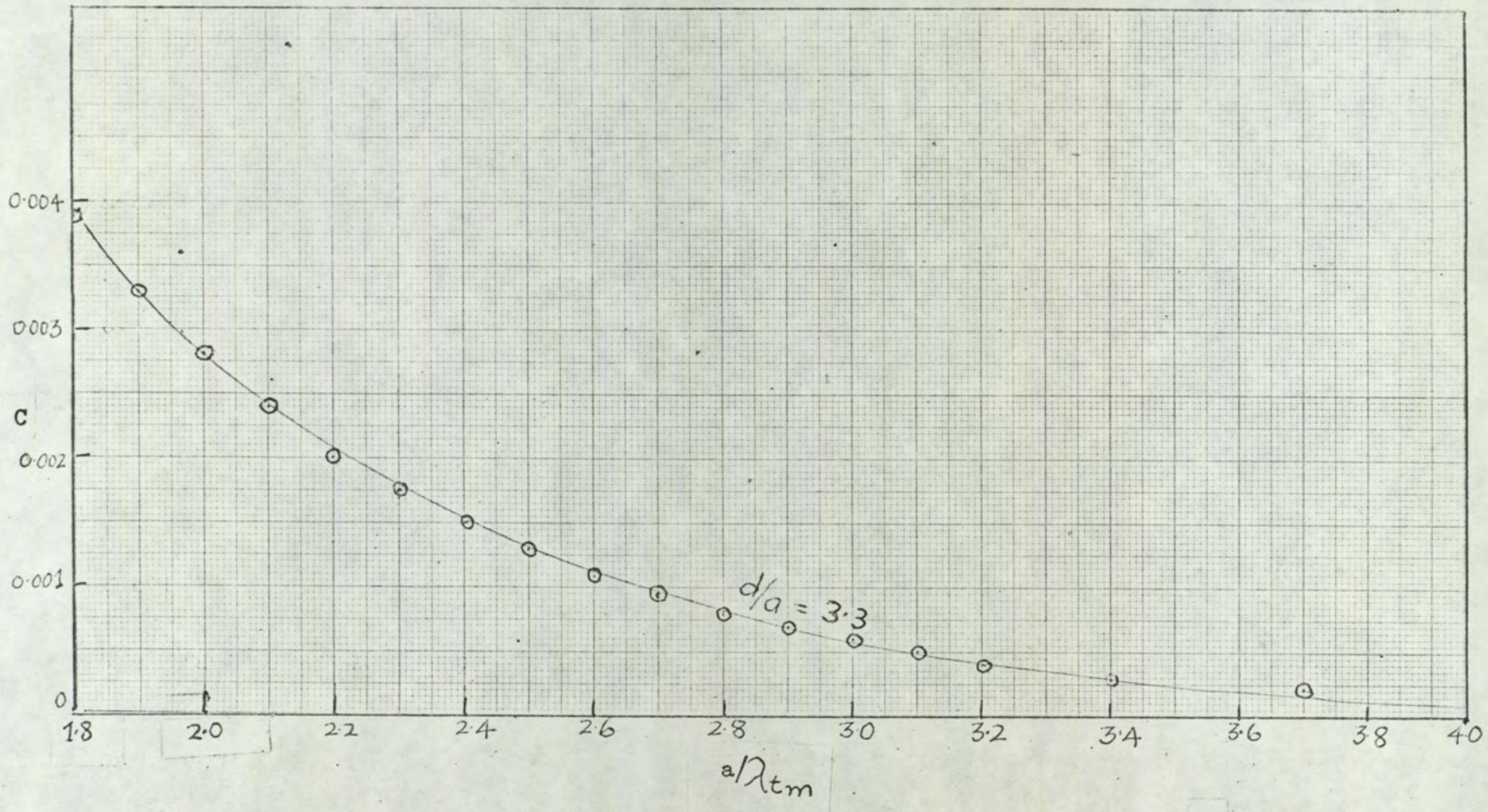

FIG.A.6.2 DANCOFF FACTOR C AGAINST RADIUS a (IN UNITS OF $\lambda_{tm}^{(3)}$)

A.6.2 contd.

$d_1\sqrt{2}$ from the centre of A. The Dancoff-Ginsberg correction factor due to these two groups of rods i.e. r_1, r_2, r_3, r_4 on one hand and R_1, R_2, R_3, R_4 on the other hand is to be determined. From the tables of C_i given in ANL-5800[3] a graph of C is plotted against a/λ_{tm}. This is shown in Fig.A.6.2 and relates to the d/a values for the subcritical assembly. The d/a values of interest in this calculation are 3.3 and 4.7 for the rods r_1, r_2, r_3, r_4 and R_1, R_2, R_3, R_4 respectively [d_1 = 1.9 in. and a = 0.575 in]. From Fig.A.6.2 the value of C corresponding to a/λ_{tm} for each condition of voids in the assembly is read off. The value of C obtained in each case is multiplied by 4 as there are four rods in each group under consideration. This calculation yields the total Dancoff-Ginsberg correction factor, C for the assembly.

Now as the effect of interaction between fuel elements in a closely packed lattice is equivalent to a reduction of surface area of a single element by a factor 1-C it is therefore necessary to multiply the actual surface area, S_f of a bar by 1-C. The value $S_f(1-C)$ is the effective surface area which is used in the determination of the effective resonance integral.

The value of a/λ_{tm} for the subcritical

A.6.2 contd.

assembly was of the order of 3.9 giving a C value of about 0.0002 which is a very small correction.

APPENDIX 7

PARAMETERS RELATED TO THEORETICAL CALCULATION OF B_m^2

TABLE A.7.1 Calculated Number Densities

Void Fraction	Number Densities - $N_i \times 10^{24}$						
	H_2O**	H	O	Natural Uranium*	U^{235}	U^{238}	Aℓ
0%	.022399	.044798	.022399	.0133692	.000096	.013273	.002259
5%	.021279	.042558	.021279	.0133692	.000096	.013273	.002259
10%	.020159	.040318	.020159	.0133692	.000096	.013273	.002259
15%	.019039	.038078	.019039	.0133692	.000096	.013273	.002259
20%	.017919	.035838	.017919	.0133692	.000096	.013273	.002259

*Density of Natural Uranium adopted was 18.36 gm/cc. The figure was obtained from the dimensions and weight of fuel as given by the U.K.A.E. who supplied the fuel.

** The density of water was taken as 1 gm/cc for zero % void fraction, 0.95 gm/cc for 5% void fraction, 0.90 gm/cc for 10% void fraction and so on.

TABLE A.7.2 Calculated Thermal Microscopic Absorption Cross Sections.

Void Fraction	Thermal Absorption Cross Section in Barns				
	U^{235}	U^{238}	Oxygen	H	Al
0%	544.03	2.239	0	.272	.189
5%	541.78	2.230	0	.271	.189
10%	539.00	2.220	0	.269	.188
15%	536.17	2.209	0	.268	.187
20%	531.86	2.190	0	.266	.185

TABLE A.7.3 Calculated Values of N_H/N_f for Various Void Fractions.

Void Fraction	N_H/N_U
0%	3.35
5%	3.18
10%	3.02
15%	2.85
20%	2.68

TABLE A.7.4 Calculated Microscopic Transport and Scattering Cross Sections for Hydrogen.

Void Fraction	σ_{tr} barns	σ_{s} barns
0%	33.02	38
5%	32.89	37.90
10%	32.74	37.76
15%	32.57	37.63
20%	32.33	37.47

TABLE A.7.5 Calculated Macroscopic Absorption Cross Sections.

Void Fraction	Macroscopic Absorption Cross Section cm^{-1}				
	H	Oxygen	U^{235}	U^{238}	Aℓ
0%	.014451	0	.029640	.016820	.000374
5%	.013644	0	.029935	.016990	.000375
10%	.012776	0	.030352	.017082	.000375
15%	.012001	0	.030605	.017387	.000374
20%	.011115	0	.031434	.017848	.000372

TABLE A.7.6 Calculated Macroscopic Transport Cross Sections

Void Fraction	Macroscopic Transport Cross Sections. Cm^{-1}				
	H	Oxygen	U^{235}	U^{238}	Al
0%	1.754367	.096697	.000543	.074899	.002701
5%	1.655884	.091630	.000551	.075958	.002710
10%	1.554973	.086440	.000561	.077414	.002720
15%	1.458476	.081499	.000569	.078472	.002729
20%	1.350977	.076053	.000589	.081251	.002744

APPENDIX 8.

TABLE A.8.1 Resonance Integrals for U^{238} at 300°K
(Taken from ANL-5800[3])

$\frac{S_f}{M_f}$ cm²/gm	I_{eff}
0	4.93
0.01	6.83
0.05	9.33
0.10	11.44
0.20	14.64
0.30	17.22
0.40	19.45
0.50	21.43
0.60	23.23
0.70	24.88
0.80	26.46
0.90	27.94
1.00	29.34
1.20	31.94

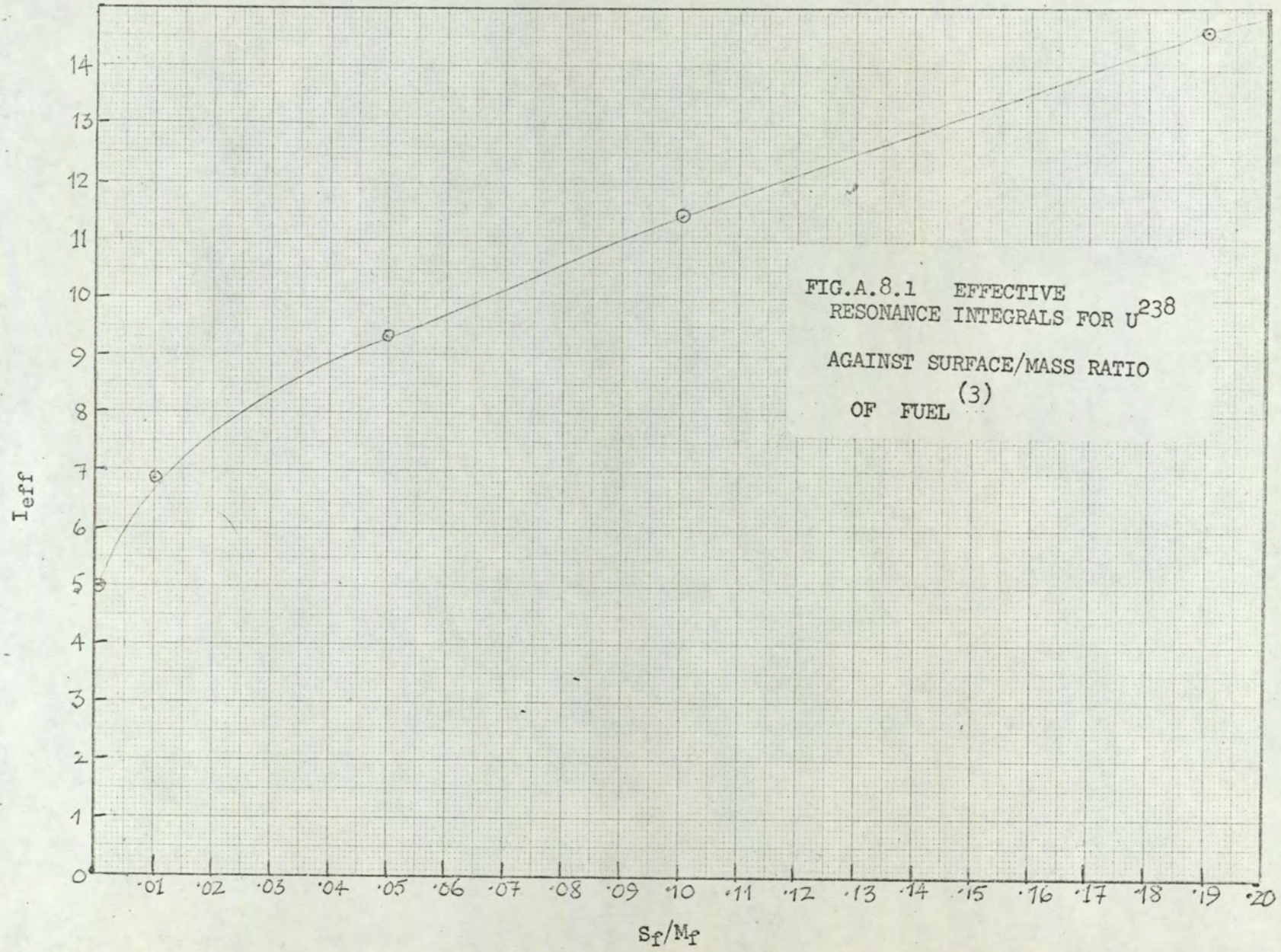

FIG.A.8.1 EFFECTIVE RESONANCE INTEGRALS FOR U^{238} AGAINST SURFACE/MASS RATIO OF FUEL (3)

APPENDIX 9

FAST FISSION FACTOR, ϵ
AGAINST RATIO OF HYDROGEN
TO FUEL ATOMS (N_H/N_f)

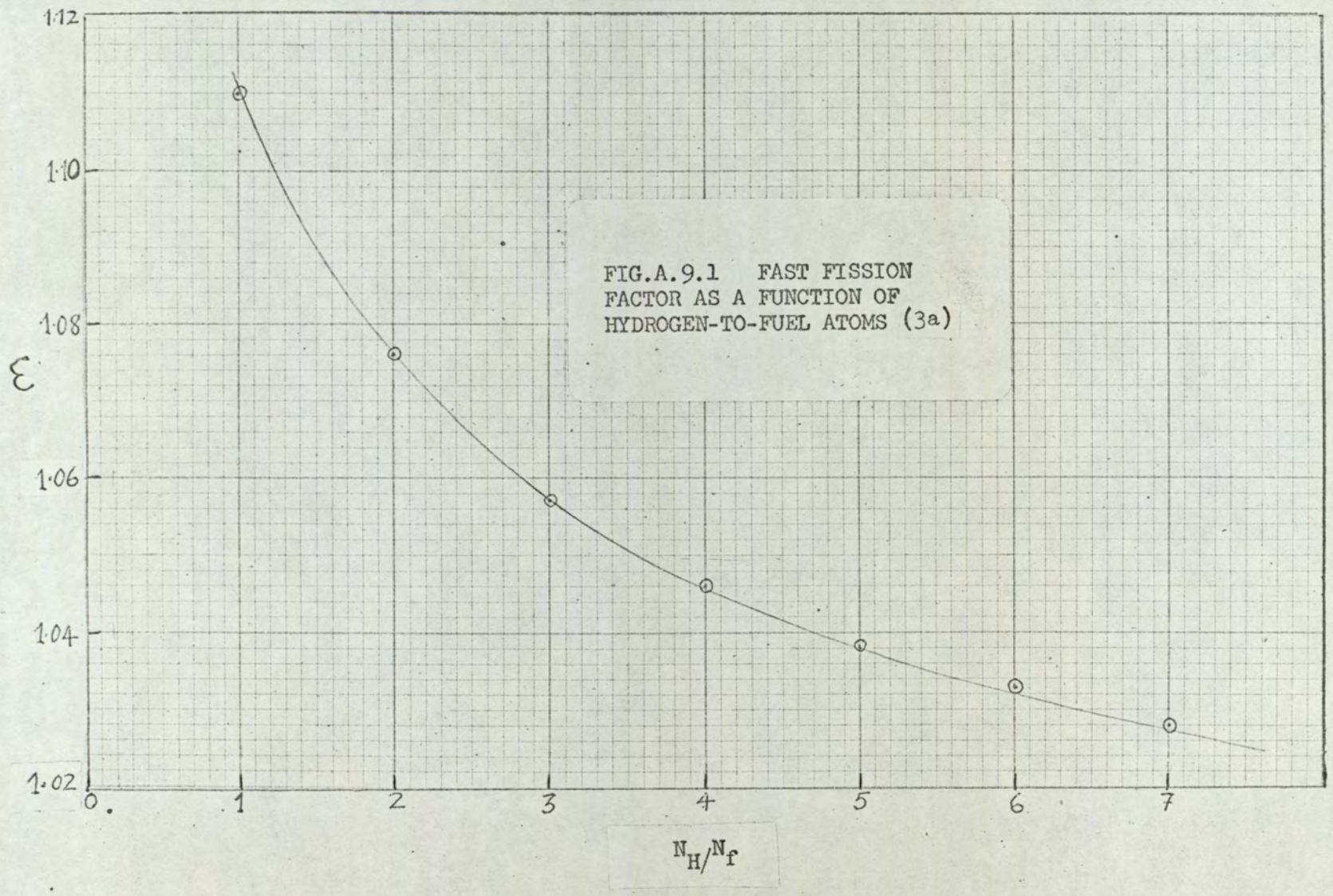

FIG.A.9.1 FAST FISSION FACTOR AS A FUNCTION OF HYDROGEN-TO-FUEL ATOMS (3a)

LIST OF REFERENCES

1) Glasstone,S. and Edlund,M.C. "The Elements of Nuclear Reactor Theory". D.Van Nostrand Company, Inc.,(1963)

2) "Catalogue of Radioactive Products", The Radiochemical Centre, Amersham, (1964)

3) Argonne National Laboratory, "Reactor Physics Constants." USAEC, Report ANL-5800, 2nd Edn. (1963)

3a) Argonne National Laboratory, "Reactor Physics Constants". USAEC, Report ANL-5800, 1st Edn. (1958)

4) Goldstein,H. "Fundamental Aspects of Reactor Shielding". Addison-Wesley Publishing Company, Inc.,(1959).

5) Blizzard,E.P.(Ed.). "Reactor Hand Book Vol.III. Part B. Interscience Publishers, London, (1962)

6) Lyon,W.S. "Guide to Activation Analysis". D.Van Nostrand Company, Inc. (1964)

7) Down,H.J.,Dickie,J. and Fox,W.N. "A method of Simulating Voids in Experimental Studies of Boiling Water Reactors." AEEW-M314 (1963)

8) Stephan, L.A. "Quarterly Progress Report". IDO - 16537 (1959)

9) Shapiro,J.L. Nucl.Sci. and Eng., 12, 449(1962)

10) Kleijn,H.R. "Proceedings Koninklijke Nederlandse Academie Van Wetenschappen". Series B, Vol.LXIX. (1966)

11) Thie,J.A.,Biedelman,J. and Hoglund,B. Nucl.Sci. and Eng., 11, 1(1961)

12) Hooker,H.H., and Popper,G.F., "A Gamma Ray Attenuation Method

12) contd.

for Void Fraction Determination in Experimental Boiling Heat Transfer Systems."ANL-5766 (1958).

13) Perkins,H.C., Husuf,M., and Leppert, G., Nucl.Sci. and Eng.,11, 304(1961)

14) Petrick,M., and Swanson,B.Sc., Rev.Sci.Instr., 29, 1078 (1958)

15) Price,W.J., "Nuclear Radiation Detection ". McGraw-Hill Book Company. 2nd Edn. (1964)

16) Lederer,C.M., Hollander,J.M., and Perlman, I., "Table of Isotopes". Sixth Edn. John Wiley and Sons Inc., New York (1967)

17) Tittle,C.W.,Nucleonics, 8(6), 5(1951) and Nucleonics 9(1), 60(1951)

18) Kouts,H.,et al. Proc. 1955 Geneva Conf., 5, 183

19) Wade,J.W., Nucl.Sci. and Eng.,4, 12(1958)

20) Khan,N.A., et al. Nucl.Instr. and Methods, 65, 140(1968)

21) Nuclear Enterprises (G.B) Ltd. Catalogue, 1967.

22) Bothe,W., Z.Physik, 120, 437(1943)

23) Ritchie,R.H., and Eldridge,H.B., Nucl.Sci. and Eng., 8, 300(1960)

24) Sola,A., Nucleonics, 18(3), 78(1960)

25) Hanna,G.C., Nucl.Sci. and Eng., 15, 325(1963)

26) Meghreblian,R.V., and Holmes,D.K., "Reactor Analysis", McGraw Hill Book Company, (1960)

27) Weinberg,A.M., and Wigner,E.P., "The Physical Theory of

27) contd.

Neutron Chain Reactors. "The University of Chicago Press, (1958).

28) Meem,J.L., "Two Group Reactor Theory". Gordon and Breach Science Publishers, New York, (1964)

29) Murray,R.L., "Nuclear Reactor Physics". Prentice Hall Inc. (1957)

30) Kouts,H., et al. Proc. 1958 Geneva Conf., 12, 446

31) Amster,H.J., "A Compendium of Thermal Neutron Cross Sections Averaged over the Spectra of Wigner and Wilkins." USAEC Report WAPD-185(1958).

32) Cooper,P.N. "The Physics Design of an Organic Moderated Reactor". AERE-RS/L 255, (1964)

33) Deutsch, R.W., Nucleonics, 15(1), 47(1957).

34) Amouyal, A., Benoist,P., and Horowitz, J. "Nouvelle Methode de Determination du Facteur d'utilization Thermique d'une Cellule." J.Nuclear Energy, 6, 79(1956)

35) Lamarsh,J.R., "Introduction to Nuclear Reactor Theory". Addison-Wesley Publishing Company, Inc., Reading, Mass; (1966)

36) Macklin,R.L., and Pomerance,H.S., Proc. 1955 Geneva Conf., 5, 96

37) Campbell,C.G., and Freemantle,R.G., "Effective Cross Section Data for Thermal Reactor Calculations." AERE RP/R 2031. (1957)

38) Campbell,C.G., and Grant,I.S., Proc.1958 Geneva Conf.,12, 728

39) Gurevich,I.I., and Pomeranchouk,I.Y., Proc.1955 Geneva Conf., 5, 466.

40) Hellstrand,E., J.Appl.Physics, 28, 1493(1957)

41) Chernick,J., and Vernon,R., Nucl.Sci. and Eng.,4, 649(1958)

42) Vernon, A.R., Nucl.Sci. and Eng.,7, 252(1960)

43) Aldler,F.T., Hinman,G.W., and Nordheim,L.W.,
Proc.1958 Geneva Conf., 16, 155.

44) Spinrad,B.I.,Chernick,J., and Corngold,N.,
Proc. 1958 Geneva Conf., 16, 191

45) Dancoff,S.M., and Ginsberg,M., "Surface Absorption in a Close-Packed Lattice." CP-2157, (1944)

46) Cooper,P.N., "Nuclear Data for H.A.R. Systems."
HARD(A)/N.20. (1956)

47) Frisch,O.R., and Littler,D.J., Phil.Mag.,45, 126(1954)

48) De Hoffmann,F., "The Science and Engineering of Nuclear Power," Vol.II. Addison Wesley Press Cambridge,Mass.(1949)

49) Feynman,R.R., De Hoffmann,F., and Serber,R.,
J.Nuclear Energy, 3, 64(1956)

50) Courant,E.D., and Wallace,P.R., Phys.Rev. 72(11), 1038(1947).

51) Min, Lu, Shabalin,E.P., and Yazvitskii, Yu.S.
J.Nuclear Energy, 19, 107(1965)

52) Pal,L.I. Nuovo Cimento, Suppl.7, 25(1958).

53) Marion,J.B., and Fowler,J.L., "Fast Neutron Physics". Vol.IV Part I. Interscience Publishers, Inc., New York (1960)

54) The Reactor Hand Book: Physics, USAEC Report AECD-3645 (1955)

55) Davison,B., Proc.Phys.Soc., London, A64, 881(1951)

56) Zaretsky,D.F., Proc. 1955 Geneva Conf., 5, 526.